ADDIS ABABA UNIVERSITY

SCHOOL OF EARTH SCIENCE

TITLE: CHARACTERIZATION AND GENESIS OF KULFAMBA MANGANESE - IRON OCCURRENCE, NORTH WOLLO, ETHIOPIA

PREPARED BY

ADISE ZEMELAK SISAY

A thesis submitted to the School of Graduate Studies of Addis Ababa University in partial fulfillment of the requirements for the degree of Master of Science in Resource Geology (Mineral Deposit)

Jun, 2020 G.C

Addis Ababa, Ethiopia

ADDIS ABABA UNIVERSITY
SCHOOL OF GRADUATE STUDY
SCHOOL OF EARTH SCIENCES

CHARACTERIZATION AND GENESIS OF KULFAMBA MANGANESE - IRON OCCURRENCE, NORTH WOLLO, ETHIOPIA

BY

ADISE ZEMELAK SISAY

ADVISOR: WORASH GETANEH (PhD)

CO-ADVISOR: DEREJE AYALEW (Prof.) and

BALEMWAL ATNAFU (PhD)

A thesis submitted to the School of Graduate Studies of Addis Ababa University in partial fulfillment of the requirements for the degree of Master of Science in Resource Geology (Mineral Deposit)

Jun, 2020 G.C
Addis Ababa, Ethiopia

ADDIS ABABA UNIVERSITY

SCHOOL OF GRADUATE STUDY

SCHOOL OF EARTH SCIENCES

CHARACTERIZATION AND GENESIS OF KULFAMBA MANGANESE - IRON OCCURRENCE, NORTH WOLLO, ETHIOPIA

BY

ADISE ZEMELAK SISAY

Approved by the Examining Committee

1.	Dr. Balemwal Atnafu	_____	26-06-2020 G.C
	Head, School of Earth Sciences	Signature	Date
2.	Dr. Worash Getaneh	_____	26-06-2020 G.C
	Advisor	Signature	Date
3.	Prof. Dereje Ayalew	_____	26-06-2020 G.C
	Co-advisor	Signature	Date
4.	Prof. Gezahegn Yirgu	_____	26-06-2020 G.C
	Examiner	Signature	Date
5.	Prof. Solomon Tadese	_____	26-06-2020 G.C
	Examiner	Signature	Date

Declaration of Originality

I hereby declare that the thesis is my original master degree work under the supervision of Dr. Worash Getaneh, Prof. Dereje Ayalew and Dr. Balemwal Atnafu, School of Earth Sciences, Addis Ababa University during the year 2020 G.C. I further declare that this work has not been presented or submitted to any other university or institution for the award of any degree or diploma. All sources and materials used for the thesis have been duly acknowledged.

Adise Zemelak Sisay _____ 26-06-2020 G.C

Signature Date

This is to certify that the above declaration made by the candidate is correct to the best of my knowledge.

Dr. Worash Getaneh (Advisor) _____ 26-06-2020 G.C

Signature Date

Prof. Dereje Ayalew (Co-advisor) _____ 26-06-2020 G.C

Signature Date

Dr. Balemwal Atnafu (Co-advisor) _____ 26-06-2020 G.C

Signature Date

Abstract

The Kulfamba Manganese-Iron occurrence is located in the top parts of Wollo plateau, northern Ethiopia, about 83 km west of Woldia. The main purpose of the research is to characterize and determine the origin of the ore body. To accomplish this secondary data collection, field observation, rock and ore analysis, and data presentation and interpretation methods have been applied. The geology of the study area is mainly characterized by presence of volcanic rocks and terrestrial sedimentary rock such as sandstone and mudrock. The ore body occurs within the volcano-sedimentary sub-basin associated with most probably late Oligocene intertrappean beds.

In order to define the genesis of the ore body, field observation, petrographic and geochemical examinations were undertaken. The field observation informs that the ore body is found in the form of stratabound - stratiform, vein, concretion and coating. From these, the layered ore is prominent over the other morphology. Based on petrographic observation, manganese oxide (mainly pyrolusite), hematite and goethite have been identified as ore minerals. Similarly, colloform growth banding, well developed crystals, vein fillings structures and secondary replacement are the ore mineral textures.

Geochemically, the mean Fe/Mn ratio of the upper and lower parts of the ore body shows strong fractionation of Fe and Mn, which are 0.045 and 20.52 respectively. The concentration of Ba is also high in the Mn-rich part, which is >10000 ppm. Contrary, the average concentrations of heavy metal such as Co, Ni and Cu have been very low in the ore body. The mean ∑REE concentrations of Mn and Fe ore body are extremely high, which is 1839.8 and 3056.2 ppm respectively. Likewise, the ∑LREE/∑HREE ratios of the ore body exhibit high concentrations of LREE over HREE. The primitive-mantle-normalized diagram of both whole rock and ore body samples reveals the presence of slight negative Eu anomalies, and both positive and negative Ce anomalies. Therefore, the different investigation suggests that Kulfamba Mn-Fe occurrence is formed by mixing of hydrothermal and sedimentary processes. In addition, the occurrence of Mn - Fe ore in the form of concretion and coating reveals a contribution of secondary weathering process later on.

Key words: Kulfamba, Manganiferous, Terrestrial bed, Genesis and Morphology

Acknowledgment

The completion of this thesis would have been impossible without the assistance of the almighty God and many people. First and for most, I would like to express my deepest gratitude to Woldia University, for sponsoring me to attend my MSc program in Addis Ababa University and providing me different geological equipment's and vehicle during field work. I am also thankful to Addis Ababa University, school of Earth Sciences, for funding the research project.

I would like to give special sincere gratitude for my advisor Dr. Worash Getaneh who made this work possible. It is not only for his excellent guidance and endless encouragement throughout the study but also for his humanity and fatherhood approach to give valuable suggestion, daily constructive comment and directions how to carry out a research. My heartfelt gratitude extends to my co-advisor Prof. Dereje Ayalew and Dr. Balemual Atnafu for their vital comments and suggestion. All advisors give me a chance to do the field with them and each of them affords a detail description on the exposed rock units and resources. Moreover, they provide me a full financial support for 18 geochemical sample analysis and field work activities.

I would like to express my warmest thanks to my class meet Getnet Gezahegn for his technical guidance, maintenance and valuable suggestions in my thesis work. He helps me by showing different software's that used to present and elaborate field data and geochemical analysis result.

I am very much thankful to Woldiya University geology department staff members, especially Mr. Siraj Beyan (department head), Mr. Takele Mengste, Mr. Dejen Teka, Mr. Assaye Getnet and Mr. Abere Tesfaye who give secondary data, valuable suggestion and comments during field work and after field work. I am also extremely grateful to Mr. Abate Assen and Mr. Samuel Getachew who give a tireless comments and suggestions. My appreciation also goes to Mr. Biniyam Samson (Woldiy University drivers) for his respectable hospitality and cooperation during fieldwork. I would also like to thank ALS SERVICES PLC, for their timely submission of the geochemical analysis and for providing a discount for the analysis.

Eventually, my deep gratitude is awarded to my brothers Brhanu Dessu and Getachew Belay for their determination and encouragement on my study and gives a solution for any difficulty. Finally, I give thanks a lot to all my families for their moral support and encouragement they offered me during my study.

Table of Contents

List of figures

List of Tables

List of Acronyms

CFB - Continental Flood Basalt

DEM - Digital Elevation Model

Fe - Iron

Fig. - Figure

GIS - Geographic Information System

GPS - Global Positioning System

GSE - Geological Survey of Ethiopia

HREE - Heavy Rear Earth Element

ICP-AES - Inductively Coupled Plasma Atomic Emission Spectroscopy

ICP-MS - Inductively Coupled Plasma Mass Spectroscopy

LOI - Loss On Ignition

LREE - Light Rare Earth Element

Mn - Manganese

My - Million years ago

PPL - Plane polarized light

ppm – Parts per million

REE - Rare Earth Element

UTM - Universal Transfer Mercator

Wt% - Weight in percent

XPL - Cross polarized light

CHAPTER ONE

INTRODUCTION

1.1 Background

The geology of Ethiopia can be considered as the national text book of geology for different types of geological investigations. The general tectonic setting and the distribution of many types of rocks throughout the country has made it more attractive and comfortable place for different systematic investigation in different approaches of geosciences. The Precambrian geology, the sedimentary basins, the main Ethiopian rift (MER), the Cenozoic volcanics, and the Afar depression are the main areas that create a center of attention for many researchers. This diverse geology of Ethiopia comprises a variety of mineral resources (metallic, gemstone and industrial mineral), energy resource and water resource. As a result of this, Ethiopia is one of the African countries with considerable mineral resource potential and is endowed with substantial amounts of metallic and non-metallic resources (Solomon Tadesse, 2003) and has a long history of mining activities. Although it is not detail, both governmental and privet exploration groups are active in searching the different economical mineral resources of the country.

The study area is comprised of the volcanic rocks of Ethiopia, in the northern plateau of Wollo. The volcanic sequence of Ethiopia was emplaced with the opening of the East African continental rift during the Oligocene, about 30 million years ago (Dereje Ayalew and Gezahegn Yirgu, 2003; Dereje Ayalew and Gibson, 2009). These volcanic rocks, mainly represented by basalts (traditionally referred to as the trap succession), have an estimated area coverage of not less than 750,000 km^2 before erosion, with a total volume of 350,000 km^3 (Mohr, 1983). Their great areal extent and volume are due to the exceptional supply of mantle material connected with hot plumes (Schilling, 1973; White and McKenzie, 1989) and less viscosity of dominantly basaltic magma. Wollo province is worldwide known area for play-of-color opal resource in the past ten years. In early 2008, a new source of play-of-color opal was discovered by farmers near Wegel Tena in northern Ethiopia associated with thick volcano-sedimentary sequence of alternating layers of basalt and rhyolitic ignimbrite (Fritsch and Rondeau, 2009; Mazzero et al.,

2009; Rondeau et al., 2010). Although the resource is not used at this time, the Wollo area is known by the occurrence of energy resource like sub basalt sedimentary basin petroleum resource, intertrappean coal and oil shale deposits in Woreillu and Wuchale area respectively (Tilahun Mammo, 2010; Wolela, 2008). According to Wolela (2008); the fluvio-lacustrine coal and oil shale bearing sedimentary succession are deposited on a basaltic substratum of Ashangi Trap series.

In addition to the gemstone and energy resources, the area is also characterized by the occurrence of manganese - iron ore in kulfamba area. The resource is new occurrence and found associated with intertrappean sediments that are bounded by trap volcanic rocks. Accordingly, this research tries to study the geology, geochemistry and genesis of Kulfamba manganese iron mineralization.

1.2. Geographic Setting of the Study Area

1.2.1 Location

The research area is located in the northern part of Ethiopia particularly in Amhara regional state, north Wollo zone of Angot woreda. It is about 604 km from Addis Ababa to the north and 351 km east of Bahir Dar. Geographically, the area is bounded by UTM coordinates 1309000m to 1318000 m N and 537000 m to 544000 m E covering a total area of 70 km^2. According to the Ethiopian mapping agency topographic mapping configuration, it is found in the Godgwadit map sheet (1139-A2). The study area is accessible by Asphalt road from Addis Ababa to Woldiya which is 521 Km toward the North, another asphalt road that extend from Woldiya to Bahir Dar about 65 Km toward West of Woldiya and finally the gravel road which is about 18 km toward southeast direction from Babasat (Fig. 1.1).

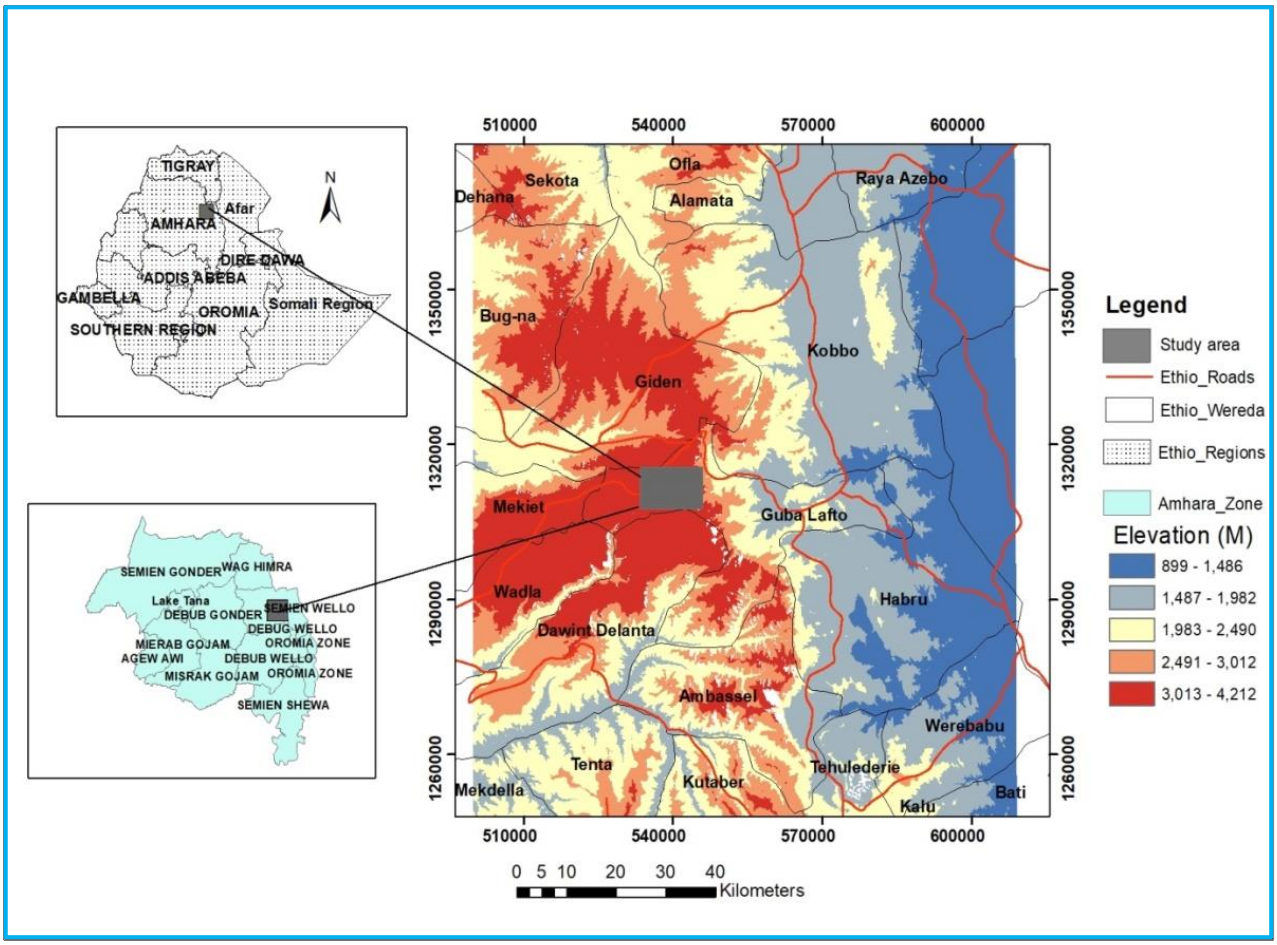

Figure 1.1:- Location map of the study area

1.2.2 Physiography and Drainage

The area is found in north western highlands, part of northern central plateau, and forms typical plateau topography, which is often extensively eroded and dissected by deep gorges. The area is highland with elevation ranging from 3300 m to 3800 m above sea level (Fig. 1.2) with an elevation difference of more than 500 m. It is characterized by relatively flat topography (plateau) with full of valleys, hills, ridges and other erosion remnant landforms. The area includes Lam Bochama Ridge and Alech Ber ridge in the north part of study area and other small erosion remnant secondary formed mesa and butte structures. Most of the river starts from the east and north east parts of the study area and flows toward south west direction. Shelekit, Tikur Wuha, Baba and Samaw are the main streams that are found in the area and they are

characterized by dendritic to sub parallel drainage patterns. Finally, all these mentioned streams flow towards Zita River, west direction as shown in (Fig. 1.2).

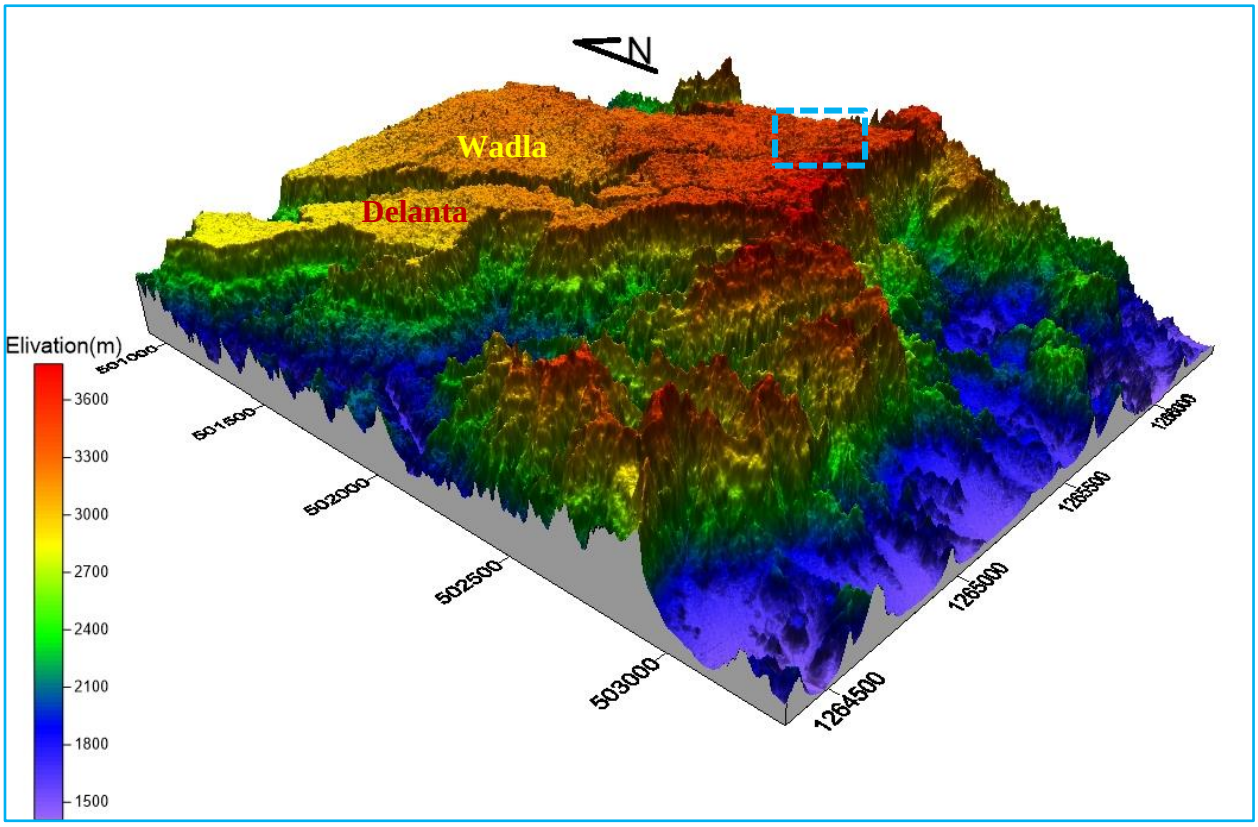

Figure 1.2:- Physiographic map of the whole Angot plateau, which comprises the study area Kulfamba as indicated in blue broken rectangle and Wadla-Delanta area.

1.2.3 Climate and Vegetation

The variability in topography has an influence on the climate of the earth surface. According to Daniel Gemechu (1977), climate can be classified with respect to elevation as Desert climatic zone (Bereha), Tropical (Kola), Subtropical (Weynadega), Temprate (Dega), and Alpine (Kur) with elevation less than 800 m, from 800 m-1500 m, from 1500-2300 m, from 2300-3300 m and greater than 3300 m respectively. Accordingly, the study area (Kulfamba) which included in Debot climate data is categorizes as Alpine (Kur) since it falls with the range of greater than 3300 m in elevation. According to the data accessed on 28/03/2019 from *https://en.climate-data.org/africa/ethiopia/amhara/debot-564611/*, the maximum temperature recorded in Debot and its surroundings is 18.6 °C during June and the minimum temperature is 6 °C during

December. The average annual temperature of the area is 16.6 °C. The rain fall in the study area is characterized by much more rainfall distribution in the summer than winter season. The average rainfall in a year is 758 mm and the difference in precipitation is 221 mm between the driest and wettest months. In general, the climatic condition of the study area is summarized in (Fig. 1.3).

Since most of the area is used for Agricultural farming practice for the local people, it has a great influence for vegetation cover in the study area. The common crop productions in the study area are barley, wheat and legume. Eucalyptus, grass and guwassa are some of the common vegetation in the study area.

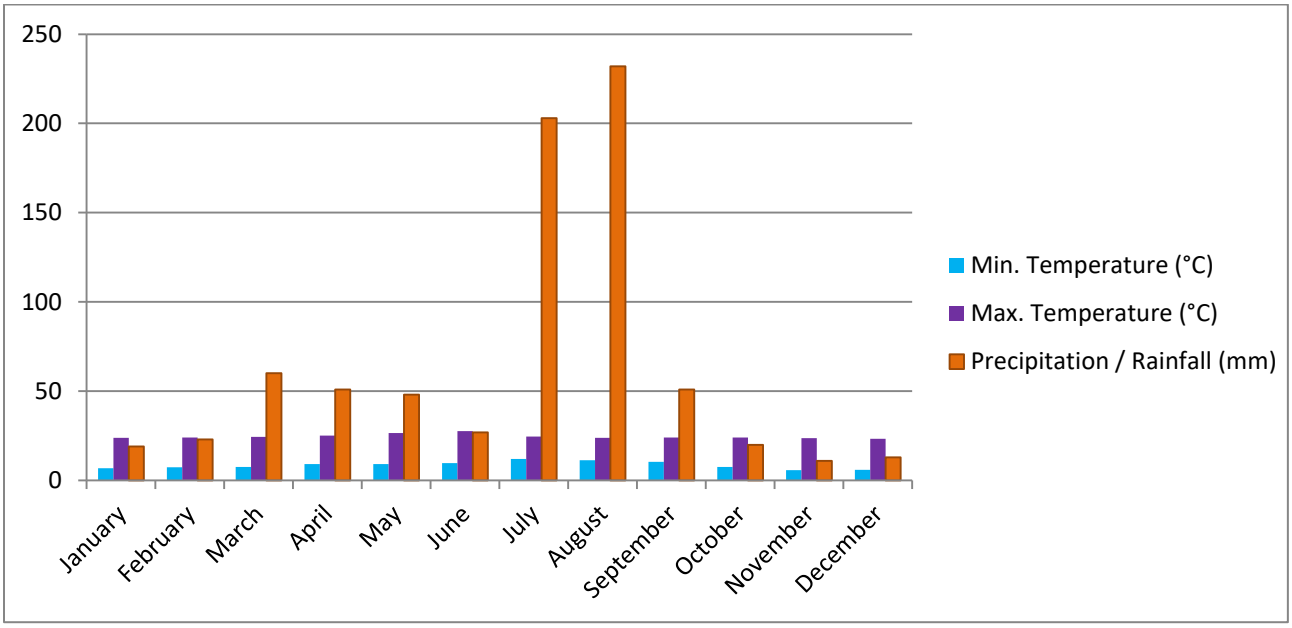

Figure 1.3:- Show monthly rainfall distributions in the study area
(Source: https://en.climate-data.org/africa/ethiopia/amhara/debot-564611/ accessed on 28-03-2019)

1.2.4 Settlement

The settlement of the population is mainly in rural villages that are scattered in west, north east and central part of the study area. In those part of the study area; the population settlement is sparsely distributed. Whereas, in northwest and north part of the study area (Keberomeda and

Irobit), the settlements are relatively dense. Keberomeda and Irobit are small towns that are located on the ignimbrite unit.

1.3 Statement of the problem

Wollo province has been well known by colored gemstone mineral resources namely opal for the last decade. According to Rondeau et al., (2010), the opals are found in a specific layer of a thick volcanic sequence of alternating basalt and ignimbrite of Oligocene age. In addition to the gemstone, the area is also characterized by the occurrences of manganiferous ore around Kulfamba locality on which the present study focuses. This resource is new occurrence and is found associated with sandstone and mudrock formation above Trap volcanics. Beyond the occurrence of the resource, the intertrapean beds that host the Mn-Fe mineralization have important implication on the stratigraphic sequence of Cenozoic volcanics. However, the area is not studied well until now. As a result, this research conducts a detailed investigation on the geology, genesis and geochemical features of the resource occurrence. On the other hand the research will help to further elaborate the stratigraphy of the Cenozoic geology of Ethiopia.

1.4 Objectives

1.4.1 General Objective

The main objective of the research is to characterize and determine the genesis of Kulfamba manganiferous occurrence.

1.4.2 Specific Objective

The specific objectives are set to be the following:

- Describe the geology of the study area
- Prepare geological map of the study area at scale of 1 : 50,000
- Identify the processes of formation of the ore body
- Hypothesize the genetic model of the resource occurrence

1.5 Methodology

1.5.1 Methods

In order to accomplish the stated objectives of the study the following methods are used directly or indirectly.

1.5.1.1 Secondary data collection

Before directly going to collect primary data from the field, important office works have been conducted. These include: checking the accessibility of the study area from Google earth, collecting and investigating different published and unpublished literatures, base map preparation and field work planning. These relevant data are obtained from institutes, internet and advisors.

1.5.1.2 Field Observation and Geological mapping

The field work activity was conducted in January 2019. During the field work primary data have been collected and recorded. These are identification and description of different lithological units based on their texture, color, mineral composition; recording aperture and spacing of joints, record stratigraphic section logs data, and describe the ore body based on its morphology and thickness. Moreover, standard representative samples were collected from actual mineralization, host rock and country rocks. Those samples were collected randomly according to the outcrop of the rock types and ore bodies. All the information taken and observed on the ground, and GPS reading at different stations are used to prepare 1:50,000 scale map with the help of GIS software. In general, the field work investigation serves as a source of primary data for the understanding of the processes of formation and genetic model of the Mn-Fe ore occurrence.

1.5.1.3 Rock and Ore analysis

The mineralized and non-mineralized rock samples that were collected from all exposed outcrops and sections have been selected and prepared for major oxide, trace element, and rare earth element, mineralogical and petrographic analysis. The mineralogical and analytical results

obtained were used to understand the mineralogical assemblage, processes of formation, environment of deposition, average grade and genetic model of the manganese occurrence.

A. Geochemical Analysis

A total of eighteen samples (thirteen rocks and five Mn-Fe ore samples) were performed by ALS laboratory in Ireland. Samples were first crushed to 70% of < 2 mm size and pulverized with a riffle splitter to have whole rock geochemical analysis. Pulverize split to 85% <75 µm and crushing tested with Quality Control (QC) test. The analytical data of major and trace elements were generated using Inductively Coupled Plasma Atomic Emission Spectrometer (ICP-AES) and Inductively Coupled Plasma Mass Spectrometry (ICP- MS) respectively. From the analysis mentioned above, major oxides such as SiO_2, MgO, CaO, Fe_2O_3, Al_2O_3, Na_2O, TiO_2, K_2O, Cr_2O_3, MnO, P_2O_5, SrO, and BaO were analyzed with whole rock package ICP-AES (ME-ICP06) and trace elements such as Ba, Ce, Cr, Cs, Dy, Er, Eu, Ga, Gd, Hf, Ho, La, Lu, Nb, Nd, Pr, Rb, Sm, Sn,Sr,Ta,Tb, Th, Tm, U, V, W, Y, Yb, Zr are analyzed with whole rock package of Lithium Borate Fusion by ICP-MS (ME-MS81). In addition, base metals such as Ag, As, Cd, Co, Cu, Li, Mo, Ni, Pb, Sc, Tl and Zn were analyzed with ICP-AES (ME-4ACD81) 4-acid digestions. Finally, the geochemical analysis result helps to determine the origin of the Mn-Fe occurrence and its depositional environment.

B. Petrographic Examination

Microscopic examination of polished and thin section through reflected and transmitted light microscope help to determine the mineralogical assemblage and textural features of ore and gangue minerals respectively. As a result a total of ten thin section samples were prepared in the mineralogy and petrographic laboratory of Addis Ababa University and in geological survey of Ethiopia. In order to determine the mineralogical proportion of the host rock (sandstone); the study uses visual estimation technique. On the other side, five polished section samples from mineralized ore body were prepared in geological survey of Ethiopia (mineralogical and geological laboratory of Ethiopia). The interpretation and mineral identification was done at Addis Ababa University. From the texture of ore minerals, the origin of Kulfamba Mn-Fe ore body has been established.

1.5.1.4 Data presentation and interpretation

Finally, all the data collected from literatures, field work and laboratory analysis were interpreted and presented. The interpretation and presentation has been shown in the form of text, tables, graphs and maps. The text mainly provides a description of the lithology, ore body and petrographic observation of the ore. On the side, the geochemical analyses, lithological section logs and climate data have been presented in table and graph format, in addition to the discussion of the results. This is a final method that gives a full result of the study. All collected data and discussion of the interpretation have been written up in the final thesis report and at last the thesis has been submitted to School of Earth Science.

1.5.2 Materials

For the success of this research different materials are used from the starting until the compilation of the research. Among these:- topographic map, geological hammer, Global positioning system (GPS), transmitted and reflected light microscopy, sample bag, printer and scanner, camera, laboratory equipment's (ICP-ES and ICP-MS) and different stationary materials are used. In addition, ArcGIS 10.3, Google Earth, Global Mapper, surfur 10, Strater 4, Grapher 8 and excel software packages are used at different phase.

1.6 Outcomes and significance of the study

The outcomes of the research are:

- Complete description and lithological characterization of the study area
- Well-organized and integrated detailed geological map at a scale of 1:50,000
- Interpretation and description on the genetic process and morphology of the Mn-Fe mineralization
- Most probable genetic model of a resource occurrence

Some of the significances of the research:

- It contains a detail petrographic, geochemical and geological description of the rock units and the ore body that found in Kulfamba area. As a result, it serves as initial or additional source for any beneficiaries of the thesis.

- As far as the sediment is not limited to the present study area, rather it is continuous towards south, south west and west part of the area and it has new stratigraphic succession information on the Wollo volcanic rock. Therefore, this work initiates the researcher for further study over the neighboring areas in order to know the extent of the basin, interpret the paleo - environment and to find other associated resources.

1.7 Structure of Thesis

This thesis is organized as eight chapters.

- **Chapter one:** deals with general introduction which includes research background, detail descriptions of the study area, problem of the statement, objectives of the research work, significance of the study and methodology adopted in the present research work.
- **Chapter two:** the literature review is mainly focus on the manganese characteristics, distribution and its geochemical association with iron.
- **Chapter three:** focuses on detail descriptions of the regional geology of Ethiopian Cenozoic volcanic particularly northern Ethiopian plateau, lithological units of the Wollo province and intertrappean sediments.
- **Chapter four:** provide the detail description of each lithological units and structures (both primary and secondary) that found in the study area. In addition, geological map of the study area, cross section and stratigraphic log section of various rock units are provided.
- **Chapter five:** Includes general introduction about kulfamba manganese - iron occurrence, its geological setting and a detail examination of the ferromanganese mineralization (including morphology of the ore body and host rock).
- **Chapter six:** The mineralogical and geochemical results (major element, trace element and REE result) of the resource and associated rocks are presented.
- **Chapter seven:** The identification and determination of Kulfamba Mn-Fe resource origin based on field observation, microscopic and geochemical analysis.
- **Chapter eight:** In the final chapter, the conclusion and recommendation of the present study is provided.

CHAPTER TWO

LITRUTURE REVIEW

2.1 Introduction

Manganese is the tenth most abundant element in the Earth's crust, which is depending on the model used for crustal composition and makes up about 1000 ppm (0.1%) of the earth's crust (Maynard, 2010). It is a hard, silvery white, brittle, naturally occurring metallic element that is found in many types of rocks. However, it is not found in a native state; rather it is often found in minerals in combination with iron. It reacts with many nonmetals at increased temperature, but it is unreactive at room temperature. It has a density of 7.2 - 7.46 g/cm3 and a melting temperature of 1244ºc (Kuleshov and Maynard, 2017).

Manganese has a wide range of application in the modern industry and consumed in large amount in all industrialized countries. Although its early uses were limited largely to pigments and oxidants in chemical processes and experiments, the metallurgical industry has accounted for the most of the world manganese consumption in the modern industry (Cannon et al., 2017; Kuleshov and Maynard, 2017). Globally, almost 90 to 95% of Mn is used in the metallurgical industry as a requisite deoxidizer and desulfurizer in steel making and as an important alloy component (Fan and Yang, 1999; Corathers, 2006). The main importance of manganese in steel production is to enhance strength, stiffness, hardness, toughness, wear resistance as well as forging and rolling qualities (Zhang and Cheng, 2007; Maynard, 2010). The remainder of the Mn (5 to 10%) has also played a vital role in the chemical industry, light industry, national defense applications, building materials, dry cell battery production, electronics, and environmental protection (Corathers, 2006; Zhang and Cheng, 2007).

2.2. Geochemistry and Mineralogy of manganese deposits

Naturally, manganese is found in divalent (Mn^{2+}), trivalent (Mn^{3+}) and quadrivalent (Mn^{4+}) valance states. However, it is present mainly in divalent form in a wide range of igneous minerals where it substitutes for iron (Post, 1999). The divalent forms of manganese are highly soluble and reactive, while the higher valance forms are insoluble and both chemically and

physically resistant (Kogel et al., 2006). Manganese is similar to iron in its chemical and physical properties (Kogel et al., 2006; Kuleshov and Maynard, 2017) and show a common association in different rocks, especially in igneous rocks, where the ratio of Mn/Fe often lies between the limits of 1/100 and 1/10 (Krauskopf, 1957). Both are redox sensitive elements with weakly oxidized ionic species ($Fe^{2+,}$ Mn^{2+}), which are fairly soluble in water in surface environments under oxygen-deficient (anaerobic) conditions and both are oxidized to poorly soluble Fe^{3+} and Mn^{4+} in aerobic environments (Maynard, 2003; Gutzmer and Beukes, 2009). As a result, they are intimately associated in nature and their deposition is in similar geological environment.

Although the two elements are found associatively together in all kinds of rocks, the fractionation of the two elements is a prerequisite for the origin of their specific ore deposits. Thus, silicate weathering provides a substantial source of Mn^{2+} to surface and ground waters, especially since Mn(II) is highly soluble than iron (Gross, 1965; Post, 1999). The main point here is the mechanism of iron and manganese separation. Therefore, the separation of the two elements and the deposition of manganese deposits seek a special ore formation process. In solutions, manganese is transportable in reducing environment and it undergoes precipitation and deposition in oxidizing environment (Worash Getaneh and Solomon Tadesse, 2015). Therefore, to concentrate Mn into significant sedimentary deposits, manganese needs to be oxidized to Mn(III) or Mn(IV) (Calvert and Pedersen, 1996; and Armstrong, 2008).

Unlike iron sulfide minerals like FeS or FeS_2, the sulfides of manganese (alabandite and hauerite) are very soluble under reducing conditions; instead manganese behavior at low Eh is controlled by carbonate minerals (Kogel et al., 2006; Maynard, 2003; and Krauskopf, 1957). The addition of carbonate species at low Eh condition leads to the formation of rhodochrosite ($MnCO_3$), which is stable under reducing conditions. Otherwise, when the iron forms sulfides in the early reducing (much lower oxygen) environments, the manganese claimed that in oxidizing environment. In general, the insolubility difference between the two plays a vigorous role in the separation of the two components in the natural system. In this regard, the sedimentary processes and volcanogenic hydrothermal solution activities are the most prominent conditions for this special ore formation process. The divalent form of manganese could be considerably sourced from either weathering of terrigenous surface rocks or hydrothermal volcanogenic fluids (Post, 1999; Johnson et al, 2016). During weathering, with reference to iron, manganese may be preferentially leached due to its larger ionic size, lower ionic potential and enzymatic microbial

reduction in the source area. Alternatively, if the source of both Fe and Mn elements is from terrigenous source, then during transportation Mn in ionic solution moves faster than Fe due to higher mobility and it may be separated to form its own deposit (Wolf, 1976). In another case, Fe may be separated during deposition by precipitating at lower PH and Eh and effective separation between the two may take place (Roy, 1997) as Mn passes into the solution. The given Eh–pH diagrams suggest a mechanism for separating manganese from iron (Fig. 2.1).

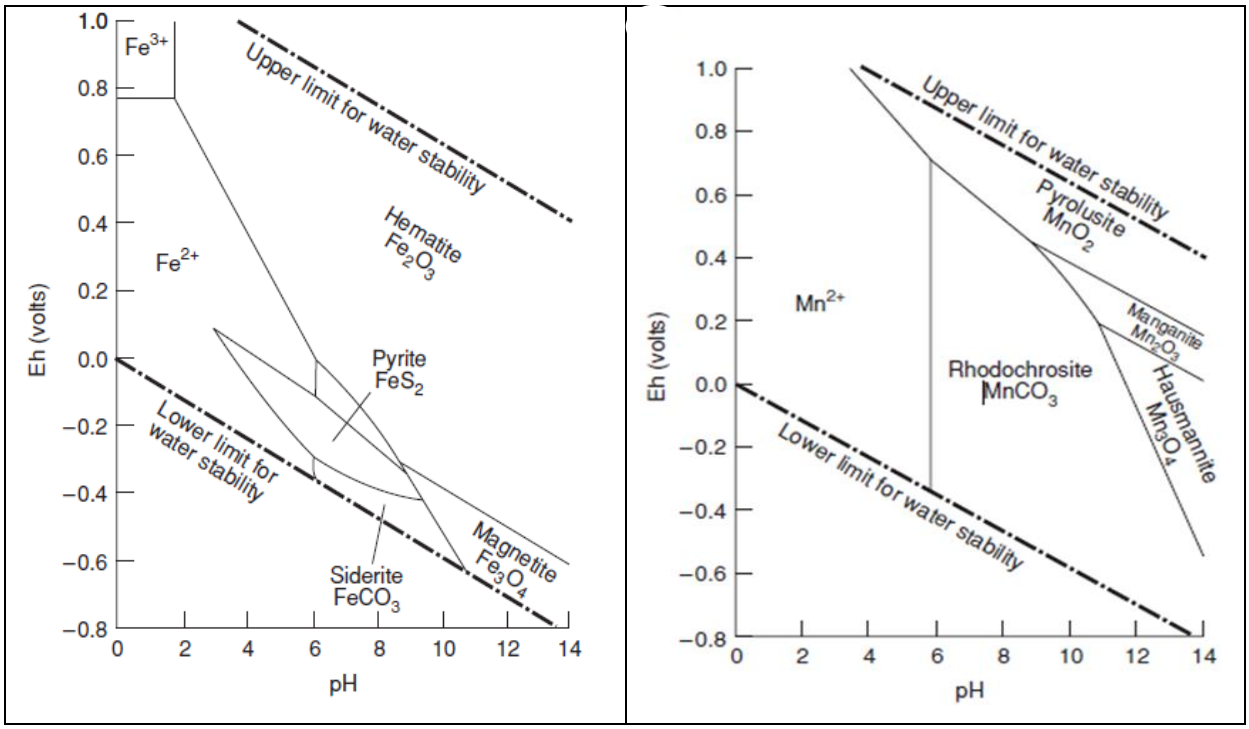

Figure 2.1:- The diagram shows the Eh–pH effects in common iron and manganese minerals formation. The conditions that apply to this particular phase diagram are: T = 25 °C, P = 1 bar, molarities of Fe, S, and CO_3 respectively, 10−6, 10−6, and 1 (diagrams modified after Garrels and Christ, 1965; Krauskopf and Bird, 1995). Note that the manganese oxides (MnO_2 and Mn_2O_3) are stable at higher Eh than the equivalent ferric oxide (hematite), and would only form, therefore, under more oxidizing conditions.

Elemental manganese readily combines with oxygen, carbon, and silicon to form a long list of manganese minerals. Manganese ores generally contain 25 to 45 percent manganese, mostly in the form of oxide (or hydroxide) and/or carbonate minerals. Such ores are widespread, but most of the world's supply is from a small number of manganese mining districts. Most manganese-rich sedimentary rocks are formed in ancient oceans under specialized conditions when changes in the oxidation state of ocean water first caused high concentrations of dissolved manganese and

later precipitated various manganese minerals that became concentrated on the sea bed (William F. Cannon, 2014). In general, the occurrence of manganese in different oxidation states benefits the deposition of manganese minerals in diverse geological and geochemical environments. According to Kuleshov and Maynard (2017), the webmail site lists 191 minerals with manganese contents of 25% or/and greater. However, approximately about 30 of the minerals are economic ores and the rest has no commercial value except their presence as a mineral.

Table 2.1: The major ore minerals of manganese, summarized after Wolf, (1976), Kuleshov and Maynard, (2017) and Kogel et al. (2006).

Oxides and Hydroxides with a higher valance of manganese		***Oxides with Lower valance of manganese***	
Mineral Name	**Formula**	**Mineral Name**	**Formula**
Pyrolusite	MnO_2	Housmannite	Mn_3O_4
Cryptomelane	Kmn_8O_{16}	Jacobsite	$MnFe_2O_4$
Nsutite	$Mn_{1-x}^{4+}Mn_x^{2+}O_{2-x}(OH)_{2x}]$ Where x=0.06 - 0.07	Bixbyite	$(Mn,Fe)_2O_3$
Birnessite	$[(Na,Ca)\ Mn_7\ O_{14}.2.8H_2O$	***Carbonates***	
Todorokite	$(Ca,Na)(Mn^{2+}.Mn^{4+})_7O_{14}\cdot 3H_2O$	Rhodochrosite	$MnCO_3$
Chlcophanite	$[(Mn.\ Zn)\ Mn_{\ 2}\ O_3\ .\ 2\ H_{\ 2}O]$	Manganoan Calcite	$[(Ca,Mn)CO_3]$
Psilomelane	$[Ba,H_2O)_2\ Mn_{\ 5}O_{10}]$	Kutnahorite	$[(Ca,Mn)(CO_3)_2]$
Hollandite	BaR_8O_{16}; R = Mainly Mn^{4+}, also Mn^{2+}, Fe, Co	Oligonite,	$(Mn,Fe)CO_3$
Manganosite	MnO	**Silicates**	
Lithiophorite	$(Al, Li)\ MnO_2(OH)_2$	Braunite	$Mn^{2+}(Mn^{4+}Si^{4+})O_3$
Romanechite	$(Ba,\ H_2O)_2\ (Mn^{+4},\ Mn^{+3})_5O_{10}$	Bementite	$[(Mn,Mg,Fe)_6Si_4(O,OH)_{18}]$
Ramsdellite	$Mn^{4+}O_2$	Neotocite	$[(Mn,Fe)SiO_{3.n}H_2O]$
Vernandite	$MnO_2.H_2O$	Rhodonite	Mn_3SiO_3
Coronadite	$[PbR_8\ O_{16}$;R = Mn^{4+} and Mn^{2+}]	Spessartite garnet	$(Mn_3Al_2(SiO_4)_3)$

Groutite	α-MnOOH		
Feiknechtite	β-MnOOH		
Manganite	γ-MnOOH		
Pyrochroite	Mn^{2+} $(OH)_2$		

Manganese occurs principally as pyrolusite (MnO_2), braunite, ($Mn^{2+}Mn^{3+}$) (SiO_{12}), psilomelane (Ba, $H_2O)_2$ Mn_5O_{10}), and to a lesser extent as rhodochrosite (MnCO3). However, in the given manganese ore minerals list in table 2.1, pyrolusite, braunite, rhodochrosite, housmannite, cryptomelane, psilomelane, manganite, and todorokite are the dominant manganese minerals in commercial deposits of the world (Mynard, 2010; Kuleshov and Maynard, 2017). Mostly those economically important manganese ores usually show a close spatial relation to the iron ores. Quartz, oxides and hydroxides of iron, clay minerals, zeolites, calcite, aragonite and rarely phosphates and sulfide minerals are the most common gangue minerals found together with manganese ore minerals in the mineral assemblages of manganese rocks (Morten et al., 1980; Heshmatbehzadi and Shahabpour, 2010, Kuleshov and Maynard, 2017).

2.3 Genesis and Geological Setting of Manganese Deposits

Manganiferous mineralization is diverse in occurrence, origin, mineralogy and geochemistry (Roy, 1981, Hein et al., 1997 and Nicholson et al., 1997). These variations reflect differences in the processes of formation and depositional environments, which in turn are a response to changes in the land-ocean-atmosphere system over the geological time. As such, Mn-Fe deposits can act as markers of major events in the dynamic evolution of the Earth's surface. Different researchers present various ways of classification of manganese deposits. For instance, Mn ore deposits are divided into six types: sedimentary, volcanic-sedimentary, metamorphosed, hydrothermally modified, hydrothermal, and supergene (Fan and Yang, 1999). This sub-type classification of manganese deposit is based on modes of origin and subsequent modifications, stratigraphic successions, host-rock types, mineral assemblages and element associations. In addition, the manganese deposits are also classified as sedimentary (non-volcanogenic), volcanogenic and hybrid (volcanogenic-sedimentary) deposits (Wolf, 1976; Kuleshov and Maynard, 2017), which is based on the composition of manganese bearing formations and

sources of manganese. The source of manganese could be from the crustal weathering or from direct volcanism. However, many of the researchers relate the diverse genetic types of manganese mineralization with direct hydrothermal activity, sedimentary processes, and continental weathering (Roy, 1981; Nicholson et al., 1997; Oksuz, 2011; Kuleshov and Maynard, 2017). Although the processes may be interrelated, each of them involves distinct mechanisms that place the deposits into specific genetic types. The distinctive characteristics of hydrothermal, sedimentary and supergene type manganese deposits are described in the following sections.

Hydrothermal manganese deposits could be volcanogenic- sedimentary or volcanogenic manganese deposits (Wolf, 1976) and have the smallest dimensions and reserves (Fan and Yang, 1999). As a result, the economic profitability of this type is low and not preferable as sedimentary and supergene manganese deposits. This type of deposits precipitates from low temperature hydrothermal fluids at the periphery or during the waning stage of a high temperature system (Oksuz, 2011; Kahrazehi et al., 2015; and Kuhn et al., 2017). Hydrothermal manganese deposits are distributed in different parts of the world in a wide range of geological setting often in the form of stratabound, but may also occur as irregular bodies and epithermal veins in a large variety of host rocks. As stratabound manganese deposits have been recognized from both modern and ancient geological setting, they are formed in the marine environment near spreading centers (active plate margins), mid-plate seamounts and subduction-related island arc settings (Bonatti et al., 1976; Glasby, 1988; Nicholson, 1990; Robertson and Varnavas, 1993; Roy 1997; Shah and Moon, 2007). While vein-type hydrothermal deposits are hosted mainly in volcanics of wide-ranging compositions as well as in a variety of sedimentary rocks of different ages.

Beyond the above geological setting, ancient hydrothermal manganese deposits also occur in continental settings as stratabound layers and veins in rocks of different varieties and ages. According to Nicholson (1990), emission of hydrothermal solution in shallow continental basins (e.g. lakes) has also produced stratabound manganese deposit. There are many stratabound hydrothermal manganese deposits in the world that are related to lacustrine formation in the Tertiary continental-volcanic province in San Francisco deposit (Mexico), Golconda (Nevada), Hokkaido (Japan) and Burmister deposit in Arizona (Hewett et al., 1963 and Hariya, 1980, cited by Roy, 1981). Zantop (1978) also concluded that a continental hot spring deposited iron and manganese in the oxygenated lacustrine basin. Besides it, hydrothermal vein deposits rich in

manganese minerals that occur in both clastic and chemical sedimentary rocks are commonly derived from terrestrial hot springs (Nicholson et al., 1997). That means the hydrothermal solution is derived from an external source and circulated through fractures in the host rocks. The veins show diverse manganese mineralogy depending on the temperature of hot solution.

The sedimentary manganese deposits are those formed as chemical sediment through precipitation in normal pressure and temperature conditions from solutions enriched in dissolved manganese irrespective of sources (Roy, 2006). This type of manganese deposit is hosted mostly in sedimentary rocks (like carbonate rock, mud rock and black shale series) and rarely in volcanic rocks. Sedimentary manganese deposits easily outclass the other types (hydrothermal and supergene manganese deposits) in respect of size and spatial and temporal distributions. The largest accumulations of manganese deposit in the world are formed by sedimentary processes dominantly in deep and shallow marine basins during marine transgression and regression phases (Cannon and Force, 1986) and small scale in continental environment (Nicholson et al., 1997; and Kuleshov and Maynard, 2017). Although the precise determination of any particular source for manganese is complex, hydrothermal and terrestrial weathering processes serve as primary sources for manganese in the depositional basins (Nicholson et al., 1997). Hydrothermally introduced manganese may be transported thousands of kilometers from the original site. On the other hand, supplies of manganese from terrestrial sources or surficial weathering are particularly active in humid tropical climates. Then the released manganese is carried by ground and surface waters to the lakes and the oceans dissolved, and Mn^{2+} would be concentrated in anoxic deep water. Finally, the mixing of fresh water and seawater in coastal zones may lead to flocculation of dissolved manganese carried by river water which may generate coastal Mn oxide deposits (Sundby et al., 1981; Frakes and BoRon, 1992 as cited in Nicholson et al., 1997).

In the earth history, large-scale deposition of manganese started from the Early Proterozoic due to oxygenation of the atmosphere and stabilization of the stratified ocean system (Nicholson et al., 1997 and Maynard, 2010). As a result, all the largest among known land-based manganese deposits found in South Africa, West African craton, India, China and Brazil are formed in this Proterozoic age. In addition, important Phanerozoic manganese deposits are also found in many parts of the world that were formed during transgression- regression cycles triggered by greenhouse conditions followed by oxygenation. In general, these hydrothermally or terrestrial

weathering generated metal may be transported a long distance from its original site to the depositional basin and directly precipitate or deposit in the basin aided by diagenesis. Marine sedimentary manganese deposits usually form by two major processes, which are hydrogenic and diagenic processes (Lange et al., 1992; Bau et al., 2014; and Kuhn et al., 2017).

A supergene manganese deposit is the third types of manganese deposit. The concentrations of supergene manganese deposits in the zones of terrestrial weathering are common and can yield commercial manganese deposits (Nicholson et al., 1997). In this type of deposit, humid tropical climate with abundant rainfall and vegetation, initial Mn content in the source rock, in concert with suitable topography (e.g. plateaus), and drainage system are crucial determinants in this process of manganese ore formation. Although the leaching of manganese and iron may take place together, selective leaching of manganese with respect to iron by enzymatic microbial reduction is very important process. On the other hand; in the A1-Fe-Mn triad the solubility of manganese is maximum and hence, during downward movement of iron and manganese in solution, a change in Eh-pH may lead to precipitation of iron in preference to manganese and an effective separation between the two may take place.

2.4 Distribution of Manganese Ore Deposits

According to Maynard (2010), three major periods are indicated for the major formation of manganese deposit in the world, namely the Paleoproterozoic (2300 to 1800 Ma), Neoproterozoic (800 to 600 Ma), and the Oligocene, at 28 Ma. The first two correspond to times of Fe deposition, but the third does not. The total land-based Mn reserves are about 26 t/km^2 of continental crust. This total amount of manganese is distributed among time periods as follows: Archean (3.5), Paleoproterozoic (88.4), Mesoproterozoic (1.6), Neoproterozoic (6.8), and Phanerozoic (17.4) (Roy, 1997). Each of the three major episodes of Mn deposition is made up of a group of individual deposits that tend to be constrained geographically. The Paleoproterozoic Mn event is made up mostly of the deposits of the Kalahari Mn field in South Africa. The second largest event, in the Oligocene, consists only of deposits surrounding the present-day Black Sea. In general, when we see the world manganese ore reserves, 380 million metric tons has been estimated. From this estimated reserve South Africa, China, Australia, Gabon, Brazil, and Ukraine holds the largest reserves of manganese resource and are leading

countries in manganese production (https://investingnews.com/daily/resource-investing/battery-metals-investing/manganese-investing assessed on 26/03/2019).

2.4.1 Manganese Occurrences in Ethiopia

The depositions and occurrence of manganese in Ethiopia have much less extent in comparison with iron deposit. According to the promotional data compiled by geological survey of Ethiopia (2013), only one primary deposit is known to exist in marine sediments of young geologic age, which is Enkafela manganese deposit. The total ore reserve was estimated to be around 75, 000 tons (Getaneh, 1985 as cited in Solomon Tadesse et al., 2003). Out of this, about 40,000 ton of manganese was mined from 1959 to 1963 (Solomon Tadesse et al., 2003). However, the recent (last year) study showed that the resource potential of Enkafela manganese deposit is estimated about 44,402 tones (Abate Assen, 2018). Therefore, as compared to the last year estimate with the former studies; 9,402 tones additional manganese deposit is present.

Besides this deposit, other manganese occurrences are found in Tigray at Mussley, Beliga, Handeda, Adi Berbere and Adi Chigono areas. However, the origin of these occurrences is not well defined (Solomon Tadesse et al., 2003). Some of them are at least partly of secondary origin which is supergene related (gossan-type, e.g. Mussley, Adi Berbere). Furthermore, there is also manganese occurrence in Melka Sedi (Kaffa) associated with laterites.

CHAPTER THREE

REGIONAL GEOLOGY

3.1 Geological History of Ethiopian Cenozoic Volcanics

The Ethiopian region records about one billion years of geological history (Abbate et al., 2015). The Precambrian basement rocks (metamorphic rocks), the late Palaeozoic to Mesozoic marine and continental sediments, Paleogene to Quaternary volcanic (dominant) with minor sedimentary rocks are the main rock types recording in the geological history of Ethiopia (Mengesh Tefera et al.,1996; Pik et al., 1998 as cited in Kurkura et al., 2012). Similarly, Asefawossen Asrat (2006) has subdivided the whole Ethiopian geological history in to Precambrian, Paleozoic, Mesozoic and Cenozoic eras. From his idea, Ethiopian Precambrian rocks are generally metamorphic rocks that are associated with intrusive igneous rocks. The Mesozoic sedimentary succession forms a group of rocks resting unconformably on the Precambrian basement rocks. Eventually, Cenozoic era is related to the formation of Ethiopian plateau as a result of the extensive flood basalt eruption between 31-29 Ma. Therefore, the Cenozoic volcanic rocks produced from flow of flood basalt have rested over the Mesozoic sedimentary successions. This era is also related to the formation of Ethiopian rift valley as result of the subsequent breaking up of the uplifted dome. All these activities had happened from the early to the middle Cenozoic era. As a result, nearly half of the country's surface is covered by thick layers of volcanic rocks of Trap series consisting of basalts prevailingly with some more acid rocks and pyroclastics. All these spectacular landscape of the Ethiopian region (typical flat-topped mountains and deep-incised valleys) with general tectonic setting and distribution of many types of rocks fascinated the European travelers since the sixteenth century. This fantastic scenario is the result of geodynamic and geomorphic processes which have shaped this territory since the Oligocene epoch. The volcanic rocks, mainly represented by basalts and traditionally referred to as the trap succession, are estimated to have covered a large area in Ethiopia that is not less than 750,000 km2 before erosion, with a total volume of 350,000 km3 (Mohr, 1983). Their great areal extension and

volume are due to the exceptional supply of mantle material connected with hot plumes. According to Dereje Ayalew et al., (2001); the Ethiopian Continental Flood Basalt (CFB) province was formed as a result of the impingement of the Afar mantle plume beneath the Ethiopian lithosphere. The extensional tectonic settings of this continental flood basalt are marked by the presence of bimodal volcanic suites. As a result this volcanic province contains major sequences of rhyolitic ignimbrites generally found on top of the flood basalt sequence (bimodal succession). Following the end of the Oligocene, the volcanism shifted toward the Afar depression, which was experiencing a progressive stretching, and successively moved between the southern Ethiopian plateau and the Somali plateau in correspondence with the formation of the Main Ethiopian Rift (Abbate et al., 2015). According to Abbate et al., (2015) the present-day morphology of Ethiopia is linked to the formation of the Afar depression, MER, and Ethiopian plateaus. Therefore, the elevated topography of Ethiopian plateaus is the result of profuse volcanic accumulation and successive uplift.

3.2 The Volcanites of the Northern Ethiopian Plateau

The volcanic rocks that cover most of Ethiopia have been subdivided into five major provinces on the basis of their lithological development, frequency of volcanic centers, type of activity, and age of effusion (Abbate and Sagri, 1980). These are (1) volcanites of the northern plateau; (2) volcanites of the southern plateau; (3) volcanites of the Somali plateau; (4) Afar volcanites; and (5) Main Ethiopian Rift (MER) volcanites. The highland volcanites were investigated from a petrographical, geochemical, and geochronological point of view by Mohr and Zanettin (1988), Hofmann et al. (1997), Rochette et al. (1998), Pik et al. (1998) and Kieffer et al. (2004).

Blanford's (1870) attempted to subdivide the northern plateau volcanites into a lower Ashangi group unconformably overlain by a Magdala Group. However, in the 1970s a more detailed lithostratigraphic approach was proposed by Zanettin and Justin Visentin (1973) and Gregnanin and Piccirillo (1974), with the distinction of the Ashangi and Aiba basalts, Alaji Rhyolites, and Termaber Basalts. Furthermore, Abbate and Sagri (1980); subdivided the volcanics of northern plateau in to five litho-tectonic units. These are: (i) pre-Oligocene (Ashangi formation), (ii) Oligocene to Miocene volcanics (Aiba basalt, Alaje formation, Tarmaber-Gussa formation), (iii) Early- to Mid-Miocene Kemise formation, (iv) Miocene Dalha Series, and (v) Quaternary

volcanics and sediments. In the northern Ethiopian plateau, huge Miocene shield volcanoes (Tarmaber-Gussa formation) were superimposed on the flood basalts.

3.3 Lithological units of Wollo province

3.3.1 Eocene-Oligocene volcanic rocks

This volcanic succession comprises Ashengi basalt, Aiba basalt and Wegel Tena ryolitic ignimberite. Ashangi formation is the earliest fissural volcanism and it attains at a maximum thickness around 1000m (Mengesha Tefera et al., 1996). It is composed of transitional to tholeitic olivine basalts, often highly zeolitized, and it alternating with subordinate tuffs (Mohr and Zanettin 1988 as cited in Abbate et al., 2015). On the other hand, petrographically this unit is classified in to three as Vesicular augite-plagioclase phyric basalt, Vesicular augite phyric basalts and Aphanatic basalt (GSE, 2010). These units had overlain unconformably on the Dessie basalt formation and Wegel Tena rhyolite and/or ignimbrite.

The Aiba basalt (after Mengesha Tefera et al., 1996 and references therein) profuse outpouring took place between 31 and 29 Ma (Hofmann et al., 1997; Pik et al., 1998; Ukstins et al., 2002). It is comprised of dominantly aphanitic, vesicular and phyric (pyroxene and olivine) basalts and towards its lower parts of the succession the basalts are interlayered with pyroclastic rocks (GSE, 2010).

Wegel Tena rhyolitic ignimbrite (its name is adopted from Hofmann et al., (1997) and Dereje Ayalew et al., (2002)) with an age of 30 Ma. This unit is exposed in Wegel Tena, Gishen Mariyam and Ambasel section. The ignimberite forms highly elevated plateau topography, which is often extensively eroded and dissected by deep gorges as it clearly observed in Wegel Tena, Dawunt and Wadla district (Ayalew et al. 2002). According to Dereje Ayalew (2003), this rock unit is dominantly porphyritic, which consists of sanidine and anorthoclase, quartz, clinopyroxene, amphibole phenocrysts and ilmenite set in a glassy or fine-grained groundmass with typical eutaxitic textures. As the writer shows, the rock units have higher Th (10–17 ppm) and Nb (73–115 ppm) concentrations, and lower Rb/Nb (0.8–1.3) and La/Nb (0.8–1.2) ratios, which suggest that only limited crustal material was involved in their genesis.

3.3.2 Oligo-Miocene Sequence

The Dessie basalt and Tarmaber Megezez formations are members of this volcanic succession. Their name is adopted from Wolfenden (2003), Zanettin et al., (1974) and Mengesha Tefera et al., (1996) respectively. Dessie basalt formation is associated with different types of aphanatic and porphyritic, massive and vesicular basalts, with subordinates of pyroclasts and ash layers (GSE, 2010). The aphanatic basalts are dominated by fine microcrystalline matrix with fine plagioclase microlites. The porphyritic basalts are varying in composition as olivine bearing basalt, pyroxene rich basalt and plagioclase rich basalt (GSE, 2011). Tarmaber Megezez formation (its age is between early to middle Miocene, ranging from 23 to 11 Ma (e.g., Kieffer et al., 2004)). A peculiar feature of the northern Ethiopian plateau is the frequent occurrence of shield volcanoes, about 30 major centers according to Mohr and Wood (1976), some of which reach as much as 100 km in diameter and 1,000–2,000 m in elevation above the plateau which is close to the volcanic centers (e.g., Semien, Guna, Choke, and Guguftu). The basalt is characterized by medium to coarse grained texture, which is commonly porphyritic with pyroxene and plagioclase phenocrysts and columnarly jointed (GSE, 2010 & 2011). It is also associated with columnarly jointed ignimbrite, which comprises blocky outcrops of ignimbrite containing pumice rock fragments, glass shards and plagioclase phenocrysts.

3.3.3 Late Miocene

The Kemissie and Dalha formations are comprised under late-Miocene volcanic succession. The Kemissie formation has been previously mapped as Kemissie rhyolite formation (Wolfenden, 2003 and Tigel et al., 2009). According to the writers, it is exposed in the central southern part along the western margin of the Afar rift, found usually as discontinuous tectonic blocks bounded by normal slip faults and consists of rhyolite, ignimbrite, tuff and ash with a thickness reaches around 100m. The Dalha formation is exposed in the north eastern corner along the rift floor and it was dated at 8.6 Ma by K-Ar (Varet, 1978 as cited in Mengesha Tefera et al., 1996). It is consisting of fissural basalt, rhyolite flows and some intercalated detrital and lacustrine sediments (GSE, 2011).

3.3.4 Quaternary volcanic

This volcanic succession includes the Adami Basalts, Wederage basalt, Merto rhyolite and some undifferentiated alluvial, elluvial and lacustrine sediments. The Adami unit forms plain and hilly topography and it has tectonic contact with Wederage basalt (GSE, 2010). It is composed of plagioclase, opaque and traces of augite mineral (GSE, 2010). The Wederage basalt is exposed along the western boundary of the rift and it is characterized by dark gray color with aphanatic and fine to medium grained texture (GSE, 2011). Merto rhyolite is patches of an isolated hill found in the Afar rift floor (GSE, 2010). It is characterized as coarse grained, dome forming unit with a composition of alkaline feldspar and vesicles found within the ashy matrix. The last unit under quaternary volcanic succession is undifferentiated alluvial, elluvial and lacustrine sediments, which are exposed in the eastern low land plain and in the central part along the western Afar marginal basin. They are characterized by black cotton and reddish brown silty to sandy soil with few outcrops of diatomite exposed along western marginal basins and on the top of the western plateau and eastern low land plain of the Afar rift floor respectively (GSE, 2010).

3.4. The Intertrappean Beds

The extensive outpouring of the Oligocene Trap basalts over eastern Africa and western Arabia was interrupted by a period of quiescence marked by the deposition of terrestrial sediments so-called intertrappean beds (Abbate et al., 2014). In the Ethiopian highlands and Yemen plateau there are some common intercalations of terrestrial sediments (intertrappean beds) that composed of red clays, sands, diatomites, and lignite seams with volcanic rocks. These intertrappean beds are characterized by relatively limited thickness, averaging a few tens of meters to few hundred meters in graben-related basins. However, in most cases those terrestrial sediments are thin, lens-shaped successions that deposited above the hummocky topography of their volcanic substratum. An average duration of the intertrappean beds is from one to three million years. This time interval is commonly matched by a few tens (or more rarely, hundreds) of meters of sediments left over after erosive episodes or depositional starvation. As the present-day outcrop shows, lateral continuity of those sediments varies from a few tens of kilometers in the Jema valley to a few hundred meters in the Agere Selam (Mekele) area. The age of this intertrappean beds can be

estimated from the age of the hosting Trap succession and by their stratigraphical position that they occupy. This is because the intertrappean beds of Ethiopia that were already studied by many authors are bounded by lower basalt and upper basalt or rhyolite/ignimbrite rock and in some case they intercalated with basalts. The close associations of radiometrically dated nearby volcanic rock with intertrappean beds help to determine the relative age of those terrestrial sediments. Accordingly, the age of the intertrappean beds as mostly encompassed in the interval from 29 to 27 Ma at the transition between the Early and Late Oligocene in the Ethiopia Trap core (Abbate et al., 2014).

In general, the intertrappean sediments are found in different parts of the Ethiopia as well mentioned by previous writer (Abbate et al., 2014). From those entire terrestrial bed outcrops, the Magdala intertrappean sediment is near to Kulfamba area (research area). Therefore, some discussion on intreappean sediment of this locality based on the previous work is needed to get information about the study area. According to Blanford (1870), in the historical locality of Magdala about 60 km southwest of Dessie, approximately 30 m of brown coarse sandstones, whitish and black shale with silicified trunks, alternating with volcanic ashes and basalts along the Jitta creek and within the upper unit of the Trappean Series were described. Hofmann et al., 1997 and Rochette et al., 1998, suggest an approximate age of Mekdela terrestrial sediment, which is between 30 Ma and 28.5 Ma. Its approximate age is estimated from the stratigraphic positions of the intertrappean beds and absolute dating result of Wegel Tena area (30.2 ± 0.1 Ma for the lower basalts and 28.2 ± 0.1 Ma for the upper basalts). Moreover, a rhyolite above the intertrappean sediments has an age of 27.7 ± 1.25 Ma (K/Ar) (Nicoletti and Petrucciani, 1973). The characteristics of the Mekdela terrestrial sediment are somehow similar to that of Kulfamba sediments.

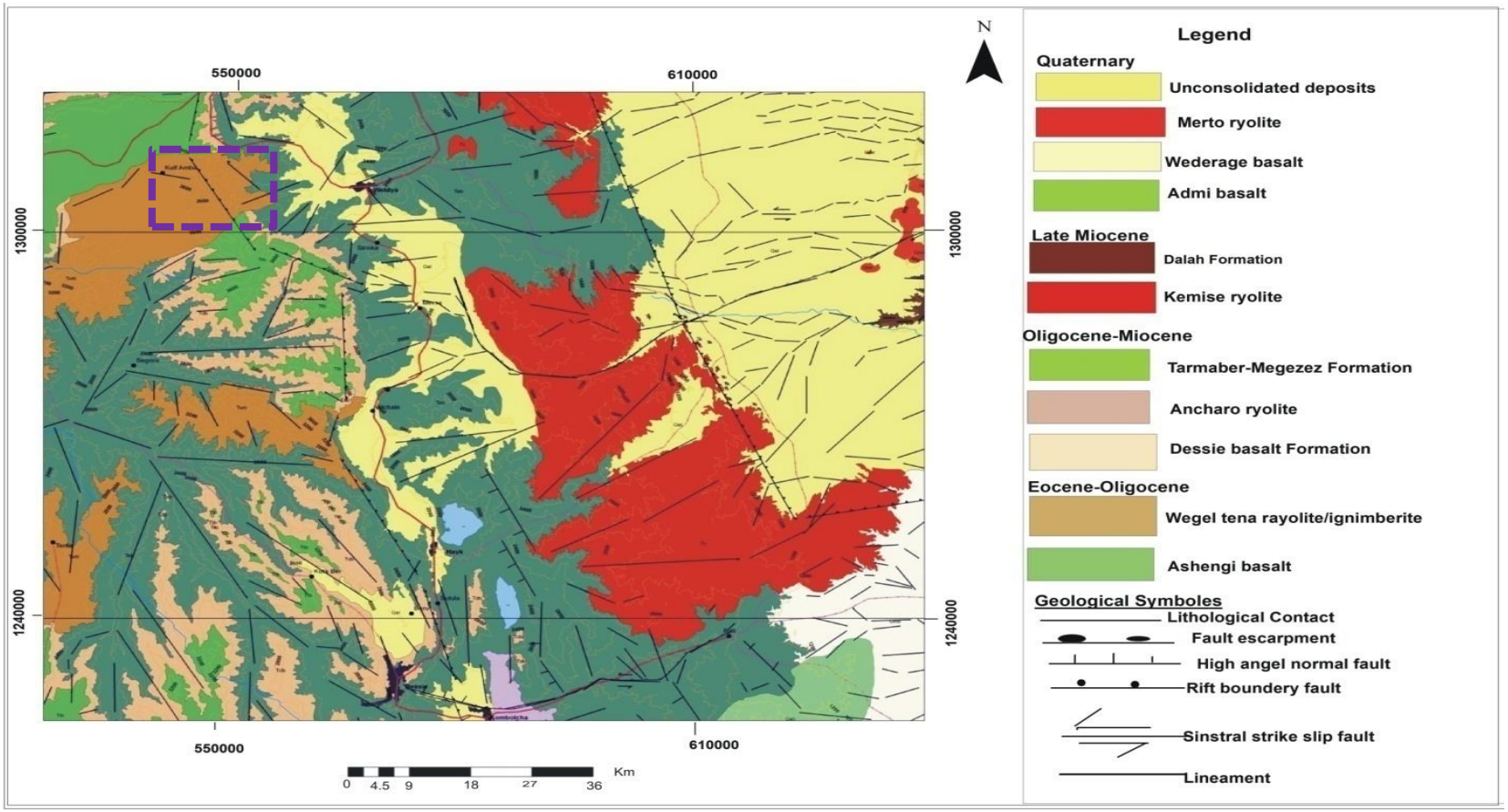

Figure 3.1:- Geological map of Dessie map sheet (GSE, 2010). The study area Kulfamba is included in this map sheet as it showed in violin color rectangle in the top left side of the regional geological map

CHAPTER FOUR

GEOLOGY OF KULFAMBA AREA

4.1 Introduction

The various lithological units in the study area are well exposed by natural events like weathering and erosion activity, river cut and human activities like road cut and quarry site. Since the dominant part of the study area is not covered by vegetation; ridge side, ridge top and hill top exposure are also important sites of rock outcrops. The contacts between lithological units are dominantly sharp contact and clearly visible due to the presence of good exposure. The study area was mapped through field survey and from different tools such as Google earth and Arc GIS. The geology of the area is characterized by an extensive outcrop of volcanic rocks specifically pyroclastic rich igneous rocks, basalt and some intertrappean sediments that host the manganiferous resource. The major lithological units that are found in the study area are listed below based on their relative/stratigraphic age, from the oldest to youngest.

1. Basalt
2. Ignimbrite
3. Mudrock
4. Sandstone
5. Rhyolite
6. Volcanic Glass
7. Agglomeratic Tuff

These rock units are described and mapped according to their lateral contact relationship. Mudrock and other altered pyroclastic materials that are found in different parts of the study area are not mapped in the current scale of mapping. Instead those unmappable rock units are well illustrated and presented in stratigraphic log section (Fig. 4.14). Whereas, the areal distribution of major lithological units such as basalt, ignimbrite/rhyolite, sandstone, volcanic glass, and agglomeratic tuff are presented on the geological map at scale of 1:50,000 scale (Fig. 4.1 A). The rhyolite and ignimbrite rocks are mapped together as ignimbrite unit. This is because the rhyolite

exposure is smaller than that of ignimbrite exposure. However, each of them is described in the coming sections in detail. Different types of structures (both primary and secondary) are also present in the study area. Generally, the detail description of both mappable and unmappable lithological units as well as structures has been presented in the following pages.

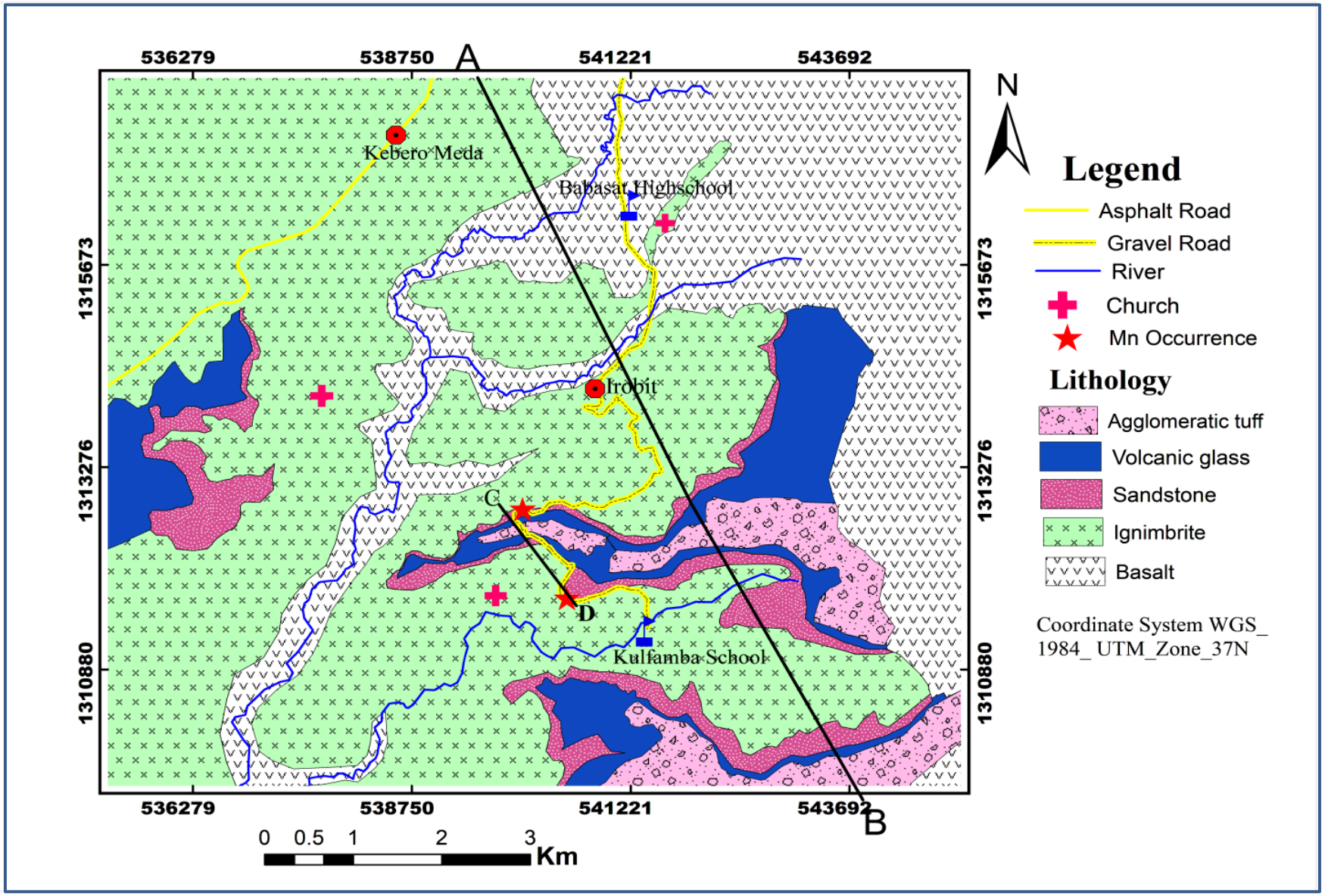
536279
538750
541221
543692
A
B
C
D
1315673
1313276
1310880
Kebero Meda
Babasar Highschool
Irobit
Kulfamba School
N
Legend
Asphalt Road
Gravel Road
River
Church
Mn Occurrence
Lithology
Agglomeratic tuff
Volcanic glass
Sandstone
Ignimbrite
Basalt
Coordinate System WGS_ 1984_ UTM_Zone_37N
0 0.5 1 2 3
Km

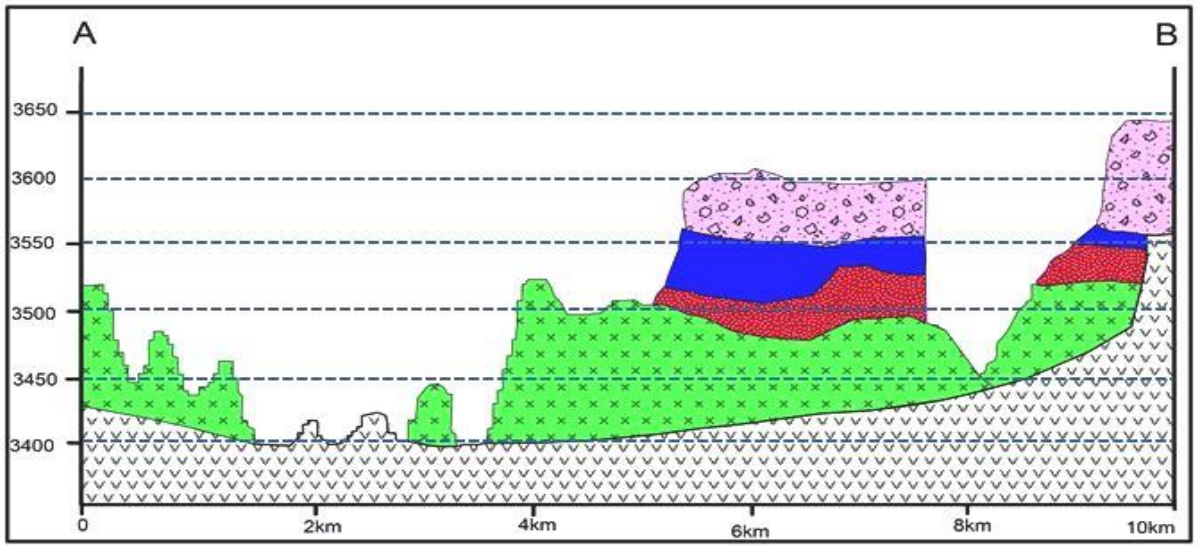

Figure 4.1:- Geological map and cross section of the study area: (A) Geological map, (B) Geological cross section along A-B profiles

4.2 Description of Lithological Units

4.2.1 Aphanetic Basalt

Basalt is one lithological unit that is found in the north and north east part of the study area. Particularly Lam Bochama Ridge including babasat and Alech Ber ridge are covered by this lithologic unit. The basalt is part of trap series/ flood basalt/ that has a large thickness and forms escarpment in the eastern and north eastern direction of the study area particularly towards Dillb and Godgwadit. It is exposed along the road cuts, quarry site and ridge top forming a chain of cliff. It is characterized by a range of colors from dark black to light grey weathered color, dark black fresh color, aphanitic texture and very hard weathering resistant rock. Associated with this unit, deep reddish to brown color, up to half a meter thick paleo-soil is observable at different sites of the study area. As it shown in (Fig. 4.2 A), the paleo-soil is exposed below light grey aphanetic basalt. Petrographic investigation of the analyzed thin sections shows the presence of fine grained identifiable pyroxene, olivine, plagioclase and opaque minerals with indistinguishable fine-grained minerals. The opaque minerals may be Fe - Ti oxide minerals.

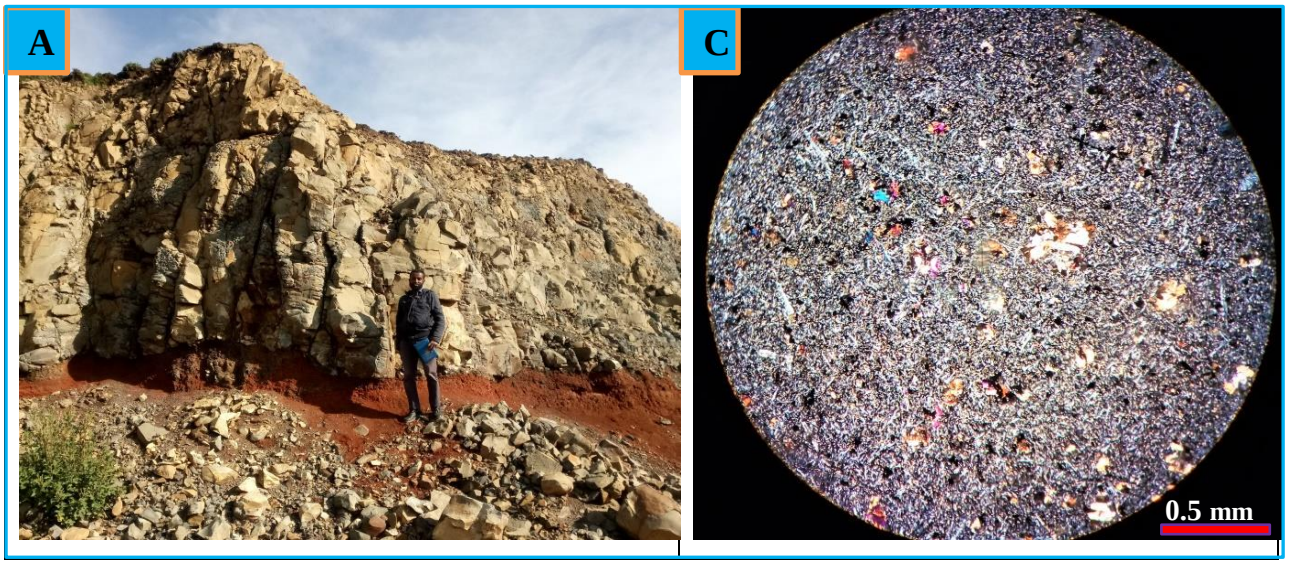

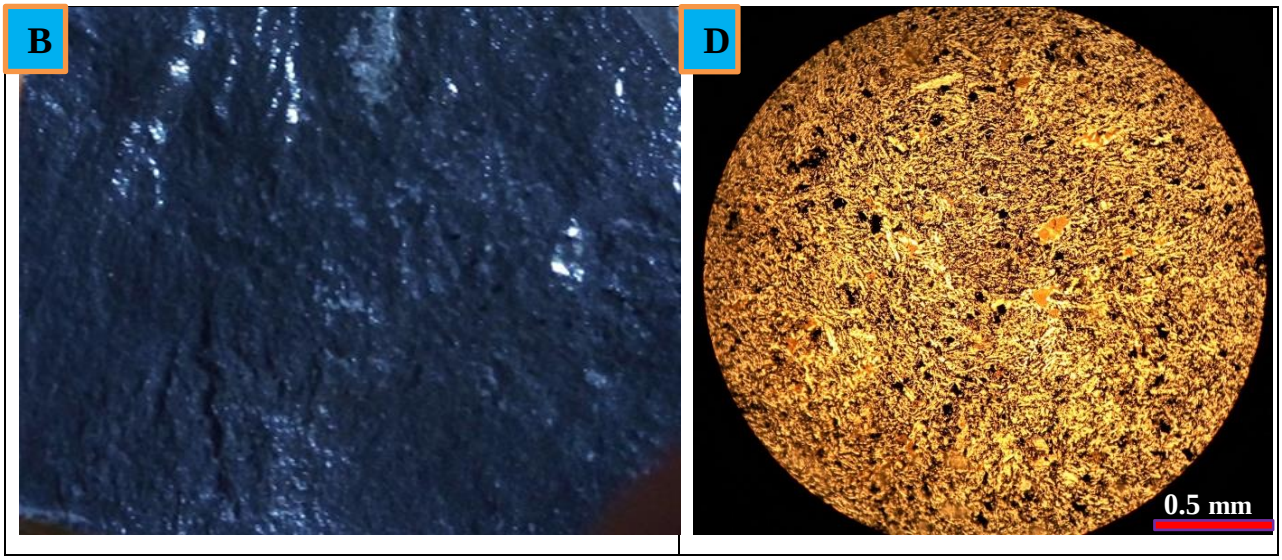

Figure 4.2:- Basalt under exposure level, hand spacemen and microscopic level under XPL and PPL (A, B, C & D) respectively. In the first image (A), deep reddish brown color paleosoil is shown below aphyric basalt. Very fine olivine, pyroxene and plagioclase minerals are visible under microscopic observation.

4.2.2 Ignimbrite

Ignimbrite is the major rock unit found in the southern, south eastern, south western, western and central parts of the study area. It is dominantly exposed by weathering and erosion activity and found above the flood basalt. This ignimbrite has two varieties based on their unique characteristics, time of flow and/or fall and place of exposure as mentioned below.

4.2.2.1 Fine Ignimbrite

This type of ignimbrite forms the lower part of the ignimbrite succession and is directly overlying the trap basalt. It is exposed by hill top and river cut and its thickness is between the ranges of 28 to 35 m. From this thickness, the lower part of the lithology approximately 10 to 12 m fine ignimbrite is highly altered and changed to kaolinite. It is characterized by light grey weathered color, light brown fresh color, presence of visible quartz minerals and some shiny elongated minerals. In addition it is uniquely characterized by presence of small pyroclastic materials/lithic fragments that have different colors (reddish brown and black color).

4.2.2.2 Coarse Ignimbrite

It is the upper part that is found above fine ignimbrite and below sandstone unit. Unlike the first type of ignimbrite, it is characterized by grey to black weathered color, grey fresh color, presence of different size (small to large) elongated pyroclastic materials and visible quartz minerals. Those pyroclastic materials also have different color like white, grey and black color. This type of ignimbrite is relatively lighter in density and broken easily. It is also containing obsidian fragment associated with other lithic fragment and its thickness is in the range between 30 to 34 m. Both ignimbrite verities have been shown in both exposure and hand spacemen level in the given image below (Fig. 4.3).

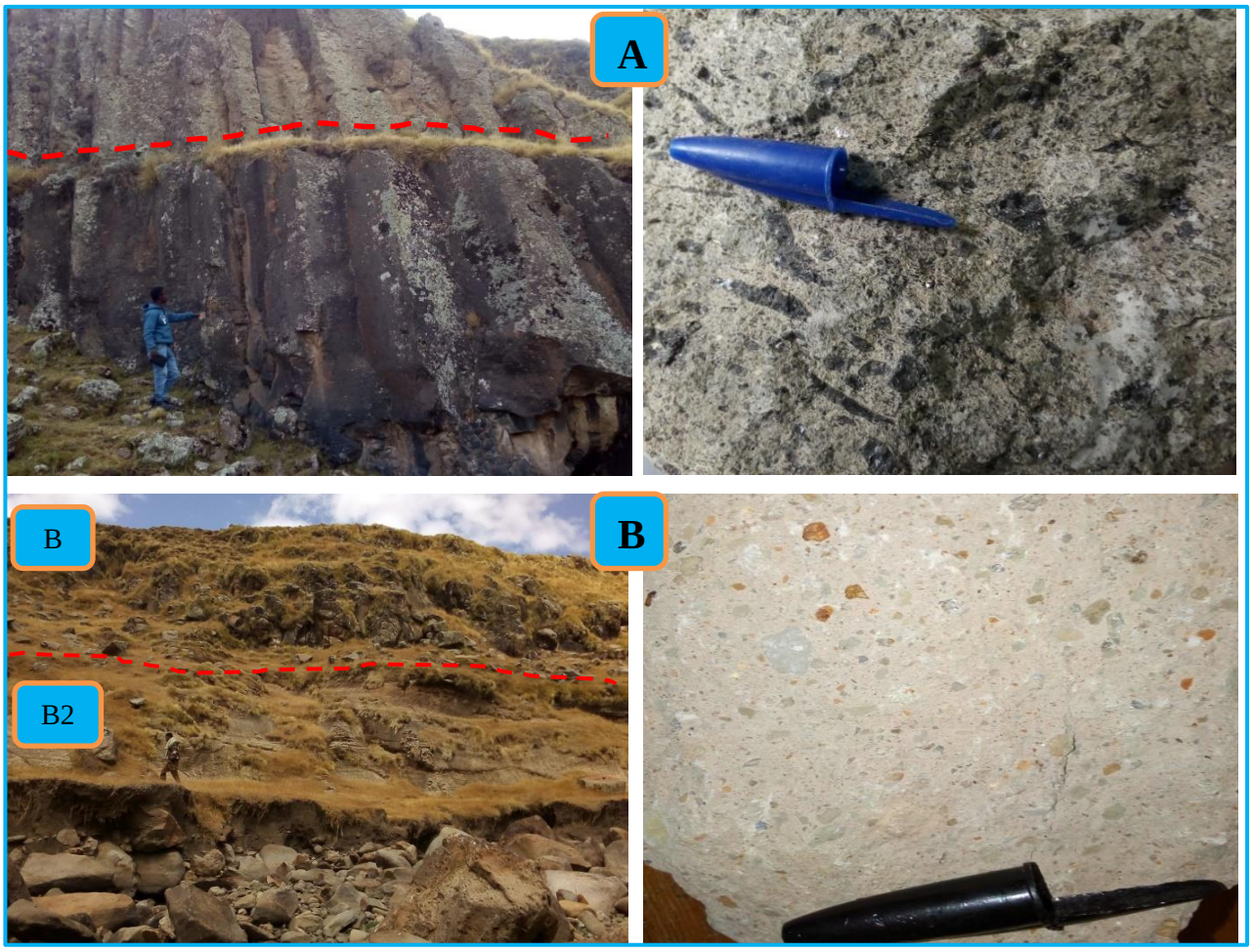

Figure 4.3:- Varieties of Ignimbrite: (A) Coarse ignimbrite in exposure and hand spacemen level, (B) relatively fine ignimbrite in exposure and hand spacemen level- (B1)-less altered fine ignimbrite and (B2)-highly altered fine ignimbrite.

Microscopic examination of this rock shows that the rock is dominantly composed of pyroclastic materials such as ash materials as a ground mass (55%), lithic fragment (25%) and other quartz, feldspar and opaque minerals account the remaining proportion (20%). The rock fragments are large; and dominantly have elongated and irregular shapes as shown in (Fig. 4.4). The quartz mineral is characterized by very small to large crystal development, more transparent and no cleavage as a whole. Whereas, the feldspar mineral exhibits cleavage as shown in (Fig. 4.4 E), and the size of the crystal also varies like quartz. In addition, fine grain opaque minerals that have black to deep red color under XPL and only black color under PPL have been presented (Fig. 4.4 C and D).

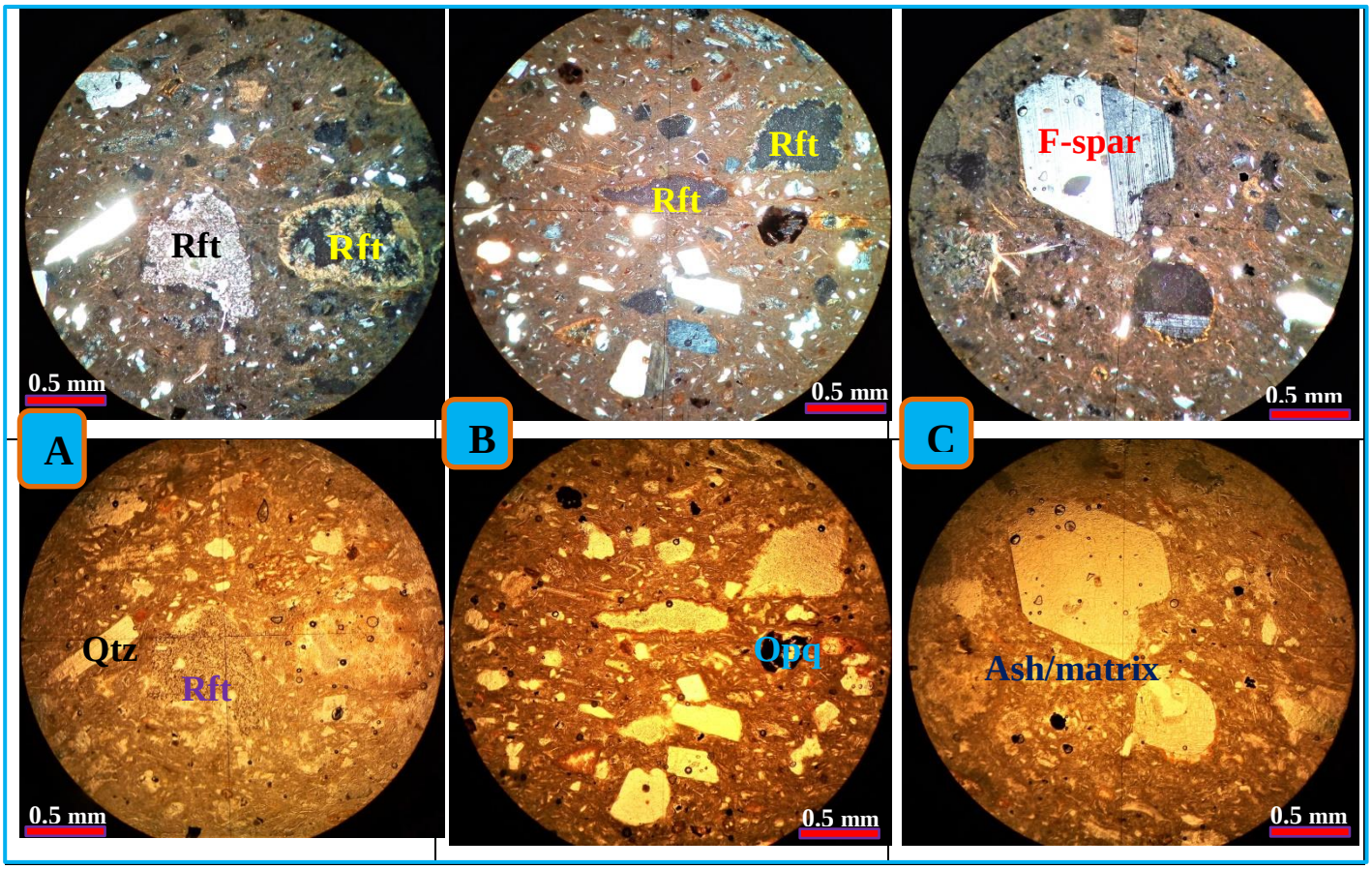

Figure 4.4:- Coarse *ignimbrite* (A) *and fine ignimbrite* (B and C) *under thin section: All photos examined under (XPL on the top and PPL on the bottom) shows welded pyroclastic materials which are composed of variety size fragment (rock -Rft), quartz (Qtz), feldspar (F-spar), opaque (Opq) and fine grain tuff (ash/matrix) materials.*

4.2.3 Mudrock

Mudrock is the general name that can be applied to any indurated sediment made up of silt and/or clay (Boggs, 2014). The mudrock that outcropped in the study area is found below the ore body and above ignimbrite unit. This rock unit is fragile, shows a mud crack structure and it is composed of clay to silt size sediments. Based on field observation, the rock has different physical characteristics in different exposure. For instance, in the north parts of the typical Mn-Fe ore bed; the whitish grey soft mudrock is exposed on the bottom of manganese layer (Fig. 4.5 B). However, in the dominant parts of the study area, reddish to brown color mudrock is outcropped (Fig. 4.5 A). The further description of the mudrock has been presented in the coming chapter.

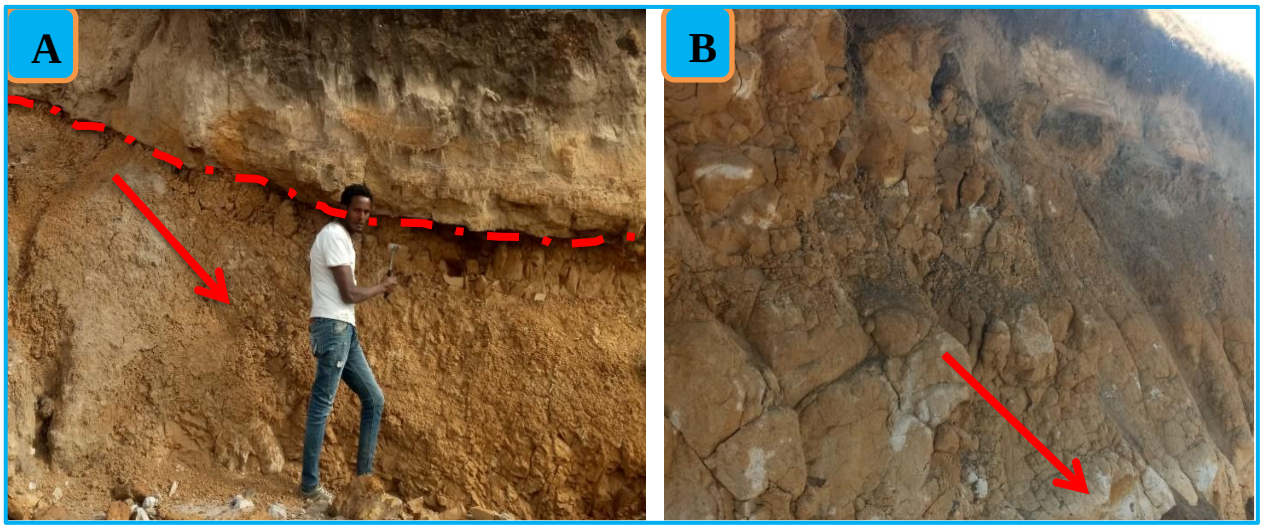

Figure 4.5:- Mudrock immediately below the ore body: *(A) reddish brown clay to silt sized mudrock, (B) whitish to grey color claystone.*

4.2.3 Sandstone

This rock is found in the central, southern, south eastern, western and north western parts of the study area as hill top, ridge side and road cut exposure. It overlies the mudrock and underlined by volcanic glass and rhyolite. It has a sharp contact with the upper and the lower lithologies. It is the host rock for the manganese mineralization in the area. The detail characteristics, petrographic description, proportion and mineral association (both ore and gangue) of this rock

unit are explained in the coming chapter (section 5.3). The sandstone can be classified in to two types based on their degree of compacting; namely compacted and friable sandstone.

4.2.3.1 Compacted sandstone

It is well indurated, less friable and whitish to light gray color. It is found at the bottom of the volcanic glass unit and above the friable sandstone. Its thickness is varying from 24 m in the central part to 52 m in the southern parts of the study area. It is uniquely characterized by the presence of large boulders of sandstone exposure in the central part and highly jointed in the southern part with high joint aperture and spacing reaches to 40 cm and 50 to 60 cm respectively (Fig. 4.11 A). It is also described by the presence of small to very big holes that are exposed on this compacted sandstone unlike the friable one (Fig. 4.6 A). These holes are the result of weathering effect; when rock/lithic fragments and other mineral constitutes are bored and removed by rain fall and other weathering agents leaving behind a hole. Associated with this rock unit, sporadic, chemically precipitated manganese coting and botryoidal/kidney form manganese mineralization are present (Fig. 5.6 G, H and I). Moreover, there are also some manganese veins that are non-systematically oriented on this unit (Fig. 5.6 K and L).

4.2.3.2 Friable sandstone

As the name indicates, it is poorly compacted, friable and purely whitish to light gray rock with average thickness ranges from 8 m to 26 m in the central part. Mostly, it is found at the bottom of highly compacted sandstone and overlies the mudstone. Furthermore, this rock is also found immediately below volcanic glass unit in some exposures and it is the main host rock for manganese ore. In this type of sandstone, some pebble and coble size rock fragments are incorporated with in it (Fig. 4.6 C and D). In general, some field exposure and microscopic observation images of the sandstone are shown in (Fig. 4.6).

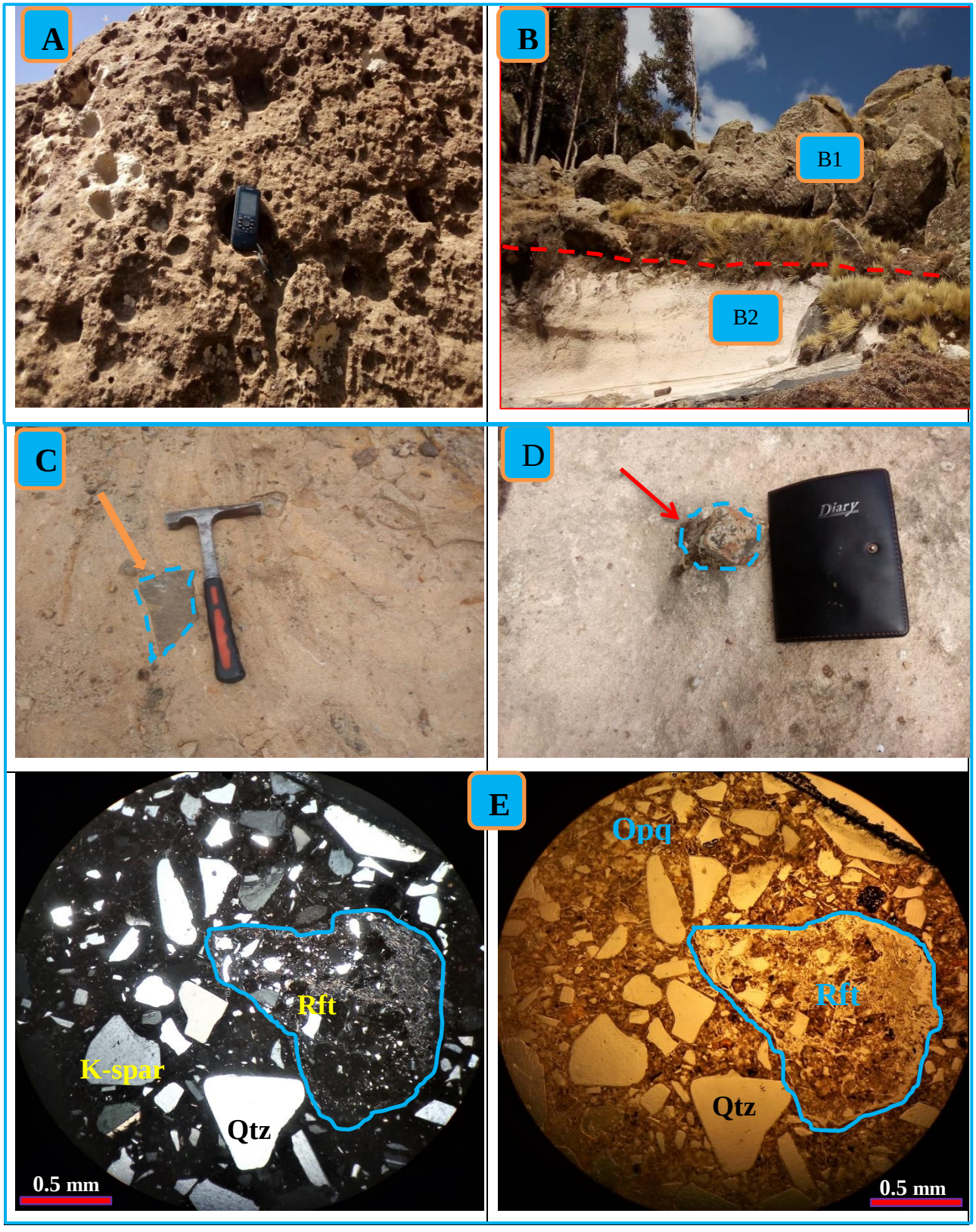
A
B
B1
B2
C
D
Diary
E
Opq
Rft
K-spar
Qtz
0.5 mm
Rft
Qtz
0.5 mm

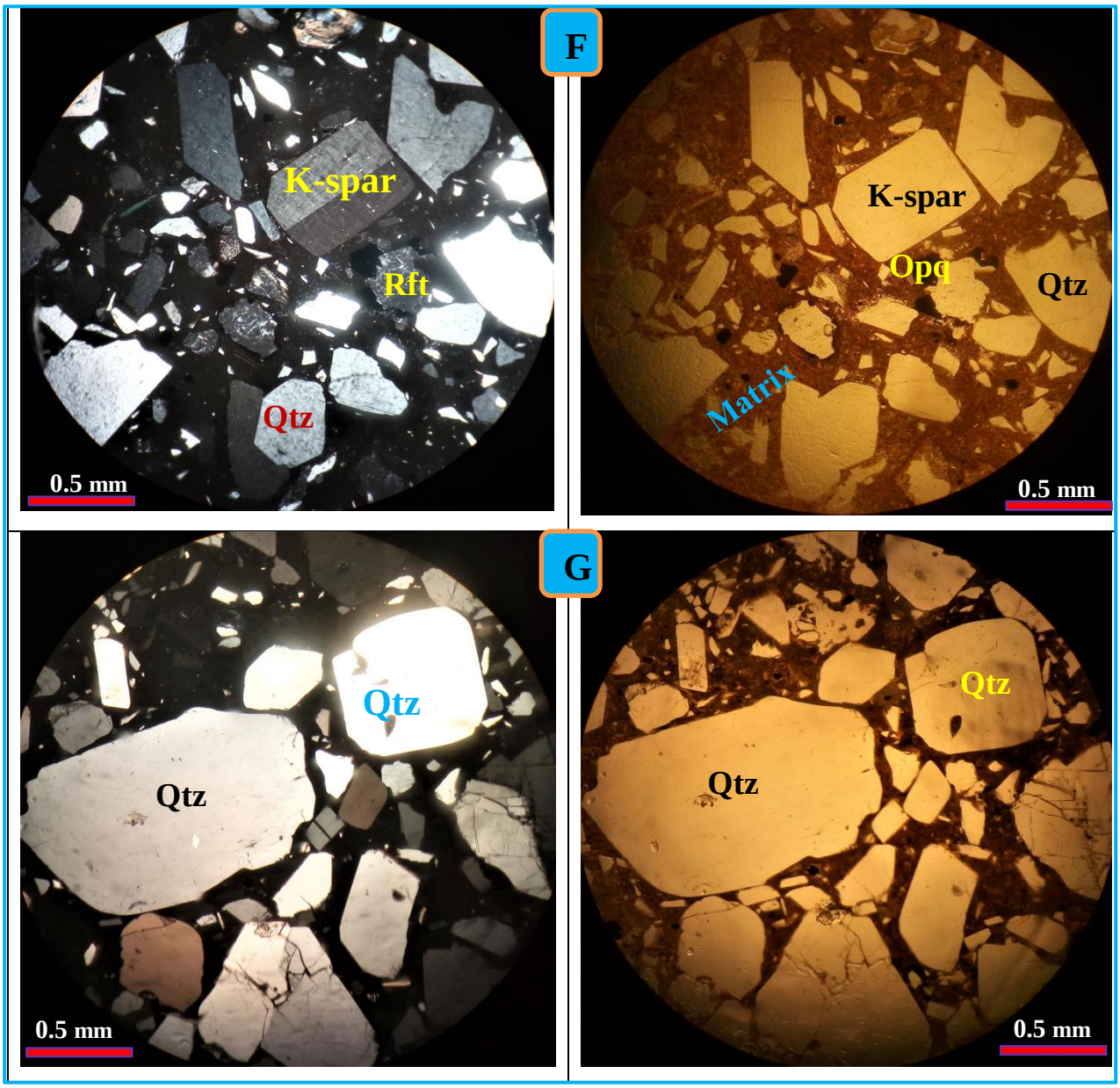

Figure 4.6:- Sandstone under exposure, hand spacemen and microscopic level: (A) Indurated sandstone which is characterized by small to big holes unlike the friable one, (B) Indurated one on the upper part (B1) and white friable sandstone below it (B2), (C, D) the arrow shows pebble to coble size pyroclastic materials incorporated with in friable sandstone rock. The last six images (crossed polarized on the left and plane polarized on the right) show the sandstone consisting of Qtz- quartz, K-spar-potassium feldspar, Opq- opaque, Rft- rock fragment and volcanic ash materials as a matrix with small broken quartz and feldspar minerals.

4.2.5 Rhyolite

Rhyolite is exposed mainly in the western, north western and central parts of the study area as a river cut, road cut, hill top and ridge side exposure. The rhyolite exposed in the western and north western part of the study area is found in two sections and each of them has their own unique characteristics. The lower rhyolite (first one) is found above the coarse ignimbrite unit and below the sandstone unit. It has a clear sharp contact with both lower lithology (ignimbrite) and upper lithology (sandstone) (Fig. 4.7 C). It is fine grained, light gray fresh color, dark gray weathered color, highly compacted, weathering resistant, with massive structure and cliff forming. It has a thickness ranging from 6 to 8 m. The second type of rhyolite (upper rhyolite) overlies the volcanic glass and there is no other lithology above it in that locality. It has a visible sharp contact with the bottom lithological unit. Unlike the first type of rhyolite, it is characterized by the presence of banding, reddish to light pink (both fresh and weathered) color, moderately compacted and its thickness varies from a half meter to 3 m (Fig. 4.7 and 4.10 A). On the other hand, the rhyolite that is exposed in the central parts has a limited extent and is found between sandstone unit (at the bottom) and volcanic glass (at the top). Its banding nature is similar with that of the second type of rhyolite (Fig. 4.7 B). However, it is uniquely characterized by grey weathered color, whitish grey fresh color and presence of small quartz. Moreover, there is highly altered, whitish and fine grain material at the contact between rhyolite and sandstone unit, which may be due to kaolinization (Fig. 4.7 D). Associated with this rock, there is also tiger eye chalcedony which is one variety of chert (Fig. 4.9 B). It has a glassy texture, yellowish to dark brown color, sub-choncohidal fracture and sharp edges when broken by hammer.

Microscopically, reddish to light pink highly banded rhyolite is examined as shown in (Fig. 4.7 E-H) below. Like its exposure and hand spacemen level, its microscopic observation inform that the rock is highly banded, rich in quartz and reddish brown fine materials, and a few opaque minerals. Banding of this rock in both microscopic and exposure level indicates that the rock is formed when a continuous successive lava flows and cools as it in contact with the surface of the earth. Some of the early crystalized quartz minerals block the flow of the lava and it turns the flow toward another direction (Fig. 4.7 E-H). As a result of this, the volcanic rock forms a psido-metamorphic/deformational like features.


A
B
C
Rhyolite
Ignimbrite
D
E
F

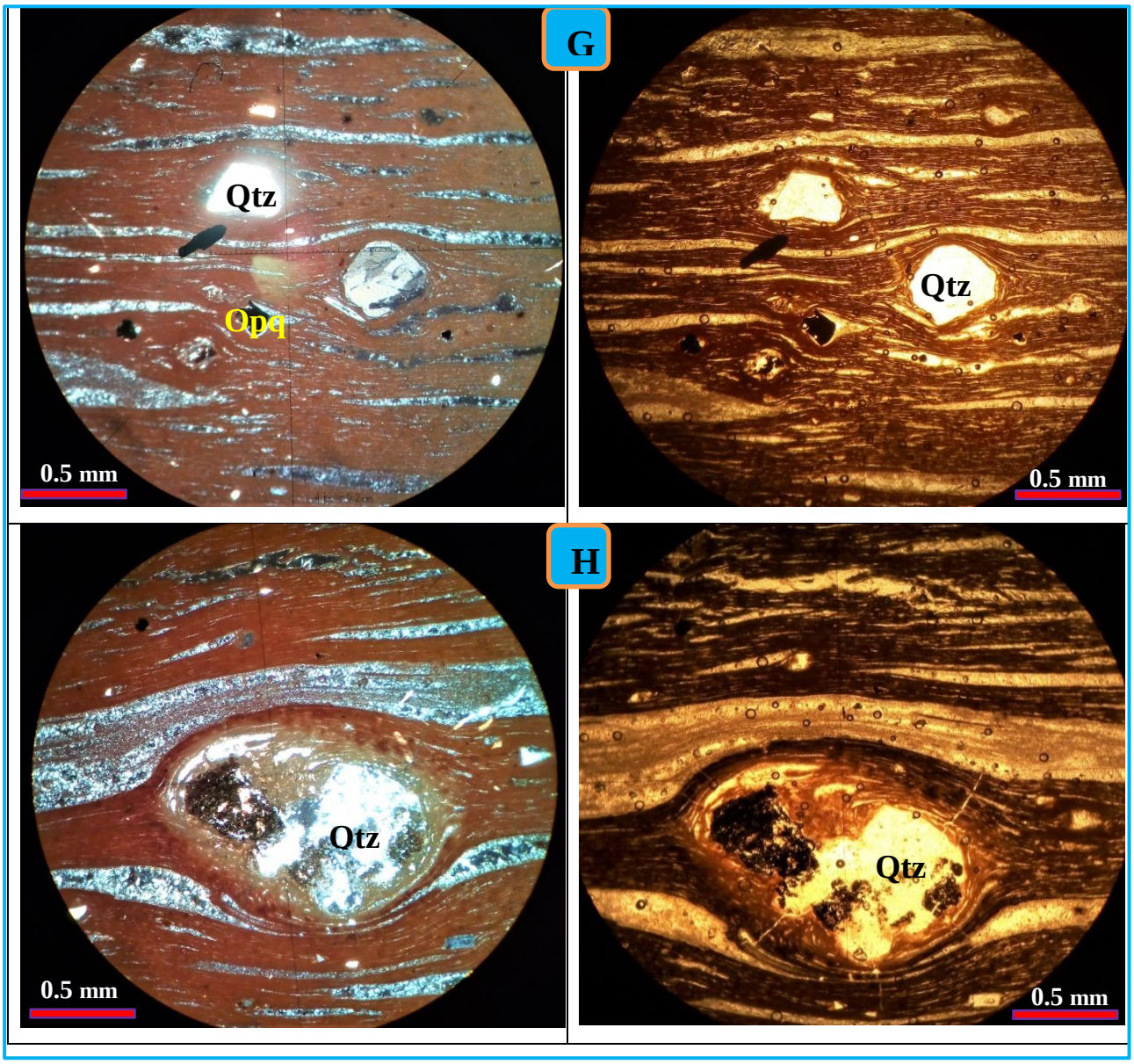

Figure 4.7:- Rhyolite exposures: (A) Highly banded uupper rhyolite that outcrop in the west part of the area (B) moderately banded rhyolite that exposed in the central part of the area (C) lower rhyolite unit immediately above the coarse ignimbrite that exposed near keberomeda and it form columnar like feature, (D) altered rhyolite overlies on the sandstone in the central parts of the area. (E) Alluvial sediments that exposed along river cut, (F) Tiger eye (chalcedony) chert that found associated with rhyolite in the central parts of the area. The last four images (XPL on the left and PPL on the right) exhibit highly banded rhyolite, which is composed of fine grain quartz layers to little medium quartz grain, opaque minerals and reddish to dark brown ground mass.

4.2.6 Volcanic Glass

The volcanic glass is found directly above the sandstone unit and below agglomeratic tuff throughout the study area. In addition, it is outcropped between the lower and upper ignimbrite unit. It is exposed mainly on ridge side, river cut and hill top. It can be described as whitish to black (when weathered), grey to black fresh color, moderate degree of weathering, massive structure, and cliff forming. The composition of this rock is mainly obsidian fragment, some grey pyroclastic materials and light gray to brown color ground mass (Fig. 4.8 A). The sizes of fragments/clasts are varying from tiny/very small (in mm size) to large fragmental size reaching about 10cm in diameter. Average thickness of this lithology varies from 15 m to 25 m. Generally, this unit shows gradational grading from the bottom part towards the top part. That means; there is pure glassy nature rock immediately above the sandstone, then some pyroclastic material with in the glassy rock and finally equal proportion of obsidian fragment with light gray ash materials as a ground mass. In some exposure, it forms a beautiful erosion remnant butte like landform. This is happening when the degree of weathering is high and its top part (agglomratic tuff) is removed and finally the weathering activity reaches to it.

4.2.7 Agglomeratic Tuff

Agglomratic tuff is found in the central, southern, south eastern and eastern parts of study area as hill top, ridge side, ridge top and erosion remnant landforms. This rock unit is crops out on the top of volcanic glass and there is no other lithology above it. Therefore, based on field/stratigraphic observation, it is the youngest lithology found in the research area. It is characterized by presence of different size rock fragments that ranges from few mm to 4 cm in diameter, dark brown weathered and reddish brown to pinkish fresh color, massive with moderate degree of weathering. As it shown in (Fig. 4.8 B), the pebbles to coble size rock fragments have been incorporated within reddish to brown pyroclastic materials. The abundance of large rock fragment in this lithological unit indicates that the source of the pyroclastic magma was very near. Since its top part is not covered by other lithology, it is highly susceptible to weathering and erosion activity. As a result, it is removed by erosion. Its thickness varies from

few meters in highly weathered area to 30 m thick in less affected area. In some exposure, the rock is highly fractured and forms a columnar joint like structure (Fig. 4.8 B).

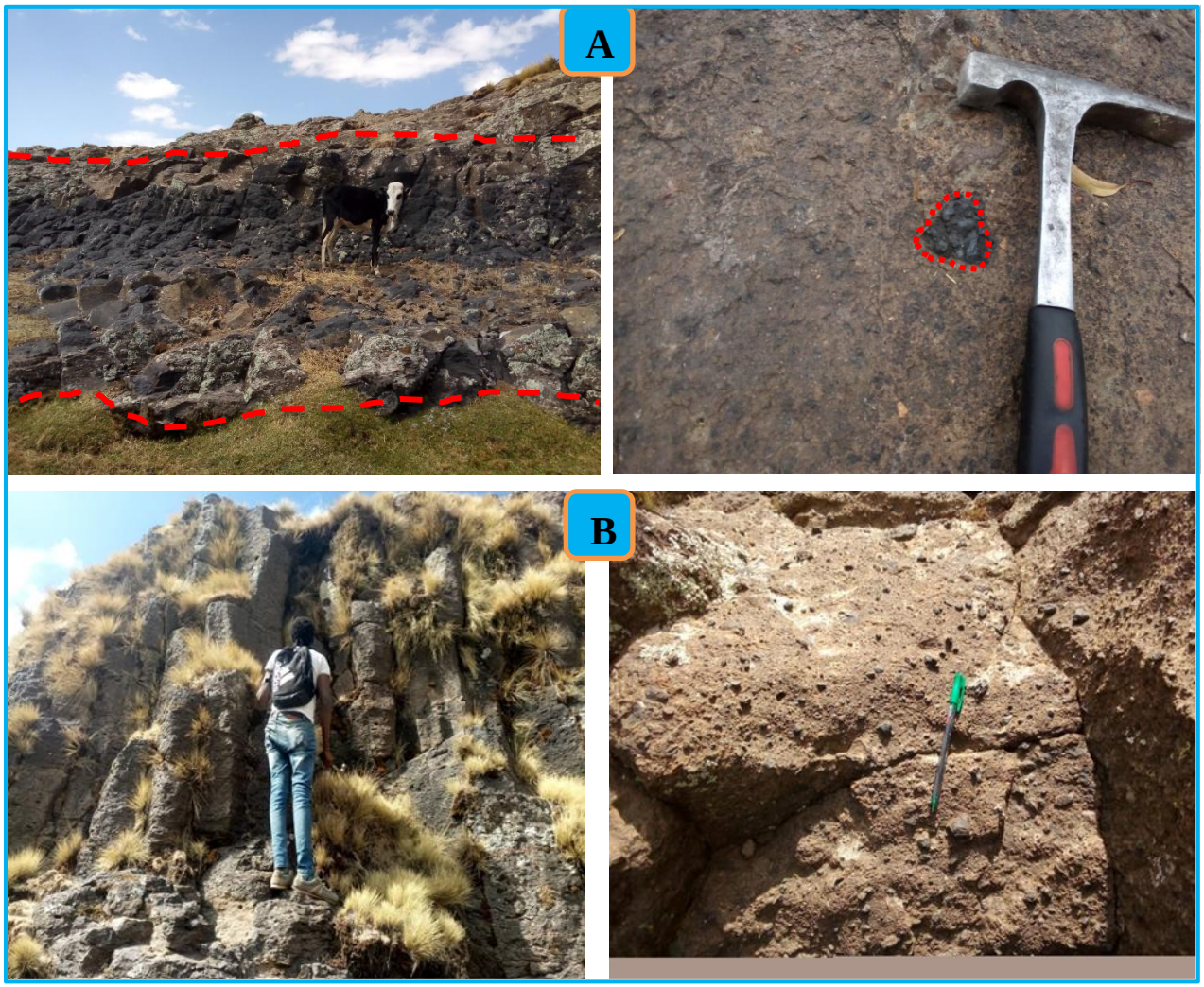

Figure 4.8:- Volcanic glass and agglomeratic tuff in exposure and hand spacemen level: (A) Volcanic glass in exposure (its thickness reaches to 6 m) and hand spacemen level, (B) Agglomeratic tuff in its outcrop and hand spacemen. The left and right image shows their outcrop and hand spacemen level observation respectively.

4.2.8 Alluvial Sediment

The sediments are exposed in the southern parts of the study area lying directly above fine ignimbrite. The sediments have different composition and different size. These alluvial sediments are formed by the intermittent river which flow from the eastern parts (which are

relatively elevated area) that are transported by flash floods during rainy season. The alluviums exhibit almost all types of debris ranging from finer clasts to coble size and very large bolder size (Fig. 4.9 A). The shape of the coble and bolder is from sub rounded to angular shape. This is because; bolder size sediments might not be transported long distance rather the source region should have been near. Its thickness reaches about 2 m.

4.3 Geologic Structures

Structures are visible features that may be observed in all types of rock (in sedimentary, igneous and metamorphic rock). These structures are formed as a result of tectonics and/or other unique processes during the rock formation (for example, sedimentary structure and metamorphic structure- the structures that are limited to a single rock type). In general those structures are formed at the time of rock formation or/and after the formation of the rock. Therefore, the structures that found in the study area can be classified as primary and secondary structures.

4.3.1 Primary structures

Primary structures may be sedimentary or igneous structures that are formed during the deposition of sediments or during the flow and cooling of magma respectively. The primary structures observed in the study area are the following.

4.3.1.1 Flow banding

Flow banding is a geological term to describe bands or layers that can sometimes be seen in rocks formed from molten rock. It is caused by friction of the viscous magma that is in contact with the surface of the earth across the lava is flowing. This structure is a typical and unique feature observed on the rhyolite rock in the study area (Fig. 4.10 A and B). As mentioned on the rhyolite description above, the western and north western upper rhyolite exposure is highly banded.

4.3.1.2 Massive bedding

The term massive bedding is applied to beds of sedimentary rock that contain few or no visible internal lamina and it is most common in sandstones. This bedding structure occurs in the typical manganese ore bed and sandstone unit in the central parts of the study area. As clearly shown in (Fig. 4.10 C and D), there is mudstone at the bottom, then mineralized clay, sandstone, manganese bed and finally sandstone bed.

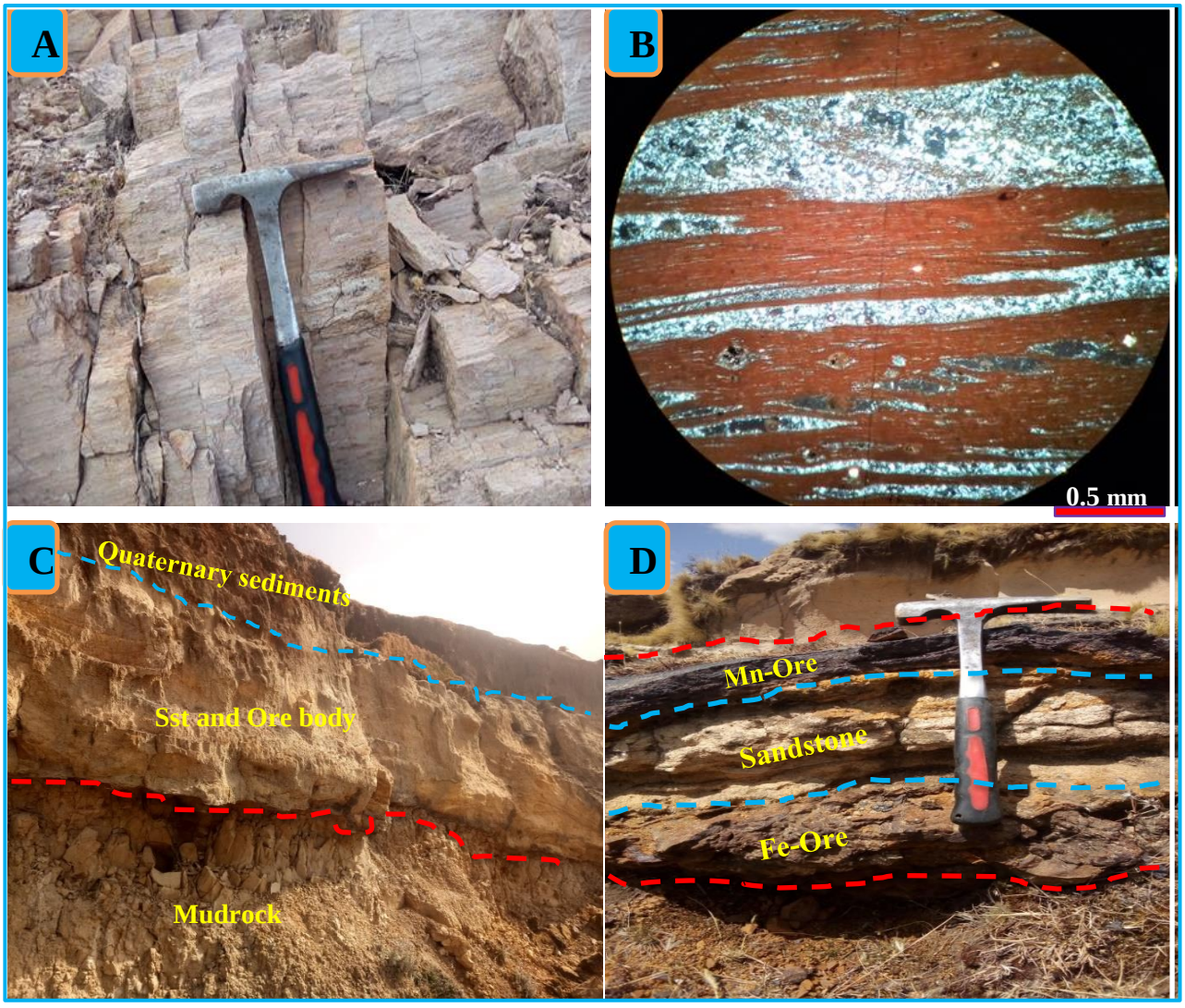

Figure 4.9:- Primary structures: *(A) rhyolite shows flow banding, (B) quartz layering under thin section, (C) massive bedding structure of mudrock at the bottom, sandstone with ore body at the middle and quaternary sediments at the top, (D) the ore body also exhibit a bedding - iron rich bed at the bottom, massive sandstone bed and manganese bed at the top.*

4.3.2 Secondary Structures

Secondary structures are formed after the formation of any types of rock as a result of external force (may be tectonic force or/and surficial activities). Therefore, these structures may be found in any types of rock. Fault, fold, joint, veins, and other erosion remnant structures are good examples of secondary structures. From the different types of secondary structures: - joint, vein, and weathering and erosion remnant structures are present in the present study area.

4.3.2.1 Joint

Joint is a fracture along which no movement has occurred. In Kulfamba, this structure is mainly exposed in volcanic glass, agglomeratic tuff and sandstone unit (Fig. 4.11). The formation of vertical joint on the sandstone unit is unusual; however this structure might be formed as a result of secondary processes like weathering and erosion (Fig. 4.11 A). Highly opened joints (wide aperture) are present in the central and south part of the study area on the volcanic glass and sandstone units. An average aperture of those two lithologies reaches about 40 cm to half meter and their joint spacing is greater than 1 m. Whereas, the aperture and joint spacing in agglomeratic tuff is relatively small, this is between 5 cm to 10 cm and less than 1 m respectively. The agglomeratic tuff exhibits a columnar joint which may expose by weathering and erosion activity (Fig. 4.11 B).

4.3.2.2 Vein

Veins are a distinct sheet like body of crystallized minerals with in a rock. They are formed when a preexisting fracture or fissure within a host rock is filled with hydrothermal fluids. In the study area there is manganese and iron veins that are associated with sandstone unit. The iron veins that are exposed in the western part of the study area are hosted by friable sandstone (Fig. 4.11

F). Whereas, manganese veins that crop out in the central parts of the study area are associated with well indurated sandstone unit (Fig. 4.11 D and E). The thicknesses of the veins are varying from few mm to 15 cm (Fig. 4.11 C and A respectively). In both parts of the study area, the ferromanganese veins are distributed non-systematically.

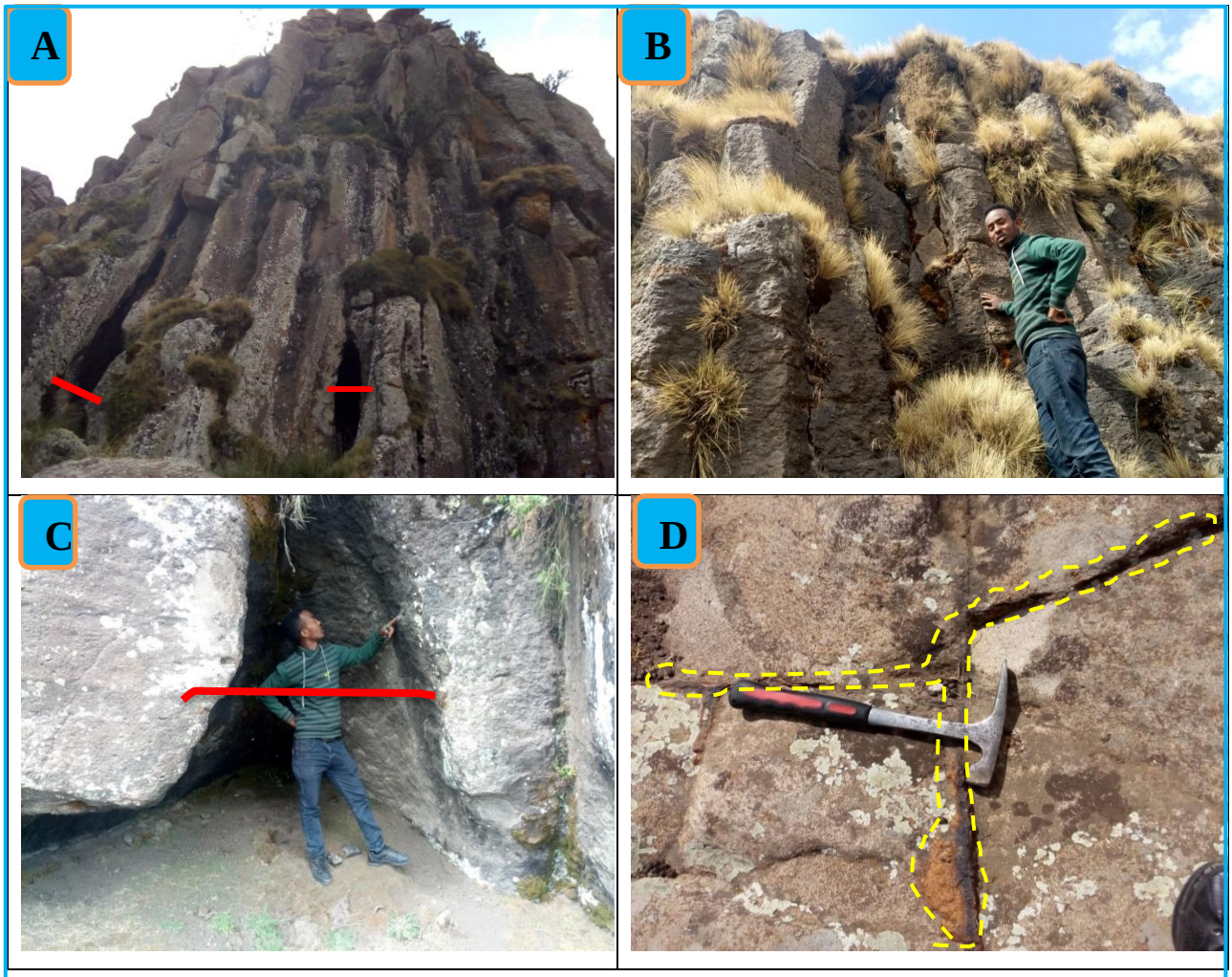

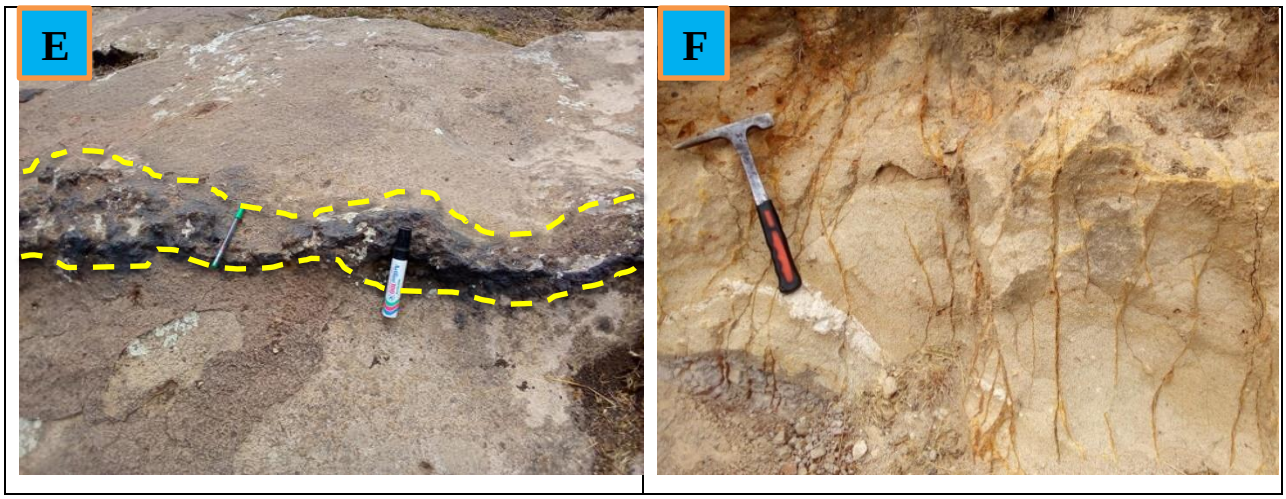

Figure 4.10:- Secondary structures*: (A and B) a vertical joint exposed on the compacted sandstone and agglomeretic tuff unit respectively, (C) very wide joint spacing and aperture on the volcanic glass exposure, (D, E and F) different thicknesses of Mn-Fe veins exposed on the sandstone.*

4.3.2.3 Weathering and Erosion remnant structures

Weathering is the physical breakup (disintegration) and chemical breakdown (decomposition) of material near the earth's surface by both mechanical and chemical processes. On the other hand erosion is the removal of weathered materials. These two processes are the major surficial activities for the formation of various landforms and exposures of different lithological units. As mentioned in before, weathering and erosions are the main activities for the exposure of different rock units in the present study area. On the other side, alteration of felsic igneous rock in to clay minerals (most probably kaolinite) by chemical weathering processes is more prominent in the area (Fig. 4.12 E and F). In general, the following mesa and butte like structures are created on the different lithological units in the area by the above mentioned surficial processes (Fig. 4.12 A-D).


A
B
C
D
E
F

Figure 4.11:- Effect of weathering and erosion on the study area: (A) the sandstone unit on the top parts of ignimbrite-rhyolite exposure in western part of the area, (B, C) agglomeratic tuff exposure on the central and south part of the study area respectively, (D) beautiful rock formation on the volcanic glass rock in the central part. All the first four image shows the different erosion remnant structures which are majorly formed by mechanical weathering and erosion activity. Whereas, the last two image shows (E, F) the effect of chemical weathering on the formation of clay minerals from alteration of felsic igneous rock.

Thickness in meter	*Stratigraphic log section*	*Legend and description of lithology*

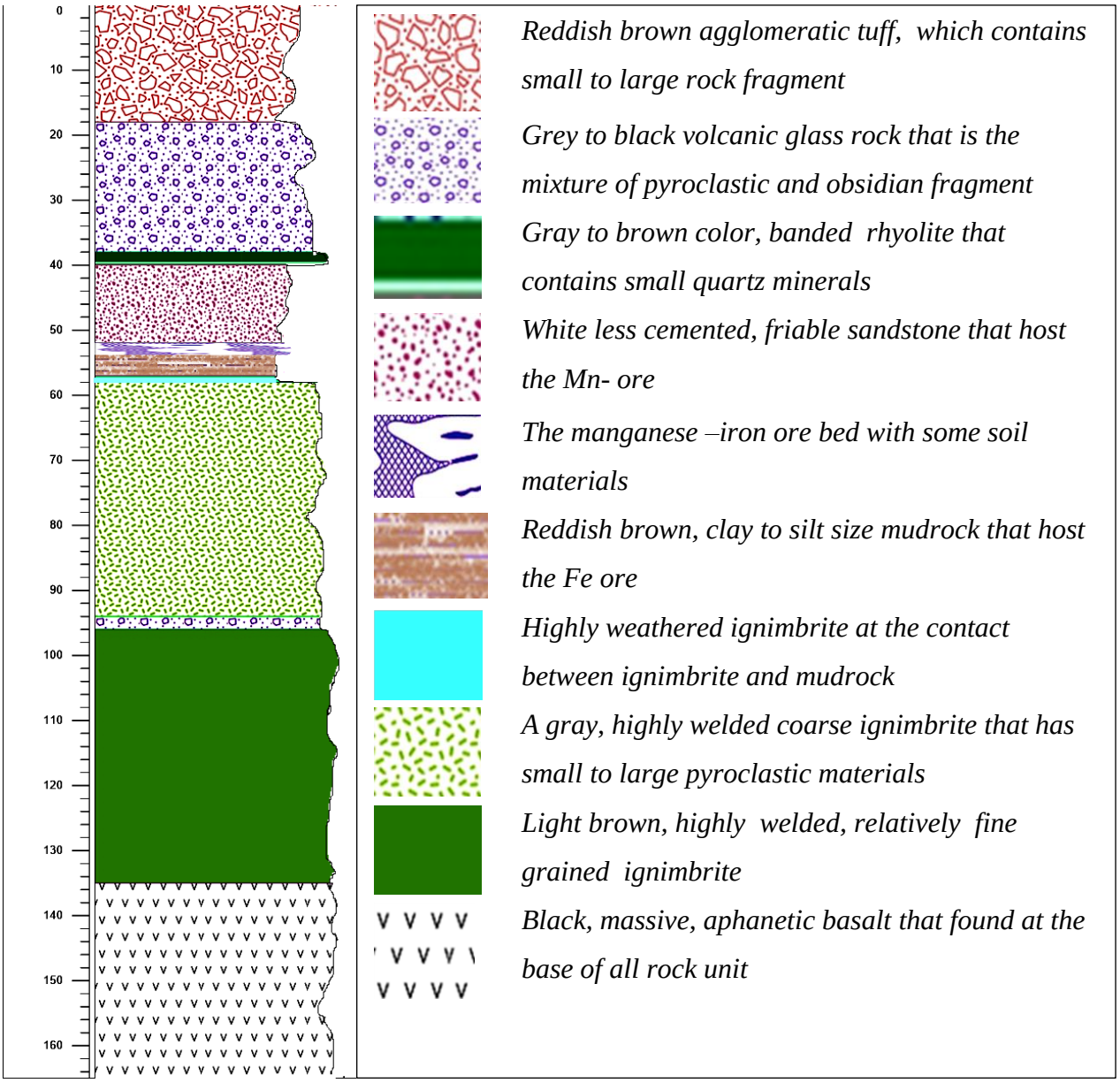

Figure 4.12:- Composite stratigraphy of the study area

CHAPTER FIVE

THE KULFAMBA MANGANESE – IRON OCCURRENCE

5.1 Introduction

The chapter comprises a detail description of the geology of Kulfamba ferromanganese occurrence. It is given in terms of its geological setting, host rocks and types of mineralization in the area.

5.2 Geological Setting

The Kulfamba ferromanganese ore is found within a volcano-sedimentary succession. According to Dereje Ayalew et al. (2001); the Ethiopian Continental Flood Basalt (CFB) province during the early Oligocene (~30 Ma), have covered a large area in Ethiopia that is not less than 750,000 km^2 before erosion with a volume of greater than 3×10^5 km^3. The extensional tectonic settings of continental flood basalt are marked by the presence of bimodal volcanic suites, which contains major sequences of rhyolitic ignimbrites generally found on the top of the flood basalt sequence (bimodal succession). The ignimbrites generally lie directly on the flood basalt sequence, but also occur interbedded with the upper parts of the basalt succession and their overall thickness locally reaches to 700m (Dereje Ayalew et, al; 2003). Similarly, in the research area the resource overlies on the top of very thick trap basalt nearly greater than 900 m and 70 to 80 m ignimbrite unit associated with terrestrial sediment. The trap basalt that is found in the study area is very thick as compared to Wegel Tena and other north western trap basalt and its elevation reaches about 3500m on the top of Dillb area. In general, the terrestrial sediment is underlain by porphyritic ignimbrite unit, which are Oligocene (30.17 +_ 0.54 Ma) in age (Dereje Ayalew et, al; 2003). The overlying volcanic sequence consists of volcanic glass, rhyolite and agglomeratic tuff, which are younger than the terrestrial sediments.

Although the upper basalt is not exposed in the present study area; the back color, very hard, and aphanetic texture basalt is found on the top of upper rhyolite rock around Istayish and other west side of Istayish including Gashena and Wadla-Delanta area. From those localities, the exposure of upper basalt in the west and south west parts of the plateau particularly in Wadla-Delanta-Debre zebit area is very thick (reaches about 160 m locally) as compared to the other parts of the plateau. Therefore, the lithological exposure in those neighbor localities indicates that, the upper basalt is

the youngest rock on the plateau. Starting from this regional field observation, the basalt could be parts of trap which might be formed at the last stage of the trap formation. Accordingly, the volcano sedimentary basin (sandstone and mudstone) that is found in the study area are most probably parts of intertrappean sediment. The Ethiopian highland is characterized by presence of some common intercalations of intertrappean beds composed of red clays, sands, diatomites, and lignite seams with volcanic rocks (Abbate et al. 2014). The age of these terrestrial beds can be estimated from the age of the hosting trap succession, nearby dated volcanic rock and by their stratigraphical position they occupy. This is because the intertrappean beds are bounded by lower basalt and upper basalt or rhyolite/ignimbrite rock and in some case they are intercalated with basalts. For instance, the approximate age of Mekdella terrestrial sediments that are determined by Hofmann et al. (1997) is between 30 Ma and 28.5 Ma. This age determination was stated from the stratigraphic positions of the intertrappean beds and absolute dating result of Wegel Tena area, which is 30.2 ± 0.1 Ma (40Ar–39Ar) for the lower basalts, and 28.2 ± 0.1 Ma (40Ar–39Ar) for the upper basalts. Moreover, a rhyolite above the intertrappean sediments has an age of 27.7 ± 1.25 Ma (K/Ar) (Nicoletti and Petrucciani, 1973). However, the present study area terrestrial sediment exposure is somewhat different from the other localities. Unlike the previous intertrappean beds, the kulfamba terrestrial sediment that host ferromanganese ore is found above the rhyolite (ignimbrite) and below other upper volcanic rocks. Moreover, those upper volcanic rocks are found below the shield volcano in the regional exposure. Accordingly, the relative age of the ferromanganese host rocks (research area sediments) is probably between 27.7 ± 1.25 Ma (K/Ar) from (Nicoletti and Petrucciani, 1973) and 23.03 Ma (starting age of shield volcano). However, in order to clearly define the exact ages of the volcanic rocks that found above the sandstone unit (rhyolite and upper basalt), absolute dating should be done.

Generally, the geology of the present study area is characterized by volcanic rocks such as basalt, ignimbrite, volcanic glass, rhyolite and agglomeratic tuff with some terrestrial sediment like sandstone and mudrock.

5.3 Description of Manganese - Iron Occurrence

5.3.1 Host rock

The resource is bounded by mudrock at its lower part and sandstone in the upper part. As a result, it is better to describe both lithologies as a host rock. Specifically, the lower parts of the ore body (iron rich bed) is associated with the muddy material, whereas the upper parts of the ore body (manganese rich bed) is hosted by sandstone. The examination of the sandstone and resource is supported by field observations and petrographic analysis.

5.3.1.1 Sandstone

The sandstones are mainly consist of framework grains ranging in size from 1/16 to 2 mm, various amounts of cement and very fine size (<-0.03 mm) matrix materials, which are present within interstitial pore space among the framework grains (Boggs, 2014). As mentioned before, the sandstone unit is one of the ore-bearing rocks and has two varieties, the lower friable and upper well indurated sandstone. It is characterized by medium to coarse grained, whitish to light gray fresh color, dark grey weathered color, massive, feldspar and quartz rich (Fig. 5.3). The constituent quartz and feldspar minerals exhibit a well-developed crystal form (octahedral and rhombic) in hand spacemen. It is also characterized by presence of differently sized pyroclastic materials, and its ground mass (matrix) is whitish to brownish grey tuff/ash materials. The size of these pyroclastic materials ranges from mm to large reaching up to 5-10 cm in diameter as shown in (Fig. 4.6 C and D). Those lithic and rock fragments are dominantly rhyolite, ignimbrite and volcanic glass fragments. The presence of these pyroclastic materials (rock fragment and ash) with in the sandstone gives insight the most probable provenance of the host rock, which is the early formed pyroclastic rock.

In addition, the presence of those rock/lithic fragments, sub angular to angular mineral grains, poorly sorted grains and more feldspar minerals in the rock tells the distance of transportation or/and the approximate location of source rock. Accordingly, the source rock was near to the depositional environment, it may happen in high relief region where rapid erosion is found. As a result of this, the transportation was so restricted and the duration time to decompose feldspar will be limited.

The sandstone that found in the study area has no any prominent sedimentary structure like cross bedding and ripple mark. This is also related with the concept of restricted transportation and environment of deposition. The absence of those sedimentary structures in the ore bearing rock is a

typical characteristic of immature sandstones with no appreciable distance of transportation (Boggs, 2014). The thickness of this rock unit is varying from 8 m to 52 m. This thickness variation may be as a result of paleo-morphological effects during the deposition of sandstone. Since surficial process such as weathering and erosion were prominent activities in the area, more than half parts of the sandstone unit is taken away (see the geological map of the study area). As a result, in deeply eroded parts toward the north east, north and south west parts of the study area the sandstone is not present. While, in less eroded area the sandstone is found.

Microscopic study of the host rock shows that, the rock is composed of quartz, feldspar, rock fragment and tuff/ash materials (matrix) with some opaque minerals. The proportions of the constituent materials can be determined by point counting and visual observation methods. Although the point counting methods help to determine the proportion of framework minerals in sandstone, visual observation method was more preferable and used in the present study. This is because; the constituent framework grains were poorly sorted (some framework mineral grains are very big as compared to the other).

In order to determine the modal composition of the constituent minerals and understand the unique features of those minerals, six thin sections were prepared from unmineralized sandstone and one thin section from mineralized sandstone (Fig. 5.4 and 5.5 respectively). Based on thin section observation (twelve fields of view for each thin section), the mineralogical composition of the host rock (sandstone) is determined as it shown in Table 5.1. In average it is composed of 30% of quartz, 26% of feldspar, 28% of matrix, 16% rock fragment, and few opaque minerals. The rock is characterized by a dark gray appearance under XPL, light brown color under PPL, sub rounded to angular and poorly sorted minerals grains, and high matrix content (fine grain tuffaceous materials) with broken feldspar and quartz minerals (Fig. 5.4 A-F).

The feldspar minerals have a tabular/flattened crystal habit, from this sanidine exhibit a Carlsbad twining (Fig. 4.6 F, 5.4 B and D). There are also untwined feldspar minerals (might be orthoclase and plagioclase feldspars) that have tabular and irregularly shaped (Fig. 5.4 E and F). Although this feldspar is untwined, it shows a one set of cleavage. It is an important characteristic of feldspar to differentiate it from quartz, since quartz did not show cleavage. The feldspar minerals have gray, light gray and pinkish to gray color, however in some extent they have very similar color with

quartz. The quartz mineral dominantly occur as a single (monocrystalline) grains and it has a white color and various forms. For instance, a heptagonal to octagonal crystal form of quartz grain minerals has been shown in (Fig. 5.4 A). It displays sweeping of extinction as the stage is rotated; this property is called undulatory extinction. Both feldspars and quartz minerals exhibit similar color (light white color) and have low relief under plane polarizer light. These two minerals are sub rounded to sub angular, fresh and less fractured in the less mineralized sandstone observation (Fig. 5.4 A and D). On contrary, in mineralized sandstone the two minerals are highly fractured and their fracture is filled by manganese and iron ore (Fig. 5.5 A-C). From the two, feldspar is highly fractured and dissected by later coming micro veins. Likewise, the rock fragments have been observed clearly under microscopic observation (Fig. 4.6 E and 5.4 C). It is characterized by presence of different size and dark grey color under XPL and PPL observation. The opaque minerals have been also observed associated with those framework grains. Those opaque minerals have dark to reddish brown color (Fig. 5.4 E).

The thin section observation could tell the compositional and textural maturity of the sandstone. According to Boggs (2014), the term maturity refers to the relative abundance of stable and unstable framework grains in sandstone (compositional maturity); and the relative abundance of matrix and degree of rounding and sorting of framework grains (textural maturity). Accordingly, in the thin section observation of the present study, the feldspar and ground mass (ash) materials are dominant over the quartz mineral, which is compositionally immature (Table 5.1). Similarly, the sandstone is ash rich and its mineral grains are poorly sorted and poorly rounded, which is texturally immature (Fig. 5.4). Therefore, starting from field observation (the presence of irregularly shaped, large pyroclastic materials, poor degree of sorting and absence of those typical sandstone structures) and microscopic examination (all the above mentioned characteristics) tells about the immaturity of the sandstone.

5.3.1.1.1 Classification of Sandstone

The classifications of sandstones are important and useful, not only for communication but also for organization of thought; a good classification can help reveal underlying regularities that need to be

explained. Accordingly, there are many different kinds of geochemical and mineralogical classification of sandstone (Klein, 1963; Okada, 1971; Pettijohn et al., 1972; Yanov, 1978; Herron, 1988 and Boggs, 2014). Most mineralogical classifications of the sandstone use a classification scheme that involves a QFR or QFL plot. These plots are triangular diagrams on which quartz (Q), feldspars (F), and rock fragments (R or L) are plotted as end members at the poles of the classification triangle. There are numerous possible ways that such a triangle can be subdivided into classification fields.

In the present study, Folk and Pettijohn sandstone classifications systems were used. The recalculated framework composition is used for classification of sandstone after (Folk, 1980). This classification system is based on only three framework minerals (QFR), but not including the matrix as it shown in (Fig. 5.1 B). As a result the ternary QFR plot exhibits that the investigated Kulfamba sandstone samples are classified as arkose and lithic arkose type. The next classification system is more descriptive than the others and it is the most widely used classification system. Accordingly, the classification of the present sandstones is fundamentally based on framework mineralogy (quartz, feldspar and rock fragment) and relative abundance of matrix; which is based on (Pettijohn, 1975). In this classification, sandstones that are effectively free of matrix (<5 percent) are classified as arenites (quartz, feldspathic or lithic) depending upon the relative abundance of QFL constituents. If matrix can be recognized (>5), the terms quartz wacke, feldspathic wacke, and lithic wacke are used instead. Consequently, the plotted diagram shows that the investigated sandstone samples are classified as feldspathic and lithic greywacke (Fig. 5.1 A).

The mineralogical classification is also consistent within the geochemical classification data. Pettijohn et al. (1972) and Herron (1988) proposed diagrams to classify the sedimentary rocks on the basis of major oxides. Based on the geochemical classification diagram of Pettijohn et al. (1972), the analyzed samples of Kulfamba sandstone are classified as arkose, litharenite and greywacke (Fig. 5.2 A & B). Similarly in the geochemical classification diagram of Herron (1988), the analyzed sandstones are plotted in subarkose and sublitharenite field (Fig. 5.2 C). The detail description and interpretation of this geochemical data of the sandstones are shown in the coming chapter of last section.

Table 5.1: Recalculated framework grains and matrix of the Kulfamba sandstone, North Wollo, Ethiopia

Sample No	Q	F	R	M

KA01-A	28	30	12	30
KA01-B	30	25	10	35
KA-13	30	28	14	28
KA-14	34	20	22	26
KA-21	28	32	10	30
WG-4	30	20	28	22
Average	30	26	16	28

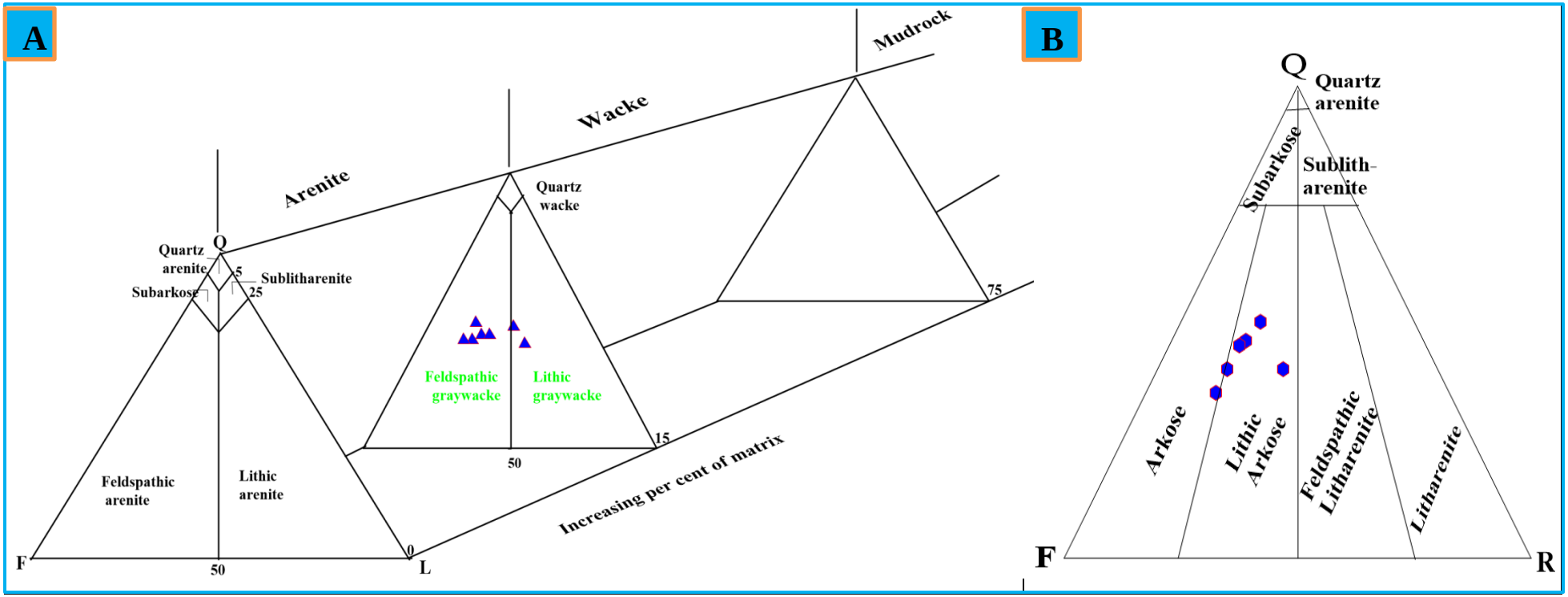

Figure 5.1:- Mineralogical classification of Kulfamba sandstone: (A) after Pettijohn (1972), which is based on framework mineralogy (Q- Quartz, F- Feldspar (potassium + plagioclase) and R or L- Rock/lithic fragment) and matrix/ground mass, (B) Folk (1980), which is based on only framework mineralogy (Q-F-R).

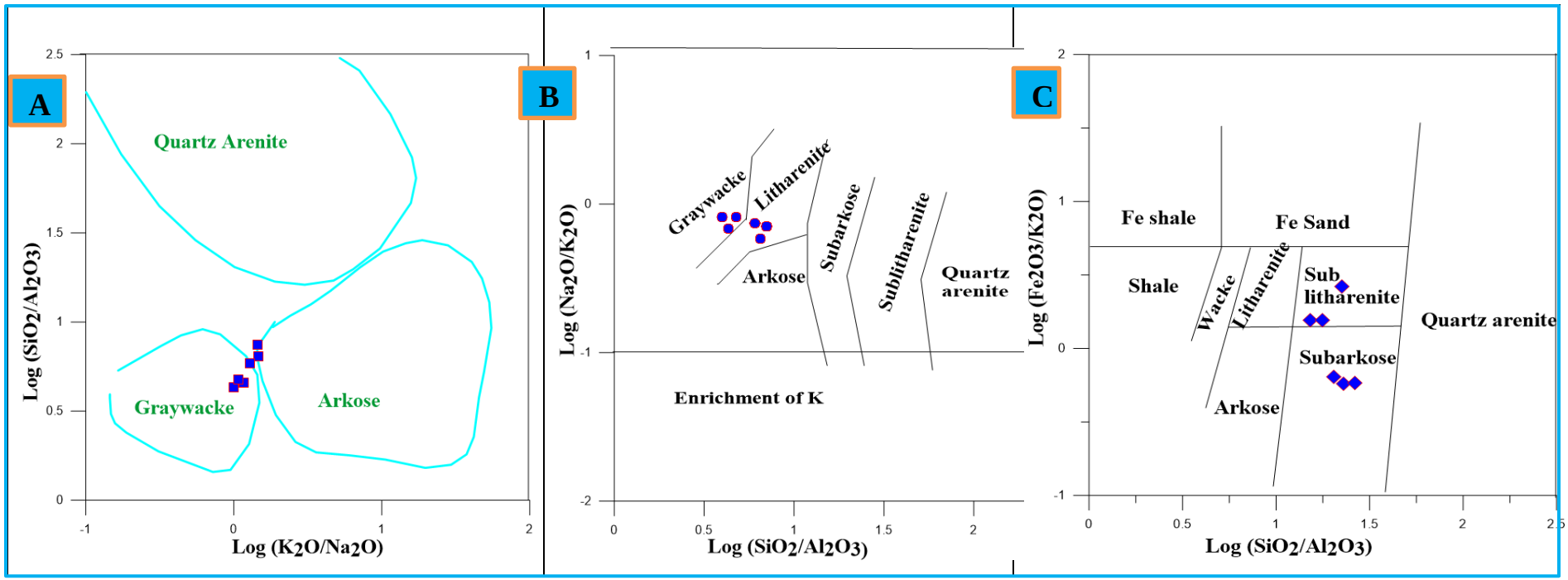

Figure 5.2:- Geochemical classification of Kulfamba sandstone: (A) Log (K_2O/Na_2O) vs. Log (SiO_2/Al_2O_3) classification after Pettijohn et al., (1972), (B) Log (SiO_2/Al_2O_3) vs. Log (Na_2O/K_2O) diagram of Pettijohn et al., (1972) and (C) the Log (SiO_2/Al_2O_3) vs. Log (Fe2O3/K2O) diagram of Herron (1988).

5.3.1.2 Mudrock

In addition to sandstone, the mudrock is found immediately below the Mn-Fe ore body and above ignimbrite. The contact between this mudrock and the underlying ignimbrite is marked by a white, highly altered pyroclastic tuff up to 1m thickness. At different exposure the thickness of this rock varies from 80 cm to 5 m. This rock can be classified as claystone and siltstone based on their grain size and color observation on the field. The Claystone is characterized by massive, white color, very fine grain, smooth, and soft materials that may reach about 2 m thick. It is localized in the northern parts of the study area. The next type of mudrock is silt sized consolidated material which is siltstone. It is distinguished from claystone by reddish brown color, rough and its silt size texture. Its thickness is varying from few centimeters in typical Mn-Fe layer to 5 m near to Kulfamba Medhanialem. It is relatively the dominant mudrock and it hosts the lower parts of the ore body or iron dominated ore (Fig. 5.3 A).

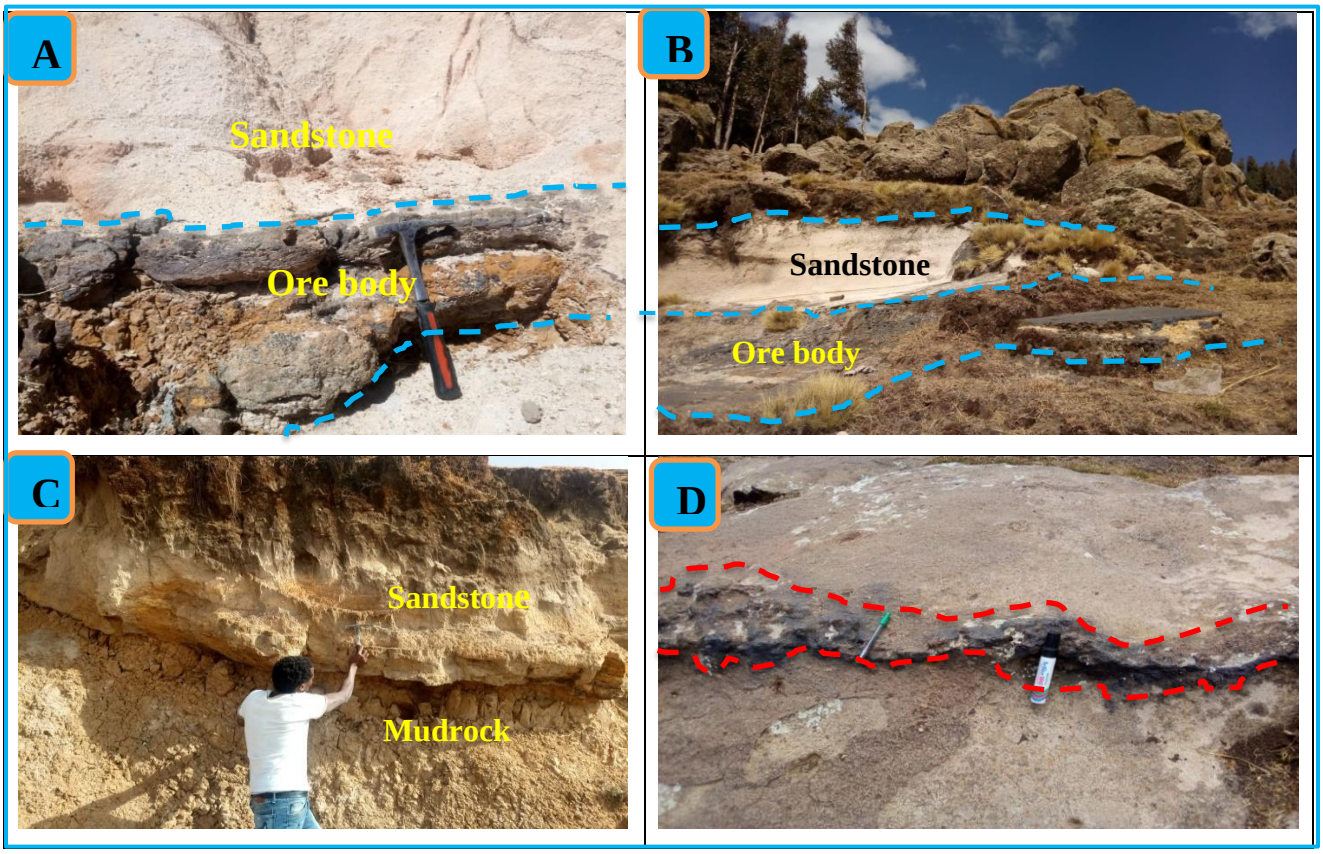

Figure 5.3:- Host rocks of the ore body: (A) Mn-Fe ore bed bounded by sandstone and mudrock, (B) Well indurated sandstone overlies on friable sandstone in the central parts of the area, (C) Mn-Fe ore body between sandstone and mudrock, (D) well indurated sandstone that host manganese vein.

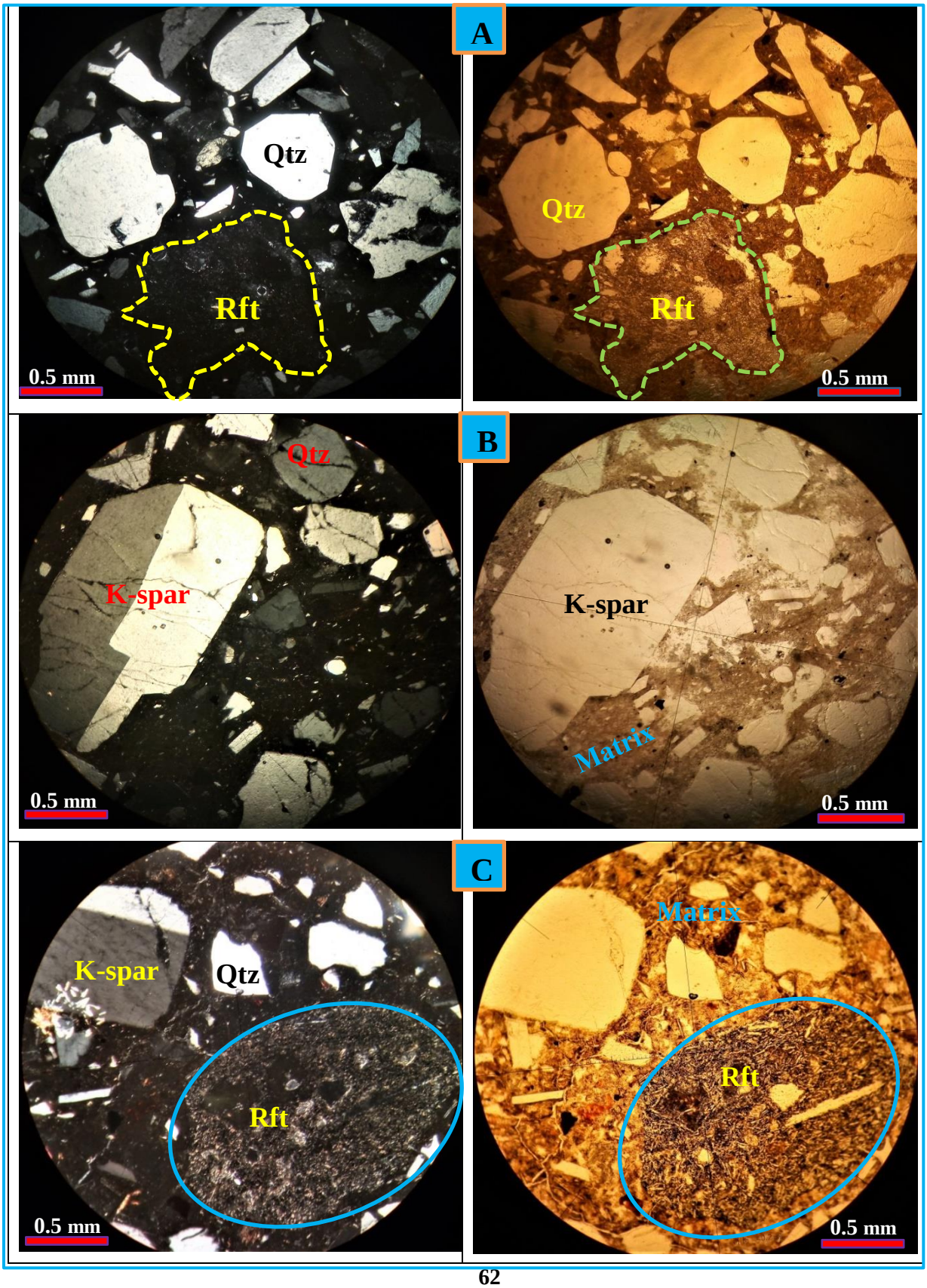
A
Qtz
Rft
0.5 mm
Qtz
Rft
0.5 mm
B
Qtz
K-spar
0.5 mm
K-spar
Matrix
0.5 mm
C
K-spar
Qtz
Rft
0.5 mm
Matrix
Rft
0.5 mm

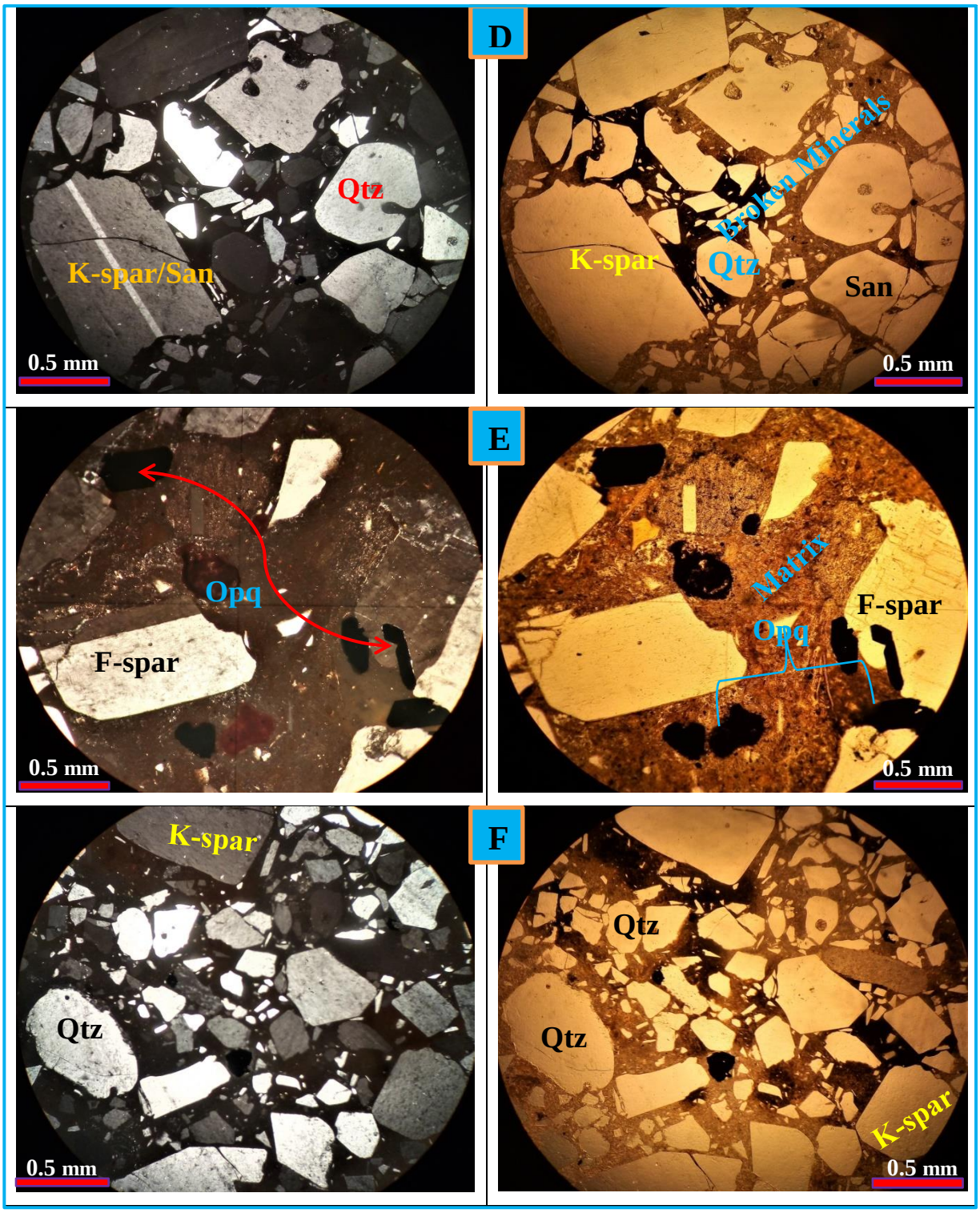

Figure 5.4:- Unmineralized sandstone under thin section: the photo above (XPL on the left and PPL on the right, show the sandstone consisting of Quartz (Qtz), feldspar (F-spar, K-spar mainly Sanidine –San and untwined feldspar), rock fragment (Rft), opaque (Opq) minerals, and volcanic ash materials as a matrix. All minerals are less fractured.

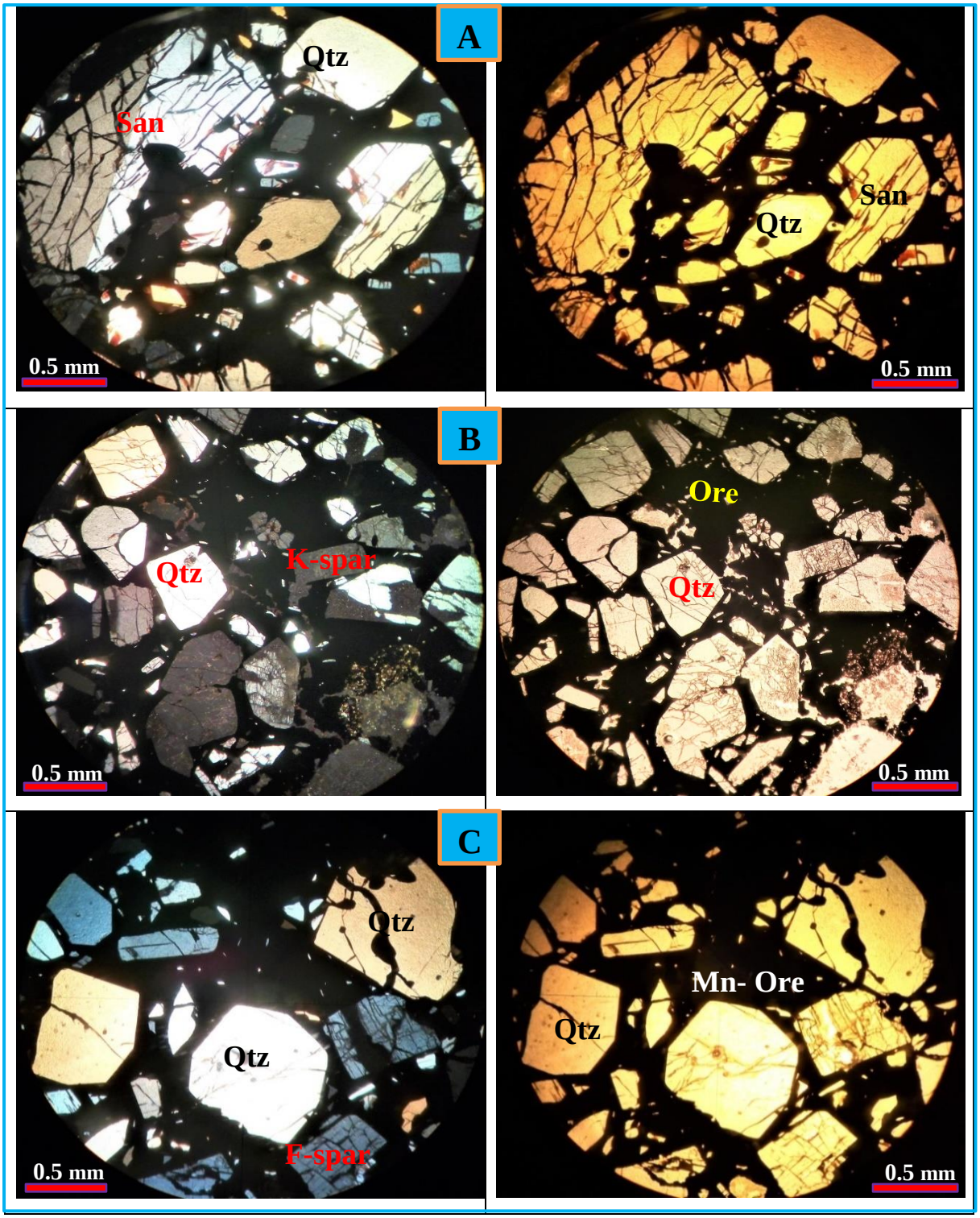

Figure 5.5:- Mineralized sandstone under thin section: the photo above (XPL on the left and PPL on the right) shows the sandstone consisting of Mn-Fe ore (all the dark part), quartz (Qtz) and feldspar (mainly sanidine –San). A sanidine shows Carlsbad twining. All gangue minerals are dissected and filled by Mn-Fe ore minerals.

5.3.2 The Manganese - Iron Mineralization

According to Hein, et al., (2015), iron and manganese mineralization can occur in five forms: (1) nodules and micronodules; (2) crusts and pavements; (3) cements and vein infillings; (4) mounds and chimneys; (5) sediment-hosted stratabound layers and lenses. Similarly, the manganese and iron ore body in the present study area found as stratabound - stratiform, botryoidally precipitated coating/encrustation, concretion and veins. However, the mineralization is dominantly occurring as stratabound - stratiform in the lower friable sandstone and in the upper parts of mudrock. The thickness of this layered manganese - iron ore varies widely within a range from 30 cm to half meter. Secondly, the manganese veins that cropped out on the well compacted sandstone unit in the central part of the study area are relatively prominent over the other ore morphology. The thickness of these vein exposures varies from few millimeters to 25 cm. In addition, in the western part of the area near Keberomeda, very thin iron and manganese veins are present on friable sandstone unit (Fig. 5.6 J). The distribution of most ferromanganese veins exposed in both indurated and friable sandstone units is non-systematic. Based on exposure in the typical Mn-Fe ore in the central parts of the study area, it is possible to construct the succession of the surrounding rock, host rock and ore body (Fig. 5.7 and 5.8). However, because of extensive weathering and erosion effect in the area, these profiles section may not be considered representative of manganese - iron deposition throughout the entire area. Beyond the effects of those surficial processes, the layered ferromanganese ore is not present in the well indurated sandstone unit; rather it is restricted in the sandstone and mudrock. For instance, the south part of the study area is characterized by absence of friable sandstone unlike the central parts of sandstone exposure. Instead, approximately 52 m thick compacted sandstone is found in that locality. Consequently, the mineralization (layered ore) in south parts of the study area is not present. Because of these two main reasons, the constructed log section in (Fig. 5.7 and 5.8) may not represent the ore body of the whole research area. In general, the morphologies of the ore body can be classified and described in to two based on their abundances of exposure.

5.3.2.1 Layered ore body

The layered ore body which is stratabound in the friable sandstone and mudrock unit is prominent over the other morphologies of the ore body in the area. This layered ore body is bounded by mudrock unit at the bottom and friable sandstone unit above it. The thickness of this ore body is varying from locality to locality. For instance, the ore body that found in the central parts of the study area is relatively thicker than the other parts. The ore bed that found in the central parts of the study area is mixed with some secondary formed soil materials and its thickness reaches 55 to 60 cm. It has two ore layers, which are separated by white friable sandstone as shown in (Fig. 5.6 A). The ore is characterized by brown to black color, coarse grained, 45 to 50 cm thick, massive manganese ore on the upper part; and reddish brown to yellow color, fine grained, 15 to 10 cm thick and massive iron ore at its bottom part (Fig. 5.6 A and E). In contrast, the thickness of the ore body in the northern parts of the study area is relatively thin, which reaches about 25 to 30 cm (Fig. 5.3 B and C).

5.3.2.2 Other Morphology of the ore body

Although bedded ore is the most common morphology in the research area, the manganese and iron mineralization appears in different form like coating, concretion and veining (Fig. 5.6 E-L). The distribution of the ore mineral in the form of concretion, coating/encrustation and veining is sporadic. In the central part, the coating and concretion of manganese ore exhibited on the compacted and friable sandstone respectively. The concretion shows replacement of the sandstone by the manganese ore as a result of surficial weathering by removing the other associated gangue minerals like feldspar and quartz (Fig. 5.6 E). Some manganese oxide coating forms a brown-black and sub - spherical botryoidal morphology and it indicates secondary precipitation of the ore body on the sandstone unit (Fig. 5.6 G and H). In addition, manganese and iron mineralization in the form of vein are observed in the central, northwestern and western parts of the study area. The manganese veins that are exposed in the central part on the well indurated sandstone unit are relatively wider and their widths are in the ranges of 10 to 15 cm (Fig. 5.6 K and L). In contrast, the veins that occur in the western and northwestern parts of the area are numerous and very narrow (fig. 5.3 J). The sandstone is traversed by a number of small veinlet's which display no preferred

orientation and varies in width from few mm to 2 cm. Furthermore, there are some pinkish to reddish brown encrustation of iron ore minerals associated with mudrock.

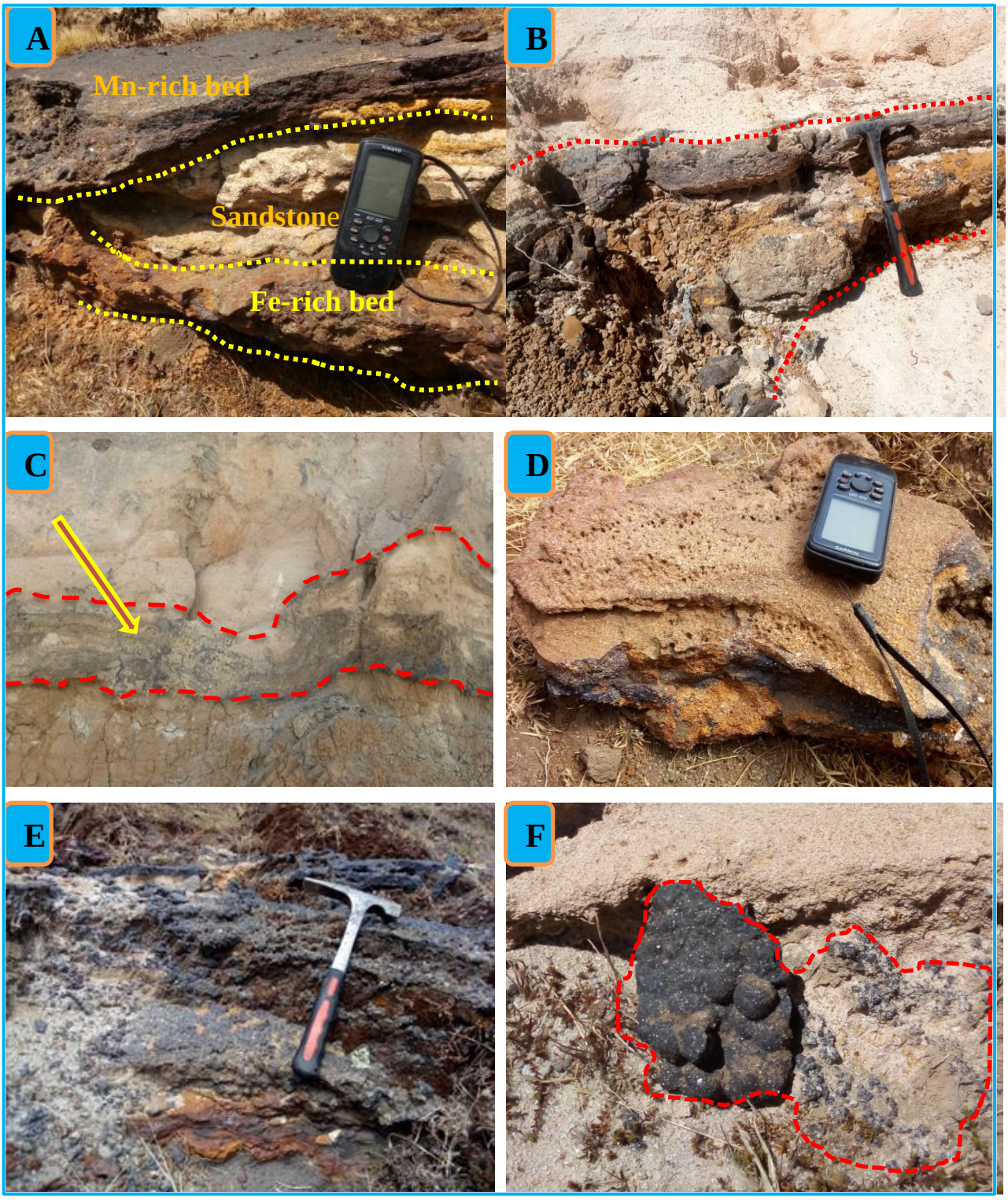

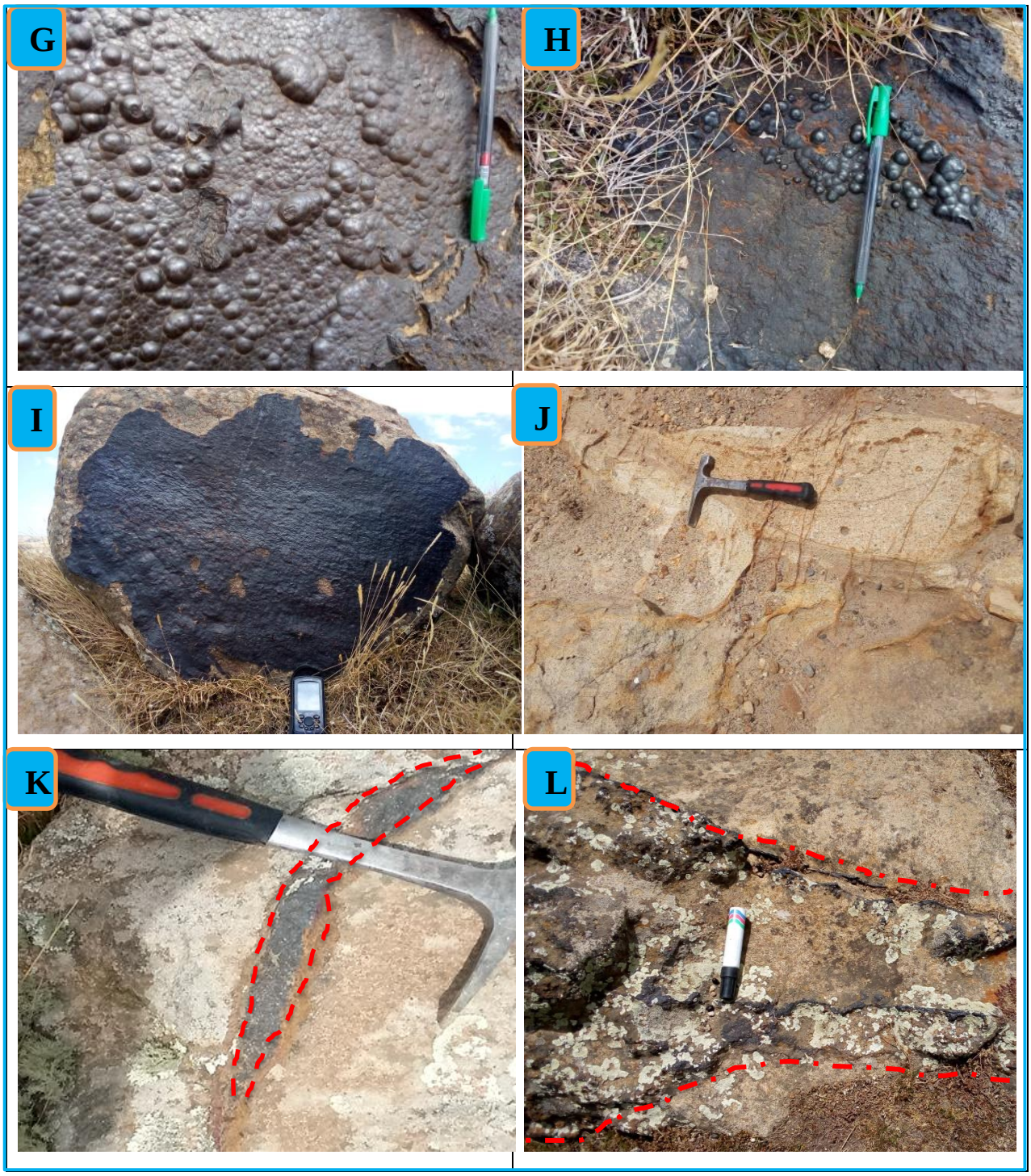

Figure.5.6:- Various morphologies of the ore body: (A, B, C, D) the first four image shows a layered Mn-Fe ore bodies in the central parts of the study area along different exposure. Image (E and F) shows the concretions of manganese ore body on the friable sandstone unit, (G, H, I) coting of manganese ore body that show kidney /botroyidal like features on the well indurated sandstone. The last three images (J, K, L) show the presence of ore bodies as a vein deposit in different thicknesses (from mm to 25 cm

Thickness in meter	Stratigraphic log section	Legend and description of lithology

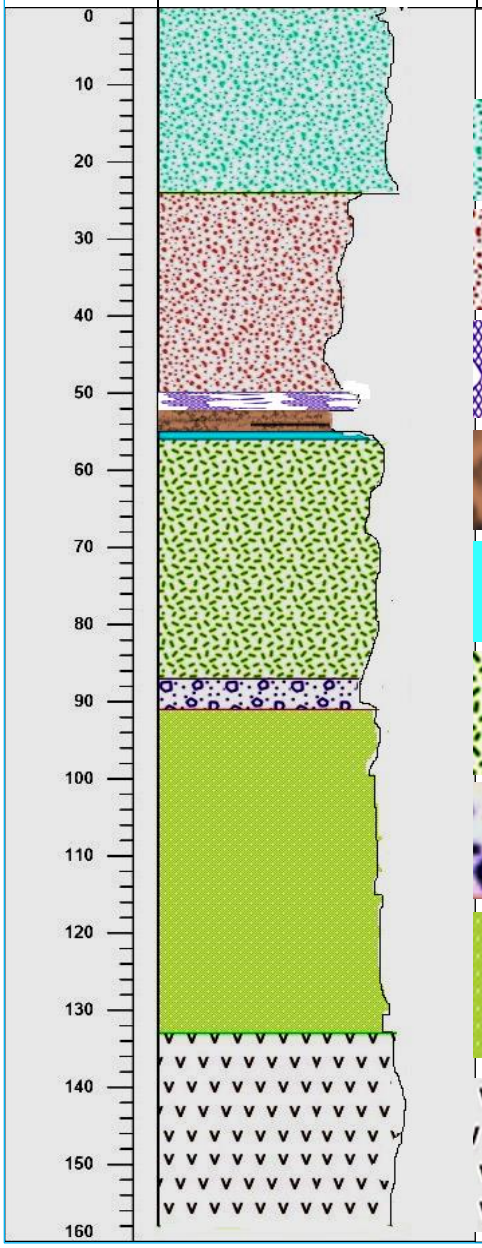

Legend	*Explanation*
	Whitish to brown color, well indurated sandstone
	White friable sandstone that host the Mn-rich parts of the ore body
	Manganese - iron ore body which is bounded by friable sandstone and mudrock
	Reddish brown, clay to silt size and fragile mudrock
	Highly weathered ignimbrite at the contact between ignimbrite and mudrock
	A gray, highly welded coarse ignimbrite that has small to large pyroclastic materials
	Black to grey color, massive volcanic glass rock that contains obsidian fragment
	Light grey to light brown, highly welded ignimbrite that contain relatively fine grained pyroclastic materials
	A black color, aphanetic texture, massive and very hard basalt that found at the base of all lithologic units in the study area

Figure 5.7:- Lithological stratigraphy of the typical manganese occurrence in the central part of the study area

Thickness in (cm)	*Stratigraphic log section*	*Legend and description of the succession*

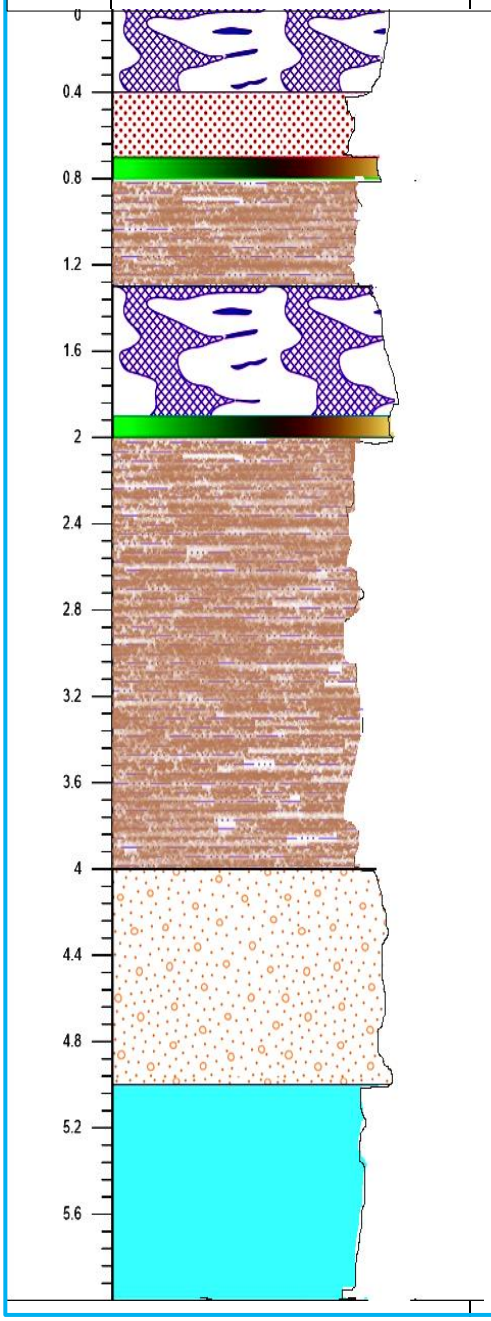

Legend ***Explanation***

Brown to black color, massive, coarse grained Mn-rich ore body

White friable sandstone between the upper (Mn- rich) and lower (Fe-rich) parts of the body

Reddish brown to yellow color, fine grained and massive iron ore

Reddish brown color, clay to silt size mudrock

Mudrock with some pinkish to reddish brown encrustation of iron ore

Highly weathered whitish tuff material at the bottom of the terrestrial sedimentary rock

Figure 5.8:- Detail stratigraphic log section of the ore body in the typical Mn- Fe occurrence

CHAPTER SIX

MINERALOGY AND GEOCHEMISTRY OF KULFAMBA MANGANESE – IRON OCCURRENCE

6.1 Mineralogy

The mineralogy of Kulfamba manganese and iron occurrence has been established only by microscopic study. The Mn-Fe ore and associated gangue minerals are identified through polished section and thin section observation under reflected and transmitted light microscopy respectively. The study revealed the presence of manganese oxide, iron oxide and iron hydroxide minerals. The upper part of the ore body is dominated by manganese oxide minerals while the lower part is dominated by iron oxide and iron hydroxide minerals. Pyrolusite, hematite and goethite are by far the most abundant ore. All of these ferromanganese ore minerals are found along the fractured and void space between framework grains, and by replacing the gangue minerals (Fig. 6.1 and 6.2). In some extent, the ore minerals are also replaced by other ore minerals. Pyrolusite is characterized by existence of fine to well-developed euhedral coarse grain crystal, massive, white to light gray (creamy) color and medium to high reflectance. Hematite is also having a white to greyish blue color, moderate reflectance and distinct anisotropism (gray blue to gray yellow) feature under polished section (Fig. 6.2 B). Moreover, the iron hydroxide mineral (goethite) show a reddish brown to gray color and low reflectance.

6.1.1 Ore mineral texture

Ore microscopy involves interpretation of ore mineral textures (spatial arrangement and relationships among mineral grains) beyond the identification of individual ore minerals. Although the textural interpretations of ore mineral are difficult, their importance in the study of rocks and ores are numerous (Barton, 1991). That means recognition and interpretation of textures is the most important step in understanding the origin and post-depositional history of an ore. Craig and Vaughan (1994), classified and explained the most common variety of textures

observed in ores as primary textures of ore minerals that are formed from melt and open space deposition, and secondary texture of ore minerals that are formed as a result of replacement, cooling, deformation, annealing and metamorphic growth.

As microscopic study in polished section shows the pyrolusite in Kulfamba mainly occurs as primary textures of open space deposition and secondary replacement on the gangue minerals. Specifically, it appears as well developed (euhedral) crystals, colloform growth banding, vein fillings structures, massive and replacement along fractures of the gangue minerals. The colloform banding of pyrolusite (monomineralic growth banding) exhibits a concavo-convex appearance and which dominantly altered the sandstone (Fig. 6.1 A and B). It illustrates a sequential growth of pyrolusite on the pore space. A well-developed (euhedral) crystal of pyrolusite is another texture and it exhibits a rhombic, hexagonal, rounded/circular and elongated/prismatic shape (Fig. 6.1 E-G). It crystalizes along the open space between the grains and within the voids of the associated gangue minerals. The pyrolusite also occurs as a micro vein filling structures within the fractured gangue minerals (Fig. 6.1 C and D). It is also clearly shown in thin section pictures (Fig. 5.3), in manganese rich sandstone. The manganese and iron ore is filled along the fractures and between the grains. In addition, big light brown color veinlet of ore crosscuts the colloform pyrolusite and randomly distributed fine pyrolusite (Fig. 6.1 A). This light brown ore also occurs as open space deposition between the gangue minerals (Fig. 6.1 J) and replacement of the gangue minerals. Furthermore, the ore mineral is occurring as a secondary replacement of the feldspar and quartz mineral along their fractured part and rims (Fig. 6.1 H and I). The gangue minerals such as feldspar and quartz are replaced partially, and in some field of view the matrix materials are completely replaced by the manganese ore.

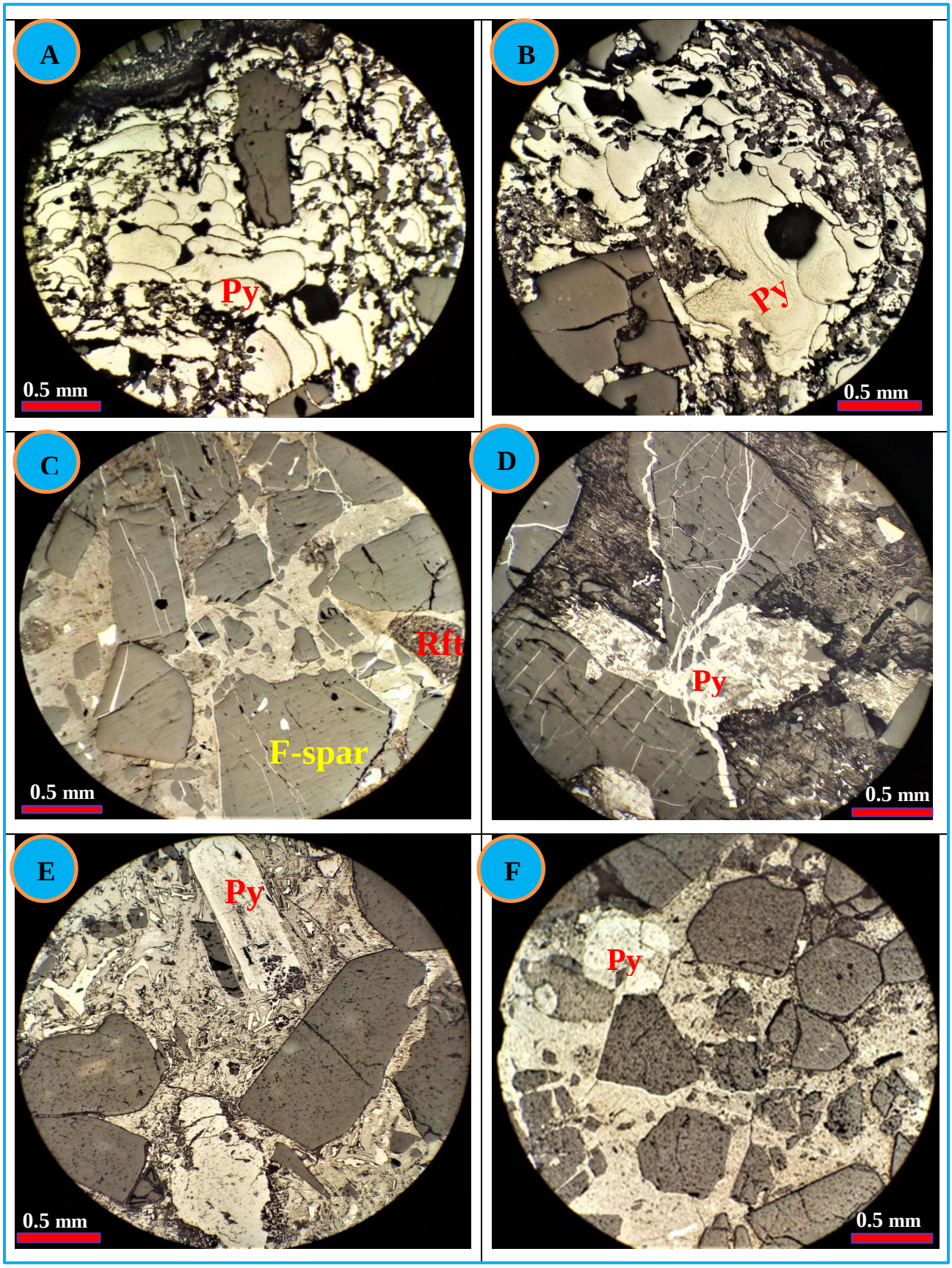
A
Py
0.5 mm
B
Py
0.5 mm
C
Rft
F-spar
0.5 mm
D
Py
0.5 mm
E
Py
0.5 mm
F
Py
0.5 mm

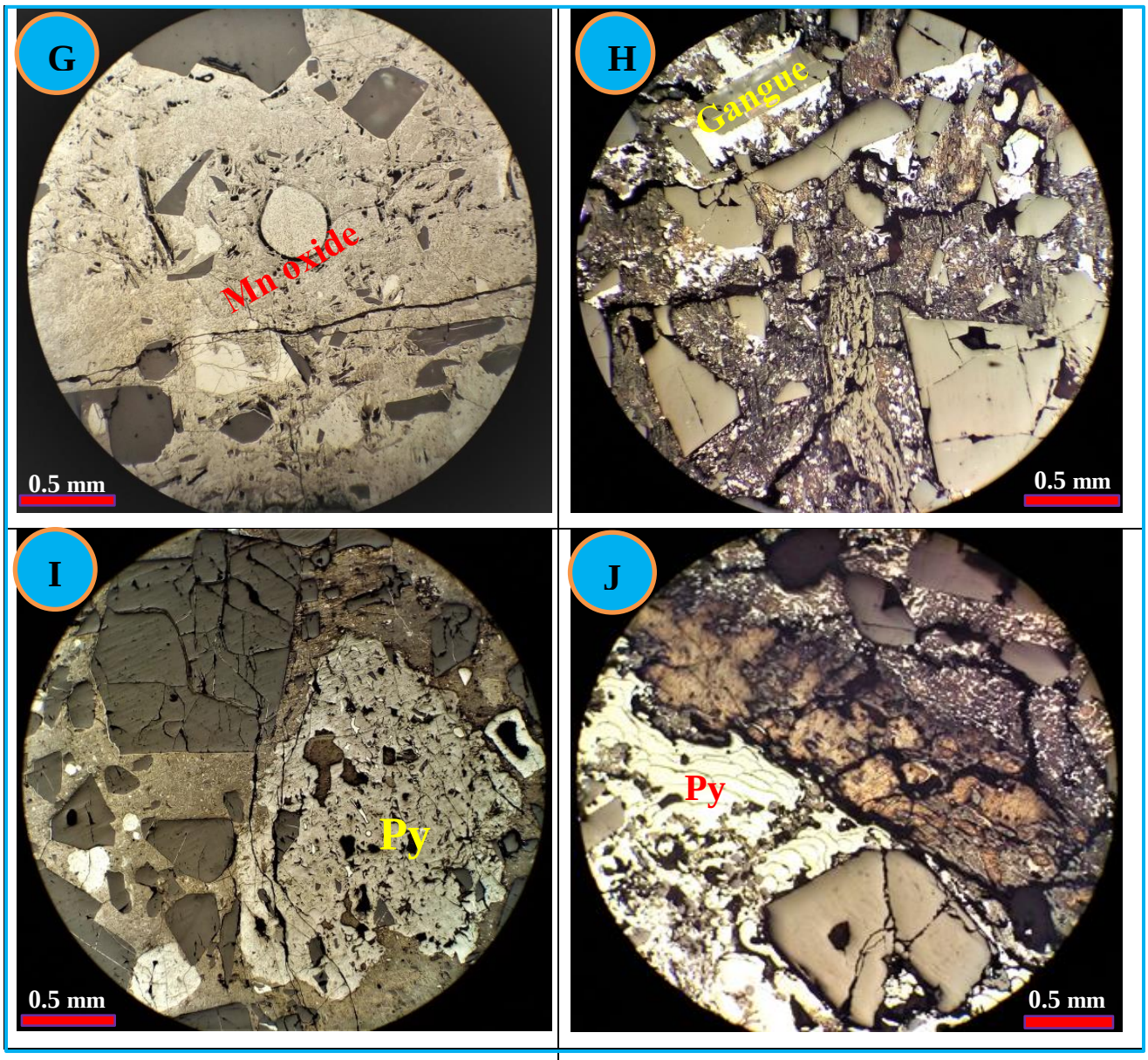

Figure 6.1:- Manganese ore minerals and their textures: (A, B) Concavo-convex coloform growth banding of pyrolusite (Py), (C, D) manganese ore infilling the fractured gangue grains, (E, F) exhibit well developed rhombic and hexagonal pyrolusite between the open space of feldspar and quartz grains, (G) euhedral and massive manganese ore, (H) replacements of pyrolusite and light brown ore along the rim and fracture of feldspar, (I) massive light gray manganese ore which replace the ground mass and gangue, (J) a coloform and fine grain pyrolusite crosscut by light brown veinlet.

Similarly, the iron oxide and iron hydroxide ore minerals in the study area mainly occur as primary textures of open space deposition and secondary replacement on the gangue and early formed ore minerals. In particular, hematite formed along the open space and highly fractured gangue minerals as fracture and void space fillings (Fig. 6.2 A-C). It also occurs as a replacement along the rim and fractures of the gangue minerals. In some field of view the hematite ore is associated with manganese oxide ore (Fig.6.2 A and E). The early formed massive hematite ore is replaced by later formed manganese oxide ore. Iron hydroxide mineral is also formed as a replacement of the hematite and associated gangue minerals (Fig. 6.2 E and F).

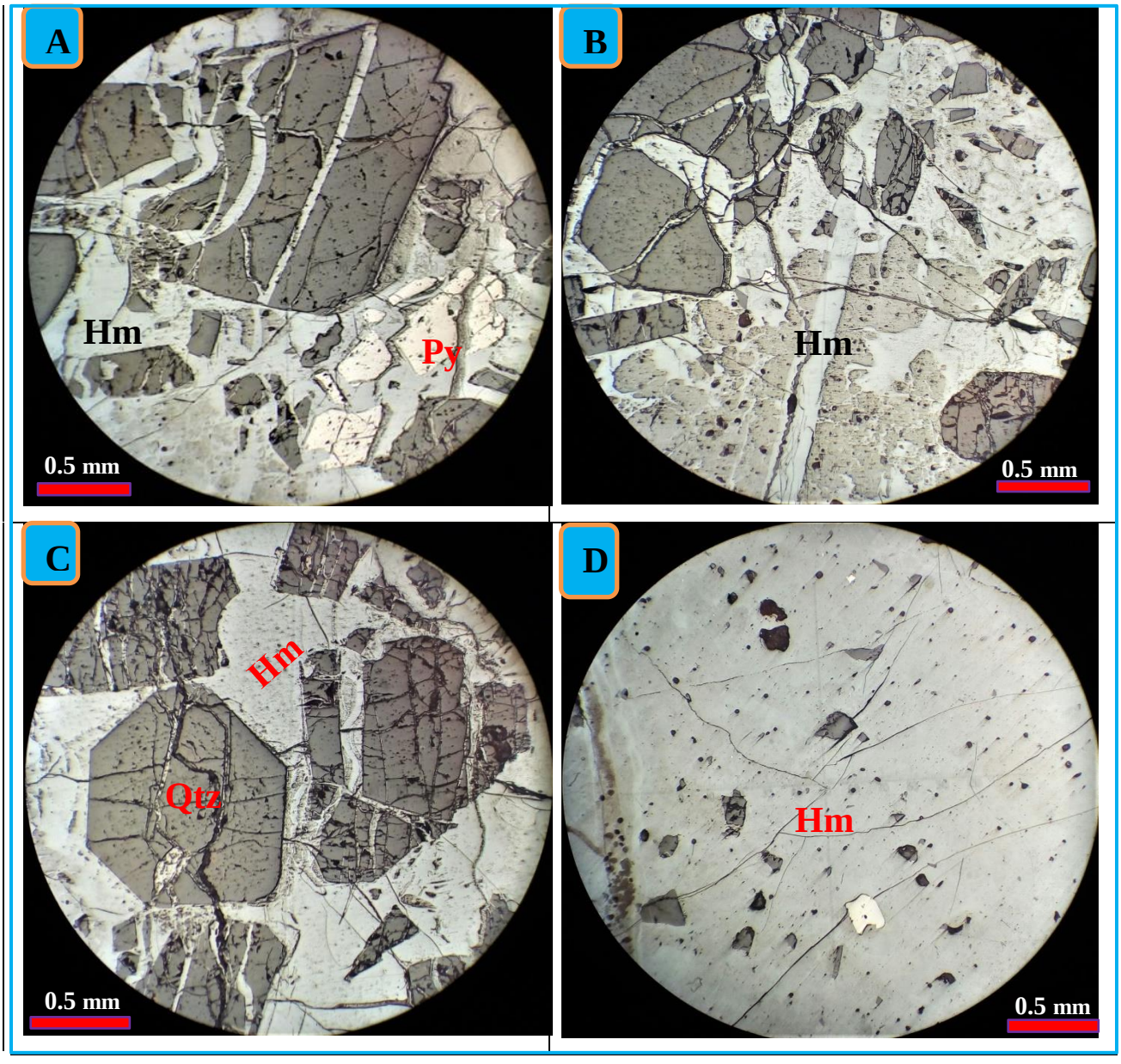

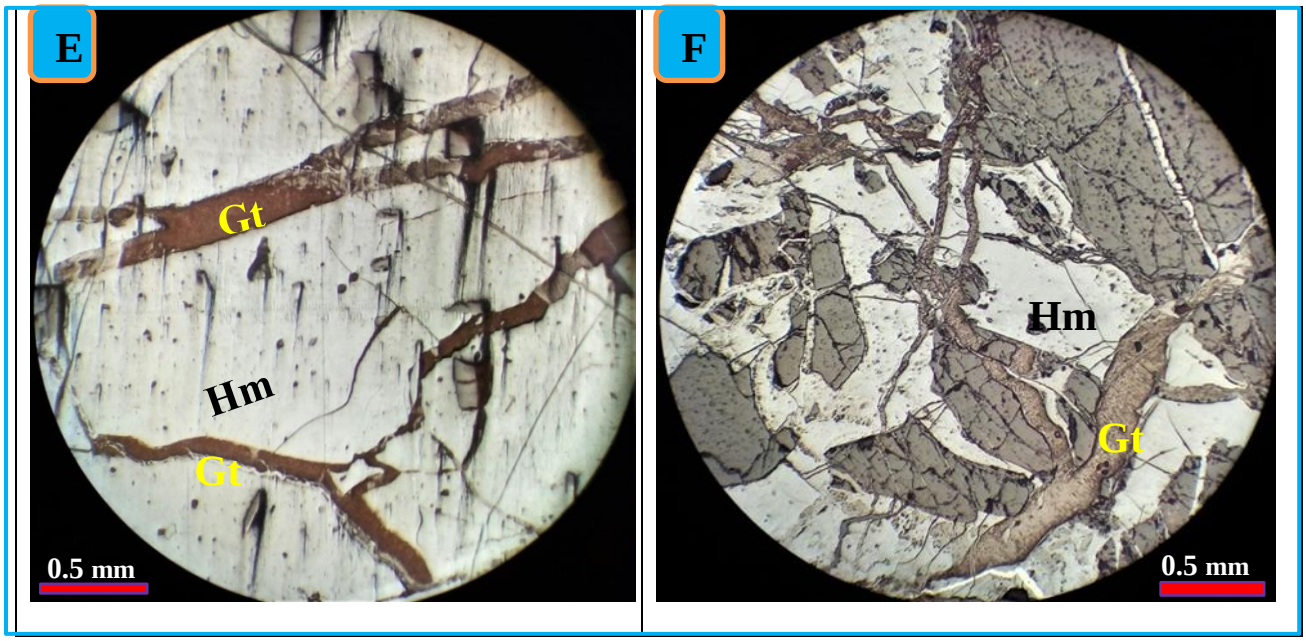

Figure 6.2:- Iron ore minerals: (A, B) massive and vein filling iron oxide ore (hematite) between gangue minerals and along fractured zone, (C) hexagonal and tabular gangue minerals replaced by hematite (Hm) along their fracture and rim part, (D) massive hematite ore with fine euhedral manganese oxide ore, (E) massive hematite ore is replaced by later formed goethite ore, (F) both gangue and hematite ore minerals are replaced by goethite ore (Gt).

6.2 Geochemical Analysis Result

Geochemistry involves measurement of the chemistry of the ore body and host rock to determine anomalous geochemical patterns related to mineralization. In order to confirm the megascopic and microscopic observation of whole sample, geochemical analysis has inimitable advantage for all investigations. Therefore, the geochemical characterization of Kulfamba manganese ore and associated host rocks is one of the main tasks of this study to support the data collected from field and petrographic observation. According to Hein et al. (2015), iron, manganese, and iron-manganese deposits occur in nearly all geomorphologic and tectonic environments. As a result, manganese - iron deposits are diverse in occurrence, origin, mineralogy, morphology and geochemistry.

In general, the diverse genetic types of manganese mineralization are related with direct hydrothermal activity, sedimentary processes, and continental weathering (Roy, 1981; Nicholson et al., 1997; Oksuz, 2011; Kuleshov and Maynard, 2017). This major classification is based on modes of origin, sources of manganese, mineral assemblages and elemental associations.

Although the processes may be interrelated, each of them involves distinct mechanisms that place the deposits into specific genetic types. The redox sensitive elements have their own unique geochemical behaviors and signature in those hydrothermal, sedimentary and supergene manganese deposits. Therefore, geochemical analysis of major element, trace elements and rare earth elements (REE) in manganese mineralization and host rock is crucial to characterize and study the processes of formation, depositional mechanism and depositional environment of ferromanganese deposits. In addition, whole rock geochemistry is important in the determination of origin and tectonic setting of the resource occurrence. For this reason, the representative samples are taken from the ore body, host rocks (sediments) and other country rock (volcanic rocks); and analyzed for those major and trace elements. The analytical results of eighteen selected samples are given in (Table 6.1). From these, thirteen samples are taken from the host and country rocks, while five samples are from ore body. Many of the ore samples are taken from stratiform ore body and one sample is from botryoidally precipitated manganese ore.

Table 6.1 Major and trace element concentration of manganese - Iron ore body, host rock and country rocks of Kulfamba area, (Sst – represents Sandstone)

Sample code	Name of sample	Wt. %	SiO_2	Al_2O_3	Fe_2O_3	CaO	MgO	Na_2O	K_2O	Cr_2O_3	TiO_2	MnO	P_2O_5	SrO	BaO	LOI	Total
KA 01	Ignimbrite	%	69.9	12.55	3.51	0.24	0.28	1.94	5.9	<0.002	0.56	0.2	0.03	0.01	0.01	5.69	100.82
KA 03	Mudstone	%	45	24.9	9.26	0.69	0.39	0.13	0.18	<0.002	1.35	0.04	0.02	0.01	0.02	18.2	100.19
KA 04	Fe-coated Mudstone	%	38	15.75	29.4	0.36	0.22	0.22	0.21	0.007	1.1	0.25	0.11	0.01	0.01	14.65	100.3
KA 06	Massive Mudstone	%	45.3	26.3	8.02	0.4	0.23	0.87	0.83	0.002	1.9	0.09	0.06	0.01	0.02	14.25	98.28
KA 08	Siltstone	%	48.8	25.7	7.28	0.31	0.16	0.86	0.82	<0.002	1.86	0.06	0.05	0.01	0.02	13.05	98.98
KA 20	White Claystone	%	48.5	27.4	8.8	0.22	0.08	0.09	0.13	<0.002	1.45	0.02	0.03	0.01	0.01	13.65	100.39
KA 05	Gray Indurated Sst	%	77.5	10.7	2.45	0.15	0.07	3.2	4.33	<0.002	0.45	0.06	0.03	<0.01	0.02	1.8	100.76
KA 13	White indurated Sst	%	73.9	12.4	3.01	0.1	0.06	3.87	4.91	<0.002	0.55	0.1	0.02	<0.01	0.02	1.19	100.13
KA 14	Brownish indurated Sst	%	77	11.4	2.68	0.12	0.09	3.31	4.53	<0.002	0.49	0.09	0.02	0.01	0.02	1.54	101.3
KA 21	Friable Sandstone	%	66.8	14.45	5.13	0.49	0.29	3.03	3.34	0.003	0.91	0.06	0.05	0.01	0.06	5.72	100.34
KA 22	Brown to reddish Sst	%	67	13.65	8.41	0.11	0.04	2.7	3.04	<0.002	0.62	0.09	0.05	<0.01	0.02	4.42	100.15
WG-4	Reddish Sandstone	%	67.2	15.3	4.82	0.58	0.44	2.79	3.29	<0.002	1	0.17	0.07	0.01	0.03	5.96	101.66
KA 19	Aphanetic Basalt	%	46.4	12.5	16.35	9.58	5.76	2.56	1.31	0.003	5.31	0.2	0.59	0.08	0.03	0.37	101.04
KA 07	Fe- ore	%	30.1	8.12	44.4	0.12	0.08	0.81	1.09	<0.002	0.63	2.33	0.08	0.01	0.32	11.55	99.64
KA 09	Massive Fe-ore	%	29.5	8.23	45.2	0.19	0.11	0.49	0.57	<0.002	0.8	1.22	0.06	0.01	0.16	12.65	99.19
KA 10	Fe-Mn ore	%	42.1	7.81	31.7	0.13	0.08	1.79	2.19	<0.002	0.32	4.74	0.01	0.01	0.73	8.32	99.93
KA 11	Mn- ore	%	34	7.36	2.66	0.14	0.07	1.74	3.47	0.004	0.35	33.1	<0.01	0.01	3.52	7.85	94.27
KA 12	Fine grain Mn- ore	%	3.76	2.36	1.28	0.26	0.07	0.22	3.19	0.007	0.12	59	0.2	0.19	4.82	12.35	87.83

Sample code	*KA 01*	*KA 03*	*KA 04*	*KA 06*	*KA 08*	*KA 20*	*KA 05*	*KA 13*	*KA 14*	*KA 21*	*KA 22*	*WG 4*	*KA 19*	*KA 07*	*KA 09*	*KA 10*	*KA 11*	*KA 12*
wt.(ppm)																		
Ba	99	159	107	205	188	124.5	177.5	176.5	174	480	163.5	252	239	2820	1390	6240	10000	10000
Ce	285	82.7	185	420	448	38.8	202	105.5	138	239	98.3	236	100	396	6150	258	755	1015
Cr	10	10	60	30	20	10	10	10	20	40	10	20	50	20	10	10	10	20
Cs	3.13	1.14	0.48	1.15	1.48	1.04	0.35	0.57	0.52	0.74	0.71	1.2	0.19	2.63	0.97	1.1	1.57	0.54
Dy	20.8	24.2	38.1	23.8	30.8	28.5	7.57	10.85	7.04	15.15	7.96	14.7	8.71	34.7	69.6	20.2	25	29.7
Er	11.15	15.2	26.3	17.1	19.95	22.5	3.64	6.42	3.71	7.55	4.3	8.17	3.99	16.55	34.7	8.64	9.57	17.7
Eu	5.51	5.72	5.62	5.71	9.21	3.69	3.05	2.68	2.23	5.22	3.05	4.77	3.82	12.95	11.7	8.93	13.25	5.79
Ga	38.1	67.9	48.9	75.7	76.4	81.8	27.1	33.4	28.4	36.1	33	37.6	26	27.4	39.8	23.1	29.8	24.9
Gd	23.7	22.7	25.1	20.1	32.6	14.25	10.55	10.05	7.67	19.55	9.76	17.5	11.9	46.5	52.5	30.5	46.7	28
Hf	33.8	53	30.9	55.7	54	48.8	7.7	15.4	9.5	14.5	13.7	15.6	10.5	14.3	15.6	7.6	8.5	5.3
Ho	4.07	5.03	8.52	5.39	6.51	6.77	1.41	2.23	1.3	2.78	1.51	2.94	1.58	6.1	13.1	3.49	4.12	6.43
La	142.5	111	64.4	194.5	344	47.8	99.2	46.2	46	150.5	84.2	118	40.6	392	78.9	240	603	145
Lu	1.39	2.35	3.67	2.68	3.05	4.04	0.46	0.85	0.49	0.86	0.8	1.1	0.39	1.95	3.12	0.79	0.85	2.03
Nb	248	302	275	284	293	273	47.3	79.6	53	77.8	76.2	82.4	53.8	85.5	91.9	36.6	36	24.7
Nd	143	115.5	77.4	165	292	53.2	97.8	54.9	54.7	134.5	81	124	58.9	432	115	278	531	126
Pr	37.4	28.7	19.5	48.2	85.5	13.9	25.1	14.2	14.3	34.8	22.6	31.7	13.3	118	27.4	72.4	143.5	32.7
Rb	223	8.1	4.2	11.8	14.6	9.2	51.3	81.7	51.1	42.3	21.4	34.6	28.4	25.2	10.3	19.8	33.4	29.1
Sm	29.1	25.2	21.3	28.4	47.5	12.9	15.95	11.65	10.3	24.1	14.2	22.2	13.3	72.4	41.4	48.7	79	27.1
Sn	9	15	9	17	16	14	3	5	3	5	4	5	3	5	5	2	3	2
Sr	19.1	42.8	20	29.6	25.8	12.8	12.9	7	8.2	61.5	7.5	44.1	667	19.5	15.8	20.8	140.5	1745
Ta	102.5	15.9	207	16.1	16	13.8	6.3	5.3	2.9	5.1	4.4	5.1	2.5	5	5.3	2.5	1.9	0.7

Tb	3.79	3.84	5.47	3.59	4.92	3.5	1.44	1.73	1.21	2.81	1.41	2.6	1.61	6.42	11.6	4.1	5.56	4.78
Th	24.7	35.4	20	36.5	36.1	30.5	5.57	10.9	6.63	12.1	9.96	10.6	3.71	10.4	11.2	5.43	6.19	4.31
Tm	1.59	2.28	4.01	2.74	3.09	3.72	0.5	0.92	0.51	0.96	0.68	1.17	0.51	2.27	4.5	1.07	1.13	2.37
U	8.85	6.59	18.15	6.55	9.87	3.88	1.64	2.89	1.62	2.54	1.6	2.62	1.13	9.76	23.2	15.35	4.51	15.75
V	47	67	192	91	77	31	12	16	15	38	27	48	511	90	121	14	12	115
W	3	4	5	6	7	4	2	2	2	2	3	2	3	9	13	1	<1	<1
Y	100.5	113	305	140.5	169	165.5	33	56.1	31.7	70.2	34.7	77	40.2	133	328	67.5	89.8	188.5
Yb	9.47	15.25	25.5	18	19.7	25.8	3.01	5.69	3.48	5.87	5.1	7.34	2.8	13.35	22.9	5.74	5.77	13.55
Zr	1340	2080	1270	2190	2200	2050	301	617	373	572	557	601	416	607	633	310	355	227
Ag	2.9	4.4	3	4.3	3.6	4.2	0.6	1	0.8	0.9	1.3	0.7	<0.5	2.9	2.5	3.2	17	33.5
As	<5	<5	14	8	11	8	<5	<5	5	<5	<5	<5	<5	76	79	5	5	5
Cd	0.5	<0.5	0.5	0.8	0.7	<0.5	<0.5	<0.5	<0.5	<0.5	<0.5	<0.5	1.6	<0.5	0.7	0.5	<0.5	18.3
Co	<1	1	28	4	1	<1	1	<1	1	4	2	6	52	45	343	6	4	48
Cu	1	<1	1	<1	<1	<1	1	<1	4	8	<1	2	308	4	1	1	1	35
Li	30	40	30	60	50	60	10	10	10	10	10	10	10	20	20	<10	10	10
Mo	6	3	18	4	3	<1	1	1	<1	1	2	2	<1	45	28	12	5	246
Ni	8	4	4	11	3	2	5	6	5	12	4	5	62	21	1	9	16	39
Pb	32	47	31	52	51	39	9	12	9	13	10	15	8	30	28	17	48	120
Sc	5	6	11	8	8	11	4	5	4	7	6	5	24	3	3	2	3	3
Tl	<10	<10	<10	<10	<10	<10	<10	<10	<10	<10	<10	<10	<10	20	10	<10	<10	<10
Zn	290	217	470	235	210	103	50	128	91	122	79	156	156	481	378	329	380	1570

6.2.1 Major Element

The major elements are the element which predominates in any host rock and ore deposit analysis. These elements are Si, Al, Mn, Fe, Ca, Mg, Na, K and P, and their concentrations are expressed as a weight per cent (wt %) and analyzed in the form of oxide. The sum of those major element oxides will total to about 100% including loss of ignition (LOI). The LOI of most sample particularly the ore sample and host rock samples are high, which is in the range between 5.69 and 18.2 wt. %. It indicates that the high water contents within the sediment and ore body.

The mean analytical results of manganese rich and iron rich parts of the ore body can be seen differently. The upper parts of the ore body is rich in MnO (av. 46.1%), SiO_2 (av. 18.88%), Al_2O_3 (av. 4.86%), BaO (av. 4.17%), K_2O (av. 3.33%), and poor in Fe_2O_3 (av. 1.97%), Na_2O (av. 1.85%), TiO_2 (av. 0.24%), CaO (av. 0.2%), P_2O_5 (av. 0.11%), SrO (av. 0.1) and MgO (av. 0.07%). As the geochemical data result shows the manganese ore bed is characterized by high manganese content, which is 33.1 to 59% MnO (av. 46.1%) and low iron content about 2.66 to 1.28 Fe_2O_3 (av. 1.97%). Contrary, the lower parts of the ore body is rich in Fe_2O_3 (av. 40.43%), SiO_2 (av. 33.9%), Al_2O_3 (av. 8.10%), and poor in MnO (av. 2.76%), K_2O (av. 1.28%), Na_2O (av. 1.03%), TiO_2 (av. 0.58%), BaO (av. 0.40 %), CaO (av. 0.14%), MgO (av. 0.09%), P_2O_5 (av. 0.05%), and SrO (av. 0.01). Unlike the upper one, the lower parts of the ore body is characterized by high iron content about 31.7 to 45.2% Fe2O3 (av. 40.43%) and low manganese concentration about 1.22 to 4.74% MnO (av. 2.98%). Therefore, the Fe/Mn ratios range from 0.02 to 0.08% with an average of 0.045% for the upper ore bed and 6.68 to 37.04% (av. 20.52%) for the lower ore body.

As the geochemical data manifest, the barium content is higher in the ore body particularly in the upper parts of the ore body. Its oxide concentration is varying from 3.52 to 4.82 (av.4.17%) and its average elemental concentration is greater than 10000 ppm in the Mn ore body. In general, the upper and lower parts of the ore body are enriched in Mn and Fe respectively, whereas they are depleted in Si, Al, K and Na as compared to the host rocks.

6.2.2 Trace Element

A trace elements are an elements which are present in a rock or ore body in concentrations of less than 0.1 wt %, which is less than 1000 parts per million (ppm). Mostly those elements occur by substituting the major elements in the rock forming minerals and are expressed in ppm (parts per million) or ppb (parts per billion). Trace elements are incorporated into the deposits either by co-precipitation, or by diffusion of the adsorbed ions into the manganese and iron oxyhydroxide mineral lattices (Hein et. al., 2015).

Although the concentrations of these elements are small in the whole rock and ore mineral analysis, they are critical for geochemical characterization of the mineralization of manganese deposits (Abate Assen, 2018). The geochemistry of Kulfamba manganese ore is characterized by low average contents of Cu (18ppm), Co (26 ppm) and Ni (27.5 ppm). Similarly, the iron rich part is described by very low average concentrations of Cu (2.5 ppm), Co (131.33 ppm) and Ni (10 ppm).

In addition, many researchers used various discrimination diagrams in order to determine the origin of the manganese – iron ore body. Accordingly, Fe-(Ni+Cu+Co)*10-Mn (Bonatti et al. 1972, Creater et al. 1982 and Öksüz et al. 2014), Fe-Si*2-Mn (Toth, 1980), Si/Al diagram (Peters, 1988), Ni-Co-Zn (Choi and Hariya, 1992) and (Co+Ni)/(As+Cu+Pb+V+Zn) (Nicholson, 1990) ternary and binary diagrams have been used in the present study. The plotting of Kulfamba manganese - iron ore samples are shown in (Fig. 6.3).

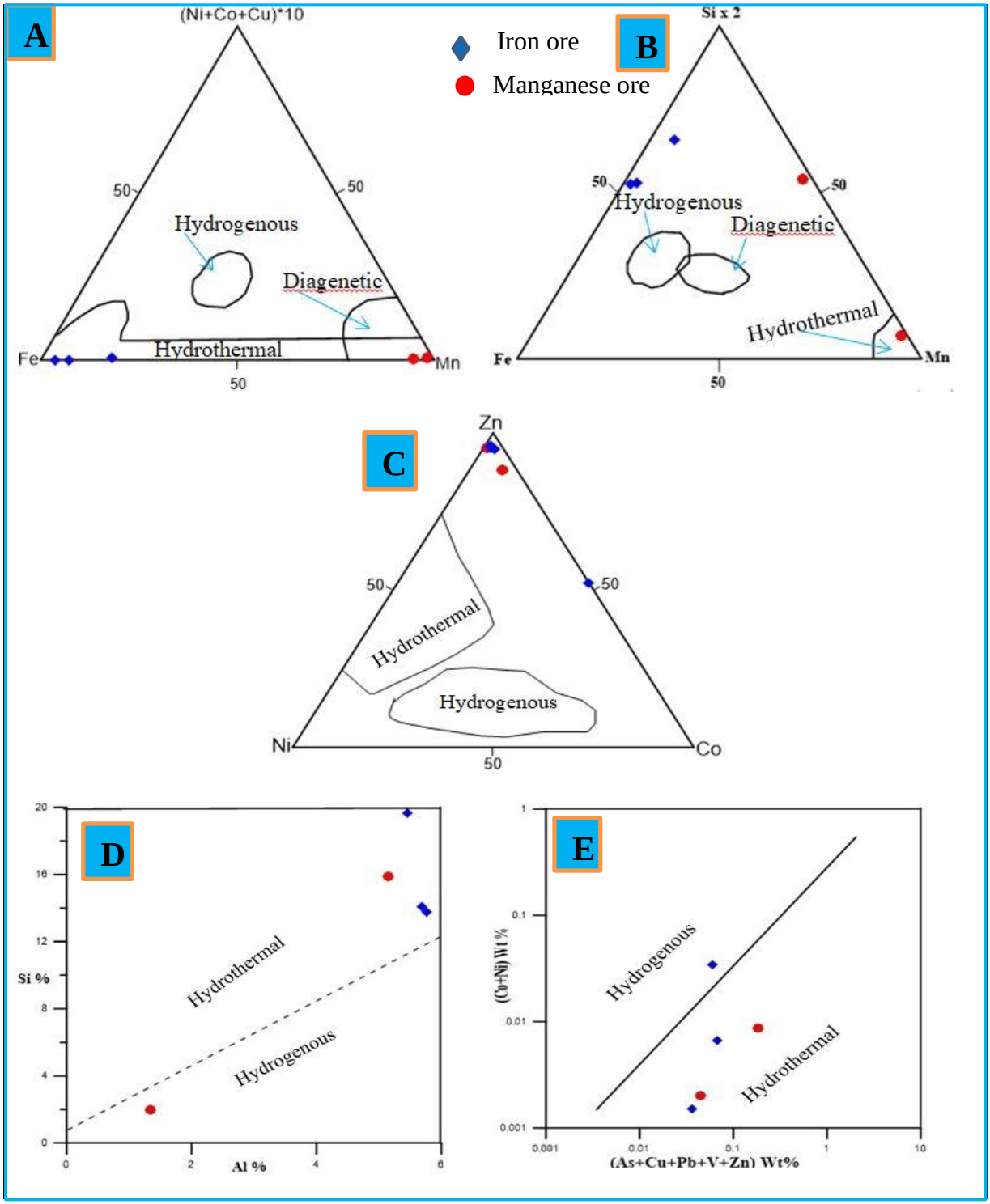

*Figure 6.3:- Discrimination ternary and binary diagrams of Kulfamba ferromanganese ore: (A) Fe-(Ni+Cu+Co)*10-Mn (Bonatti et al. 1972 and Öksüz et al. 2014), (B) Fe-Si*2-Mn (Toth, 1980), (C) Si/Al diagram (Peters, 1988), (D) Ni-Co-Zn (Choi and Hariya, 1992), (E) (Co+Ni)/(As+Cu+Pb+V+Zn) (Nicholson, 1990).*

The rare earth elements (REE), metals with atomic numbers from 57 to 71 (La to Lu) are the most useful of all trace elements and they have important applications in petrological and resource studies (Rollinson, 1993). Typically, REE can be classified to light rare earth elements (LREE) and heavy rare earth element (HREE). Although most of the REE have very similar chemical and physical properties due to the presence of stable 3+ ions, there is small difference in size and behavior. These small size and behavioral differences in REE is used in geochemistry to understand the genesis of rocks and ore deposits. The concentration of REE in the rocks is usually normalized to a common reference standard called chondritic meteorite; to eliminate the abundant variation between elements and identify any fractionation of the REE group relative to chondritic meteorites (Rollinson, 1993). The entire individual rare earth element concentration, their ratio, ∑REE, and average Ce* and Eu* values of Kulfamba Mn-Fe ore body is given in (Table 6.2). All these mentioned REE ratio and concentration could give information about the origin of Mn-Fe mineralization (Hein et. al., 2008; Oksuz et. al., 2014).

Table 6.2:- Rare earth element data of Kulfamba Manganese - Iron ore body (ppm)

Sample	La	Ce	Pr	Nd	Sm	Eu	Gd	Tb	Dy	Ho	Er
KA - 07	392	396	118	432	72.4	13	47	6.4	35	6.1	17
KA - 09	79	6150	27.4	116	41.4	12	53	12	70	13	35
KA - 10	240	258	72.4	278	48.7	8.9	31	4.1	20	3.5	9
KA - 11	603	755	144	531	79	13	47	5.6	25	4.1	10
KA - 12	145	1015	32.7	126	27.1	5.8	28	4.8	30	6.4	18

Sample	Tm	Yb	Lu	Y	∑REE	LREE/HREE	Ce*	Eu*	Y/Ho
KA - 07	2.3	13	2	133	1551	11.13	0.42	0.57	21.8
KA - 09	4.5	23	3.1	328	6637	30.28	31.6	0.76	24.9
KA - 10	1.1	5.7	0.8	68	980.5	12.15	0.45	0.58	19.3
KA - 11	1.1	5.8	0.9	90	2224	21.52	0.56	0.54	21.8
KA - 12	2.4	14	2	189	1456	12.92	3.17	0.61	29.3

- *Ce*=CeN/(2/3LaN+1/3PrN), Eu*=EuN/(2/3SmN+1/3GdN), ∑LREE=La+Ce+Pr+Nd+Sm+Eu, and ∑HREE=Gd+Tb+Dy+Ho+Er+Tm+Yb+Lu.*

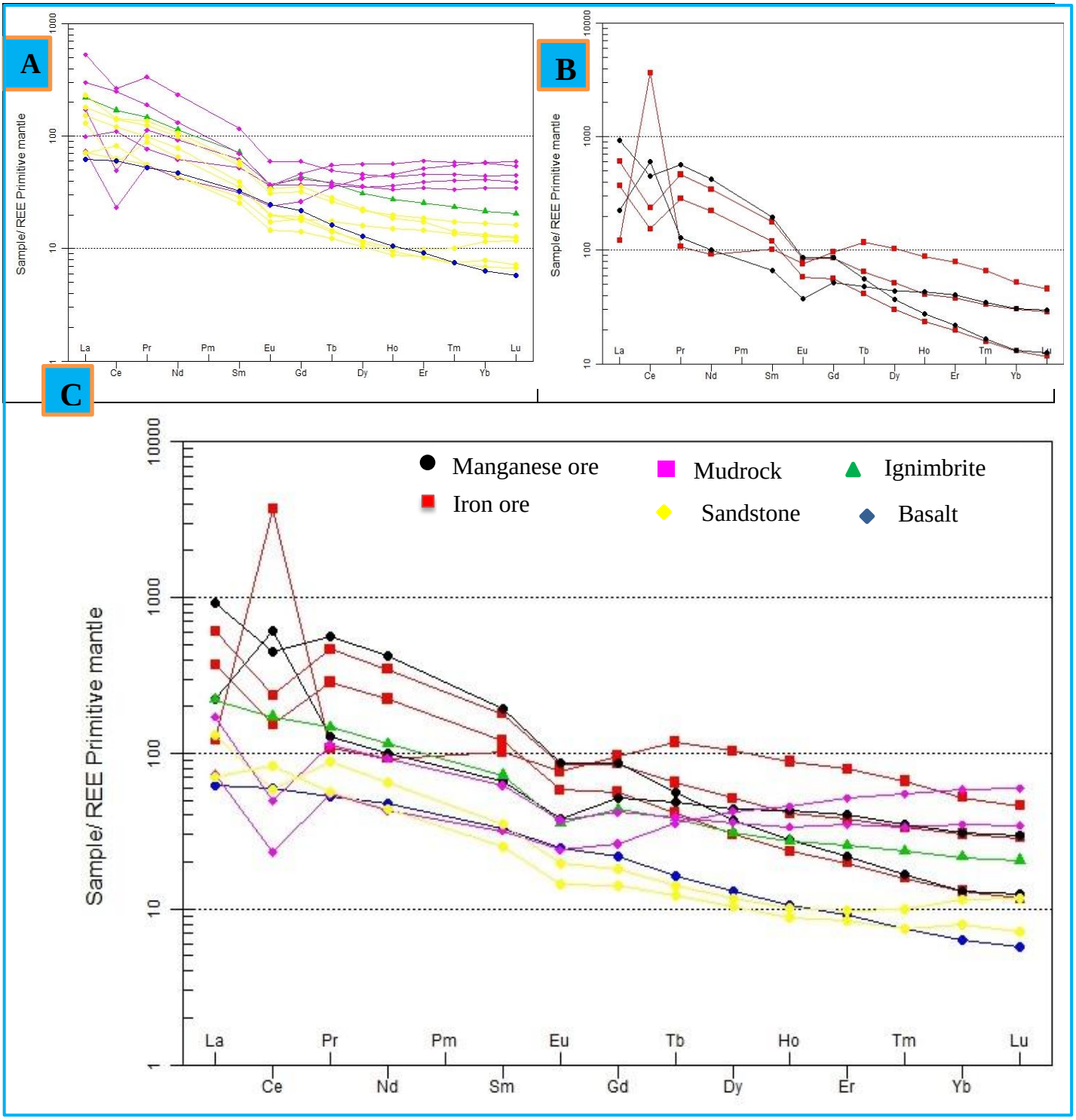

Figure 6.4:- Primitive-mantle-normalized REE distribution patterns for Kulfamba ore body and rocks are determined from MacDonough and Sun (1995). (A, B) the normalizing patterns of rocks (host and country) and Mn - Fe ore respectively, (C) normalized patterns of Mn – Fe ore and some selected rocks.

6.2.3 Whole Rock Geochemistry

Whole rock geochemical study is also helpful to insight the origin of the ore body, which is done by analyzing and interpreting the chemical signature of host rock and associated country rock. To achieve this total of thirteen fresh samples; six from sandstone, five from mudrock and two from volcanic rock (basalt and ignimbrite) were selected. Accordingly, the analytical data for major oxides, trace and rare earth element data including LOI for the analyzed rock samples are presented with ore body analysis result in table 6.1. The ore body is bounded by sandstone and mudrock. As a result many of the rock samples are selected from these intertrappean sediments.

5.2.3.1 Major Oxide content

The sandstone shows high contents of SiO_2 (av. 71.56 wt.%), Al_2O_3 (av. 12.98 wt.%), Fe_2O_3(av. 4.4 wt.%), K_2O (av. 3.9 wt.%) and Na_2O (av. 3.15 wt.%). The first three major oxide show significant variation in their amount, which varies from 66.8 – 77.5 wt.%, 10.7 – 15.3 wt.% and 2.45 – 8.41 wt.%; whereas the last two oxide show fairly uniform contents in the samples. The remained major oxide content is low, which is below one and they show little bit variation between samples. The significant variations of the major oxides are largely reflecting the relative proportions of quartz and feldspar minerals. The concentration of Fe_2O_3 is relatively higher in the sandstone. Therefore, the opaque minerals that are seen in the thin section might be iron oxide minerals. The average Na_2O contents, which is 3.15 wt.% reflects the presence of plagioclase feldspar in the studied sandstone. However, the identification of plagioclase feldspar in microscopic observation was difficult, because of the absence of its unique feature (albite twining) and similar color with quartz. In general, major oxide compositions of the Kulfamba sandstone are presented in Table 6.3.

According to Potter, (1978) and Noori, et. al., (2014), the high contents of SiO_2 and high SiO_2/Al_2O_3 ratio, which is greater than ten, reflects quartz-rich nature and chemical maturity index of the sandstone respectively. Accordingly, the present studied sandstone is characterized by high contents of SiO_2 (av. 71.56 wt.%); while its SiO_2/Al_2O_3 ratio is less than 10, (4.4 - 7.42, av. 5.67 Wt. %). This small SiO_2/Al_2O_3 ratio value indicates that the present investigated

sandstone (host rock) is chemical immature. Therefore, the immaturity of the investigated sandstone is not only mineralogically and texturally, but also it is chemically immature. The relative enrichment of K_2O (av. 3.9 wt.%) content over Na_2O (av. 3.15 wt.%) in Kulfamba sandstones may be due to significantly higher concentration of potassium feldspar than plagioclase feldspar. Their K_2O/Na_2O ratios are in the range between 1.1 to 1.36 wt.% (av. 1.23 wt %). These concentrations and ratios are also consistent with the petrographic observations, which show K-feldspar particularly sanidine is dominates over the other feldspar minerals.

Al_2O_3/TiO_2 ratios in clastic rocks are also essentially used to infer source rock composition, because Al_2O_3/TiO_2 ratio ranges from 3 to 8 for mafic igneous rocks, from 8 to 21 for intermediate rocks and from 21 to 70 for felsic igneous rocks (Hayashi, et. al., 1997). Accordingly, the Al_2O_3/TiO_2 ratios in the present studied sandstone are in the range between 15.3 to 23.78 wt %, which suggests intermediate to felsic igneous rock as a source rock of the Kulfamba sandstone. In general, the geochemical classification of the sandstone is described and shown with mineralogical classification in chapter five (Fig. 5.2 and 5.3).

Table 6.3: Major oxides compositions (Wt. %) of analyzed Kulfamba sandstones (host rock)

Sample code	*KA-05*	*KA-13*	*KA-14*	*KA-21*	*KA-22*	*WG-4*
SiO_2	77.5	73.9	77	66.8	67	67.2
Al_2O_3	10.7	12.4	11.4	14.45	13.65	15.3
Fe_2O_3	2.45	3.01	2.68	5.13	8.41	4.82
CaO	0.15	0.1	0.12	0.49	0.11	0.58
MgO	0.07	0.06	0.09	0.29	0.04	0.44
Na_2O	3.2	3.87	3.31	3.03	2.7	2.79
K_2O	4.33	4.91	4.53	3.34	3.04	3.29
TiO_2	0.45	0.55	0.49	0.91	0.62	1
MnO	0.06	0.1	0.09	0.06	0.09	0.17
P_2O_5	0.03	0.02	0.02	0.05	0.05	0.07
BaO	0.02	0.02	0.02	0.06	0.02	0.03
LOI	1.8	1.19	1.54	5.72	4.42	5.96
$Total$	100.8	100.13	101.3	100.34	100.15	101.66
SiO_2/Al_2O_3	7.42	5.96	6.75	4.6	4.9	4.4
K_2O/Na_2O	1.35	1.26	1.36	1.1	1.12	1.18
Al_2O_3/TiO_2	23.78	22.55	23.27	15.9	22	15.3

The mudrock also shows significant amount of SiO_2, Al_2O_3 and Fe_2O_3, which varies from (38 – 48.8, av. 45.12 wt. %), (15.7 – 27.4, av. 24.01 wt.%), (8.02 – 29.4, av. 12.5 wt.%) respectively. Whereas, the concentration of other major oxides in the mudrock is low that is below one. The concentration of aluminum and iron oxide in the mudrock is higher than that of sandstone concentration, but the SiO_2 content is low as compared to sandstone. Unlike sandstone, the concentration of titanium oxide in the mudrock is high that varies from 1.1 to 1.9 (av. 1.5 wt. %).

Furthermore, the volcanic rocks (basalt and ignimbrite) that found below intertrappean bed are analyzed. Accordingly, ignimbrite contains 69.9 wt. % SiO_2, 12.55 wt. % Al_2O_3, 5.9 wt. % K_2O, 3.51 wt. % Fe_2O_3 and 1.94 wt. % Na_2O. Similarly, the basalt is characterized by high contents of SiO_2, Fe_2O_3, Al_2O_3, CaO, MgO, and TiO_2, which are 46.4 wt. %, 16.35 wt. %, 12.5 wt. %, 9.58 wt. %, 5.76 wt. % and 5.31 respectively.

5.2.3.2 Trace Element Content

The sandstone, mudrock and ignimbrite are highly enriched in Zr, Nb, Zn and Ba. The concentration of Zr and Nb in these rocks is higher than that of ore body concentration. Similarly the basalt is characterized by high concentration of Sr, V, Zr, Cu, Ba and Zn. The Sr, V and Cu content in basalt is very high as compared to the ore body and other host rocks. Whereas, heavy elements such as Co and Ni were depleted in the host rock like of the ore body.

The Primitive mantle normalized (after MacDonough and Sun, 1995) REE patterns of the sediment and volcanic rock samples is smooth and it shows a high enrichment in LREEs and slight depletion in HREEs (fig 6.5). The normalized REE patterns of eighteen samples of Mn–Fe ores and wall rocks showed enrichment of LREE over the HREE. Compared with the Mn–Fe ores, the host and country rocks possess negative Eu and Ce anomalies, and lower ∑REE content. This means, the summation of rare earth elements of ignimbrite, mudrock, sandstone and basalt are 718.5 ppm, 710.3 ppm, 403 ppm and 261.9 respectively.

CHAPTER SEVEN

DISCUSSION

7.1 Genesis of Kulfamba Manganese – Iron Occurrence

Different researchers offer various ways of classification of manganese - iron deposits based on way of formation, subsequent modifications, host-rock types, source of metal, mineral assemblages and element associations (Wolf, 1976; Roy, 1981; Fan and Yang, 1999; Kuleshov and Maynard, 2017). However, many of them relate the diverse genetic types of manganese - iron mineralization with direct hydrothermal activity, sedimentary processes (hydrogenic and diagenetic) and continental weathering processes. Hydrothermal manganiferous deposits are directly precipitated from low temperature hydrothermal solutions in continental environments or volcano-sedimentary manganese mineralization deposited in marine environments (Ingram et al.; 1990, and Nicholson; 1992a). It is usually deposited in the form of stratabound, but may also occur as irregular bodies and veins in a large variety of host rocks. Hydrogenetic process refers to the slow settling of Mn-Fe colloids from the oxygenated bottom layer and all its constituents are sourced from the ambient seawater as initially colloidal particles within the water column (Bau et al., 2014). While, diagenetic processes represent the precipitation of manganese and iron from the pore water within the underlying reducing sediment and its principal source is an exogenetic source or weathering of crust from the washout of the feeding land mass (Kuleshov and Maynard, 2017). All these types of manganese deposits are characterized by different composition, morphology, ore mineral texture and different geochemical behavior.

In order to elucidate the genesis of Kulfamba manganese and iron mineralization, the present study uses field observation, petrographic and geochemical analysis. The complete interpretation of those analysis helps to accomplished the stated objectives that mentioned in chapter one. As a result, the genesis of the manganiferous occurrence has been identified based on the investigation and interpretation of the above mentioned results.

7.1.1 Field Observation

The different morphologies of the ore body that have been observed in the field have an implication on the genesis of the manganese - iron mineralization. According to Nicholson (1990), emission of hydrothermal solution in shallow continental basins (e.g. lakes) has produced stratabound and veins ferromanganese deposit in varieties of rock and ages. There are many stratabound hydrothermal manganese and manganiferous deposits in the world that are related to lacustrine formation in the Tertiary continental-volcanic province in San Francisco deposit (Mexico), Golconda (Nevada), Hokkaido (Japan) and Burmister deposit in Arizona (Hariya 1980 and Hewett et al. 1963, cited by Roy 1981). Sedimentary Mn-Fe deposits are mainly occurring as nodules and stratiform morphology (Gültekin and Balci, 2018). Stratiform or bedded ore morphology is the typical characteristics of sedimentary process. Similarly, the Kulfamba Mn-Fe ore body occurs as different morphology as described in the previous chapter; from those stratabund – stratiform (layered) mineralization is prominent over the other. This layered mineralization in the study area shows a separated iron and manganese layer. As shown in (Fig. 5.3 A and B), the ore body gradually changes from reddish brown Fe rich bed to brown - black Fe-Mn bed and finally to black Mn rich layer at the bottom, middle and top parts of the ore body respectively. It is formed as a result of iron precipitation first relatively in low oxygen environment and later the manganese is precipitated relatively in more oxidized environment. The evidence that support this statement is that the occurrence of iron enrichment in the lower parts of the ore body associated with mudrock. This means, the iron is formed with in the shallow continental basin (with in the lake), relatively in low oxygen environment. In contrast, the manganese enrichment occurs in the upper part of the ore body and it is hosted by sandstone. This indicates that the Mn-rich part of the ore body is formed in the transitional (fluvio-lacustrine), and relatively in more oxidized environment. The relative mobility of the two elements at different oxygen level has a great role for the formation of this stratiform Mn – Fe ore body. In addition, the manganese and iron vein ore bodies are exposed in different parts of the study area as described in chapter five. Therefore, the mineralization of the research area could be related with hybrid, both hydrothermal and sedimentary process. Furthermore, the sporadic manganese concretion, coating and its botryoidal/kidney like features could exhibit contribution from secondary processes latter on.

7.1.2 Petrographic observation

Petrographic observation was one method that helps to perform the objective of the present study. The most common varieties of ore mineral texture are mainly classified as primary and secondary texture of ore minerals (Craig and Vaughan, 1994). Correspondingly, the texture of the Kulfamba manganese ore mineral is identified through polished section and it shows mainly primary texture of open space deposition such as colloform growth banding, well developed crystals and vein filling structures. In addition, the manganese ore exhibit a secondary replacement texture, which replace along the rim and fractures of the gangue minerals (Fig. 6.1). The iron ore also exhibit open space deposition along the interstices between gangue minerals and replacement texture (Fig. 6.2). All the above listed open space deposition textures are the typical characteristics of hydrothermal activity. However, the replacement texture of the ore body shows the overprinting signature of secondary processes. Consequently, the petrographic observation of the study area resource origin could be mainly related to hydrothermal process with that of secondary process.

7.1.3 Geochemical characteristics of Kulfamba Manganese - Iron Occurrence

The geochemistry of major element, trace elements and rare earth elements patterns (REE) in the ore body and host rock are employed to characterize and distinguished the genesis of the kulfamba resource occurrence. According to Oksuz et. al., (2014) and Hein et. al., (2015), Fe/Mn ratios vary from 24,000 (up to 92% FeOOH or 58% of Fe) for hydrothermal seamount ironstones to about 0.001 (up to 82% MnO2 or 52% Mn) for hydrothermal stratabound manganese oxides from active volcanic arcs. Fe and Mn are characteristically fractionated on precipitation from a hydrothermal solution, producing high or low Fe/Mn ratio in exhalative sediments. In contrast, the hydrogenetic Fe-Mn deposit shows a little fractionation with a mean Fe/Mn ratio of 0.7 for open-ocean seamount crusts and 1.0 - 1.3 for continental margin seamount crusts.

Accordingly, the upper parts of the ore body (manganese rich part) and its bottom part (iron rich part) in Kulfamba has 0.045 and 20.52 mean Fe/Mn ratio respectively. The small and large ratio values (high concentration variation between Fe and Mn) shows a very high fractionation of iron and manganese in hydrothermal deposits. This high fractionation of Mn from Fe is as a result of

early precipitation of Fe in the lower parts of the deposit. As described above, the iron and manganese ore forms their ore layer. This field observation is also supported by geochemical results of Mn-Fe concentration. That means, the concentration of manganese is increased from bottom to upper parts of the ore body and the reverse is true for iron concentration (iron concentration is decreased). The abundance of Mn increases with decreasing Fe concentration. In general, insolubility difference between the two plays a vigorous role in their separation and ore mineral formation. That means the Fe is effectively separated during deposition by precipitating at lower pH and Eh, whereas Mn passes into the solution until it reach to high oxidation environment (Roy, 1997). Therefore, both high (20.52) and low (0.045) Fe/Mn ratio in the bottom and upper parts of Kulfamba ore body is conformable with hydrothermal deposits.

Like Fe and Mn contents, the Al and Si concentration in the ore body can also be used to distinguish the origin of Mn-Fe mineralization (Peters, 1988). Roy (1992) suggested that hydrothermal deposits commonly occur in close association with the ferruginous silica gel. As a result, the Si-Al binary diagram shows that all ore samples except one (sample KA-12) are fall in hydrothermal field (Fig 6.4 D). However, Fe-Si*2-Mn ternary diagram demonstrate that KA-12 is plotted in the hydrothermal field whereas the other four ore samples are dropped out of all genetic type (Fig. 6.4 B). These ore samples show the strong fractionation of manganese and iron during their mineralization. The sum up information that has got from the two discrimination diagram shows hydrothermal and hydrogenous nature.

The concentration of BaO can also tell about the origin of manganese - iron ore body. Hydrothermal solutions are more enriched in Ba as compared to seawater since they are affected from volcanic activity (Hein et al., 2008 and Pelleter et al., 2017). As the geochemical analysis result shows the concentration of barium was depleted in the host and volcanic rocks, while it is highly enriched in the ore body. As compared with iron ore the concentration of BaO is very high in manganese ore. According to Maynard (2010), Ba has a strong correlation with that of manganese. This is because, both manganese and barium do not form insoluble sulfides and are thus free to migrate from the deep to shallow environment (more oxidizing condition). Therefore, the high concentration of Ba (>10000 ppm) in Kulfamba is a characteristics of hydrothermal deposit.

The average concentration of heavy metals such as cobalt, nickel, zinc and copper; and their ratio have been also exploited in the classification of Mn-Fe deposits. High cobalt concentrations are indicative of marine environment, which is hydrogenetic deposit (Hem 1978, Oksuz 2010, and Nicholson 1992). This enrichment is related to its oxidation from Co^{2+} to its less soluble form Co^{3+} at the earth surface. The reverse is true for hydrothermal deposit. Hydrothermal deposits contain much lower concentration of minor metals such as Co, Cu and Ni as compared to hydrogenetic and diagenetic deposit. The extreme enrichment of metals in the hydrogenous deposits is usually attributed to their very slow accumulation from oxidizing seawater (Hein et al., 1997) as compared to rapid deposition of manganese and iron from suddenly cooled hydrothermal fluids, again under oxidizing conditions (Mynard, 2003). As shown in section 6.2.2, both lower and upper parts of the ore body is characterized by extremely low average concentration of those minor metals. This result is agreed with hydrothermal mineralization.

On the other hand, the Co/Zn ratio is used to differentiate between hydrothermal and sedimentary types of manganese - iron deposits where the Co/Zn ratio of 0.15 is indicative of hydrothermal type deposit and a ratio of 2.5 indicates hydrogenous type deposits (Toth 1980 and Kahrazehi et al., 2015). Therefore, Co/Zn ratio of manganese ore (upper parts of the ore body) is from 0.01 to 0.03 with its average 0.03 and iron ore (lower parts of the ore body) varies from 0.02 to 0.91 with its average 0.33. Consequently, the Co/Zn ratios of both upper and lower parts of the ore beds are near to the Co/Zn ratio for hydrothermal ferromanganese deposits.

In addition, many authors widely used the concentration of those heavy trace elements and major element in terms of discrimination diagram in order to determine the genesis of Mn - Fe ore deposit (Bonatti et al. 1972, Creater et al. 1982, Nicholson 1990, Choi and Hariya 1992; and Öksüz et al. 2014). Correspondingly, the ternary diagram of Fe - (Ni+Cu+Co)*10n - Mn shows that all samples of the ore bodies are plotted in the hydrothermal region (Fig 6.4 A). However, the manganese ore samples show mixing of hydrothermal and diagenetic process for the formation of the ore. The diagram also shows the extreme fractionations of manganese and iron with very low concentration of heavy metals. In addition, the Ni-Co-Zn discriminate diagram of all ore samples is fall out of both hydrothermal and hydrogenous region (Fig. 6.4 C). This is as a result of extreme concentration of zinc relative to nickel and cobalt. The extreme content of zinc in the ore body could be related with its source rock. As the geochemical data reveals, the

concentration of zinc in ignimbrite, mudrock, basalt and sandstones have (290, 247, 156 and 94) ppm respectively. Consequently, the coming hot solution bring high concentration of zinc by leaching the underline rock. Furthermore, the dominant ore sample in (Co+Ni) versus (As+Cu+Pb+V+Zn) binary diagram also manifest the hydrothermal nature of the resource (Fig. 6.4 E). However, one iron ore sample shows the contribution of hydrogenous process for the mineralization.

The concentration and ratio of rare earth elements also have a vigorous role to identify the origin of Mn-Fe mineralization (Hein et. al., 2008, Oksuz, 2011 and Oksuz et. al., 2014). The total REE concentrations in hydrothermal deposits range from 45 to 648 ppm, whereas those for hydrogenous deposits range from 1208 to 1918 ppm (Glasby et al., 1997; Miura and Hariya, 1997; Nath et al., 1992; Nath et al., 1997; Usui and Someya, 1997; Wiltshire et al., 1999). According to the writer, hydrogenous accumulations of Mn-Fe deposit have much higher REE concentrations and a pronounced positive cerium anomaly. Correspondingly, the total rare earth element concentrations in Kulfamba manganese and iron ore body is very high, which is in range 1456.2 to 2223.5 (av. 1839.8 ppm) and 980.5 to 6637 (av. 3056.2 ppm) respectively. This exaggerated enrichment of total REE contents are majorly as a result of high concentration of cerium (Ce), which is in the range of 755 to 1015 ppm for upper parts of the ore and 258 to 6150 ppm for its lower part. Consequently, the ∑REE content of Kulfamba Mn-Fe mineralization shows the involvements of hydrogenous processes during ore formation.

In addition, the total rare earth element enrichment of the present study might be related with the source rock. The whole rock geochemistry in section 6.2.3 indicates higher enrichments of total REE in the host rock and underline volcanic rock. The total REE content of ignimbrite, mudrock, sandstone and basalt are (718.4, 710.3, 403 and 261.9) ppm respectively. Although the sediment reworking was limited, there might be REE mobilization, and it may lead for the higher enrichments of REE in the host rock and ore body.

The ∑LREE/∑HREE ratios of the Kulfamba manganese and iron ore are in the range of 12.92 to 21.52 (av. 17.22 ppm) and 11.13 to 30.28 (av. 17.85 ppm) respectively. This ratio indicates the high concentrations of light rare earth over heavy rare earth element from their source and during mineralization. The relative enrichment of LREE is related to the mobility of REE in

hydrothermal systems. LREE are relatively more mobile than HREE in hydrothermal solution. In general, the higher enrichment of LREE over the HREE indicates the Mn-Fe mineralization of Kulfamba is association with hydrothermal solutions (Oksuz 2010). On the other side, the depletion of heavy REE relative to the light REE might be due to the presence of different accessory mineral like garnet and zircon in their source (Rollinson, 1993).

Some rare earth elements particularly Ce and Eu also exist in oxidation states other than trivalent ions in the form of Ce^{4+} and Eu^{2+} respectively. As a result, they are possible redox indicator. Hence, these two elements are most important in the assessment of Mn-Fe genesis, calculations were made for these anomalies. In order to compute Ce and Eu anomalies, LaN and PrN, and SmN and GdN values were utilized and their anomalies was found from Ce/Ce* and Eu/ Eu* respectively (Rollinson, 1993 and Oksuz 2010). Therefore, Ce*=CeN/(2/3LaN+1/3PrN) formula was used in the calculation of Ce anomalies. For the Kulfamba manganese occurrence, Ce* value is 0.43- 31.60 averaging as 7.24. Similarly, the Eu anomaly was computed from the formula of Eu*=EuN/ (2/3SmN+1/3GdN). Eu* was found to be 0.54 - 0.76 averaging 0.61 in the study area. These values are much greater than that of seawater (Oksuz, 2011) and similar to that of hydrothermal solutions.

Many authors (eg., Fleet, 1983; Derry and Jacobsen, 1990; Klein and Beukes, 1993; Bau and Dulski, 1996) have argued that modern hydrothermal fluids are characterized by positive Eu anomalies and near zero or negative cerium anomalies, whereas hydrogenous Mn-Fe deposits are characterized by a positive Ce anomaly and negative Eu anomaly. In Kulfamba Mn-Fe occurrence, the two ore samples (one from Mn rich part (KA-12) and the other from Fe rich part (KA-09) show a pronounced positive Ce anomaly (fig. 6.5 A). The oxidation of Ce^{3+} to Ce^{4+}, result in precipitate as insoluble cerianite (CeO_2) exhibiting a positive Ce anomaly (Kopp et al., 1996 and Lara et al., 2018). Whereas, the other three ore samples (KA-07, KA-10 and KA-11) REE data of the Mn-Fe oxide exhibit relatively flat patterns, which are characterized by slightly negative Ce anomalies. As mentioned above, the cerium anomalies of the first two ore samples show a positive Ce anomaly which is hydrogenous nature while the other three ores samples exhibit a negative Ce anomaly which is hydrothermal nature.

Likewise, primitive mantle normalized diagram signatures of the present study are characterized by the presence of slight negative Eu anomalies in all ore and rock samples (Fig. 6.5). It is related with the source rocks, there was plagioclase fractionation at depth during their formation. According to Rollinson (1993), the europium anomalies are mainly controlled by feldspars, for Eu (present in the divalent state) is compatible in plagioclase feldspar, in contrast to the trivalent REE which are incompatible. Thus the removal of plagioclase from a melt by crystal fractionation or the partial melting of a rock in which plagioclase is retained in the source will give rise to a negative Eu anomaly in the melt. All these may lead to the slight depletion of europium in the whole rock and its influence also goes to the ore body. In addition, the mobility of Eu depends strongly on redox and temperature conditions (Michard et al., 1983), and Eu enrichment involves hot and reduced fluids while Eu depletion involves cold and oxidizing fluids (Parr, 1992; Canet et al., 2005). Therefore, these slight negative Eu anomalies in all samples might indicate sediment contribution via dehydration and it confirms that the contribution of hydrogenous processes during Kulfamba ore formation. In general, the spider diagram shows the overprinting of hydrogenous processes over the hydrothermal processes. Both processes have their own contribution in the formation of Kulfamba manganiferous resource.

The ratio of Y/Ho is also important to discriminate the different genetic types of the Mn-Fe ore body. The element yttrium has similar ionic radius with that of Holmium (Ho). The Y/Ho ratios in the study area range from 21.8 to 29.3 (av. 25.5) for manganese ore and 19.3 to 24.9 (av. 22) for iron ore. Hydrothermal deposits are characterized by positive Y anomaly, Y/Ho>1 and hydrogenetic and diagenetic deposits show negative Y anomaly, Y/Ho<1 (Bau et al., 2014 and Konstantinova et al., 2017). The Y/Ho ratio of Kulfamb resource occurrence shows enrichment in Y element. These ratio values indicate that both upper and lower parts of the ore bodies have hydrothermal nature.

The available primitive mantle normalized REE patterns for the Kulfamba Mn-Fe ore occurrence and associated whole rock samples are presented in (Fig.6.5 A, B and C). The entire spectrum of the ore body is relatively smooth and flat except sample (KA-09) and displays a pronounced enrichment of the light rare earth element (LREE) over the heavy rare earth element (HREE), which is a typical characteristic of hydrothermal processes. Likewise, most of the whole rock

samples except (KA-03, KA-20 and KA-22), displays smooth and flat pattern with higher enrichments of LREE over HREE.

7.2 Genetic Model of Kulfamba Manganese - Iron ore

The manganese - iron ore body found in the study area, Kulfamba is hosted by intertrappean sedimentary rocks (mudrock and sandstone units), which are probably formed in the late Oligocene age. As the above described lithological log section shows, the host rocks are bounded by felsic rocks (ignimbrite in the lower part and volcanic glass in the upper part) and their most like source is pyroclastic material. Thus terrestrial sedimentary rocks are formed in continental sub-basin (fluvio-lacustrine environment). The formation of water pond sub-basin, lake and terrestrial sedimentation are started at the end of the emplacement of the ignimbrite formation. Its formation is following the paleo-geomorphology. This is evidenced by thickness variations in those terrestrial beds (mudrock and sandstone) as it shown in geological map of the study area.

The ore body is mainly formed by sedimentary and volcanic derived hydrothermal processes (Section 7.1). Some field observation (ore morphology) shows a certain contribution to secondary processes beside sedimentary and hydrothermal processes. First there was terrestrial inputs and upward movement of hydrothermal fluids following through the fractures in the underlying rocks to the water pond sub-basin. That means, the Mn, Fe and other element enrichment with in the ore body might not be only from underline rocks but also from those terrestrial sediments. That is why the Kulfamba manganiferous ore body shows hybrid morphology and geochemical result. The whole rock geochemical result also supports the host and underline volcanic rocks are relatively enriched by REE and iron oxide.

Later on, the metals start to precipitate (Fe^{2+} and Mn^{2+} will be oxidized to Fe^{3+} and Mn^{3+}, Mn^{4+} respectively) within the lake and transitional zone based on their geochemical behaviors. That means, the iron metal precipitate first, relatively at low pH and Eh (relatively in less oxidized) condition, while the manganese pass in to solution until it reach in more oxidized environment. This geochemical behavior of the two metals is also supported by their stratiform ore body formation in the field. The iron enrichment is mainly found in the lower parts of the ore body associated with the mudrock, while the manganese enrichment is formed in the upper parts of the

ore body associated with sandstone. In general, the fractionation of the two elements was the best mechanism to form Mn-Fe layered ore body. Beyond this layered ore body, the two metals are found in the form of vein mineralization associated with sandstone unit. This mineralization is formed when the metal rich thermal solutions are passing through the pore space and fractured zone of the host rock, and finally it precipitate as the physico-chemical condition have been changed. In addition, there is an involvement of continental weathering process after the formation of the host rock and ore body. For instance, the manganese concretion and coating is the results of this secondary process.

CHAPTER EIGHT

CONCLUSION AND RECOMMENDATION

8.1 Conclusion

From the present study, a number of conclusions have been presented about the geology of the study area and the origin of the ore body.

1. The geology of the present study area was mapped through field observation and from secondary source such as Google earth. Hence, five lithological units are mapped in 1:50,000 scale of map. The geological map and stratigraphic log section shows that the Mn-Fe ore body is hosted by intertrapean sediments such as sandstone and mudrock. As the petrographic and geochemical analysis shows, the sandstone is mineralogically, texturally and chemically immature. The most probable age of the host rock is between 27.7 ± 1.25 Ma to 23.03 Ma (late Oligocene). A strong surficial process such as weathering and erosion has a great role for the exposures of the host rock and the ore body.
2. The morphology of the ore body in the research area is found as a stratabound layer, veins, botryoidally precipitated coating/encrustation and concretion; however layered mineralization is prominent. The presence of these stratiform-stratabound and vein morphologies could show the hybrid nature of Kulfamba resource occurrence.
3. The mineralogy of the ore body has been identified through polished section and thin section. Accordingly, pyrolucite, hematite and goethite are the ore minerals, which dominantly occur as primary textures of open space deposition and secondary replacement on the gangue minerals. The presences of open space deposition texture such as colloform, vein felling and well crystallized textures supports the hydrothermal nature of the ore body.
4. The geochemical features of major element, trace element and REE were critical to distinguish the genesis of Kulfamba Mn-Fe resource occurrence. Most of the geochemical features show hybrid, hydrothermal - sedimentary processes. For instance,

a. The average Fe/Mn ratio value (0.045 and 20.52) of upper and lower parts of the ore body shows strong fractionation of iron and manganese during ore formation. The concentration of barium in manganese rich bad is also high (>10000 ppm). This strong fractionation of iron and manganese, and high concentration of Ba is match with hydrothermal activity.
b. Lower average content of minor metals such as Co, Ni, and Cu; and much lower ratio value of Co/Zn exhibits a hydrothermal nature. In addition, Fe-(Ni+Cu+Co)*10-Mn discrimination ternary diagram also show a hydrothermal nature. However, the other ternary and binary diagrams such as Fe-Si*2-Mn, (Co+Ni)/(As+Cu+Pb+V+Zn) and Si/Al demonstrate both hydrothermal and sedimentary processes.
c. The REE geochemistry such as ∑REE, their ratio (∑LREE/∑HREE, Y/Ho, Ce* and Eu*), and primitive mantle normalized REE distribution pattern shows mixing of hydrothermal and hydrogenous process. The extreme concentration of total REE of the upper (av. 1839.8 ppm) and lower (av. 3056.2 ppm) parts of the ore body demonstrate hydrogenous nature. While, the higher concentration of light rare earth element over heavy rare earth element values of the ore bodies demonstrate hydrothermal nature.

❖ Based on the above (field observation, petrographic and geochemical analysis), the Kulfamba manganese - iron resource occurrence was formed by hybrid, hydrothermal – sedimentary processes. Later on, the continental weathering process has its own contribution for the occurrence of Mn-Fe in the form of coating and concretion.

8.2 Recommendation

1. According to the regional geology observation, the host rock (terrestrial beds) and the ore bodies are not limited in the present study area. The stratigraphic section including terrestrial beds and thin manganese layer that found in Wogeltena area, 45 Km away from Kulfamba is similar with the present study area. From this geological observation, the sedimentation and Mn-Fe mineralization were not limited in the study are. Therefore, a detail field work is necessary to get the further continuity of the ore body and determine the extent of the basin.
2. In order to characterized and determine the origin of the Mn-Fe ore body, the ore samples are only taken from layered and fine grain manganese ore. However, the mineralization is occurring in the form of vein, concretion and coating. Therefore, it is better to take and analyzed the ore sample from those mentioned morphology to get further information about its genesis.
3. The local peoples of Kulfamba use the rhyolite and ignimbrite as a construction material, for building and cobblestone. In addition, in most part of the study area the felsic rock is altered to clay minerals (most probably to kaolinite). Therefore, a detail study is needed for those nonmetallic resources (clay minerals and construction materials).

REFERENCES

Abate Assen (2018). Characterization and genesis of Enkafela manganese deposit, Dallol area, Northern Afar depression. Unpublished MSc Thesis, Addis Ababa University, Addis Ababa, Ethiopia, 90 pp.

Abbate, E. and Sagri, M. (1980). Volcanites of Ethiopian and Somali Plateaus and major tectonic lines. Atti Convegni Acc Lincei Roma, **47**:219–227.

Asfawossen Asrat (2006). Introduction to Physical Geology. Addis Ababa University, Department of Earth Sciences. Addis Ababa University press, Ethiopia.

Bau, M., Schmidt K., Koschinsky, A., Hein, J., Kuhn, J., and Usui, A. (2014). Discriminating between different genetic types of marine ferro-manganese crusts and nodules based on rare earth elements and yttrium, Chemical Geology, **381**: 1- 9.

Boggs, S. Jr. (1992). Petrology of sedimentary rocks: Macmillan Pub. Co., New York, 707 p.

Boggs, S. Jr. (2014). Principles of sedimentology and stratigraphy. Pearson Education.

Bonatti, E., Fisher, D., Joensuu, O., Rydell, H. S., and Beyth, M. (1972). Iron manganese-barium deposit from the Northern Afar rift (Ethiopia). Econ. Geol. **67**:717–730.

Canet, C., Prol-Ledesma, R.M., Proenza, J., Rubio-Ramos, M.A., Forrest, M.J., Torres-Vera, M.A. and Rodríguez-Díaz, A. (2005). Mn-Ba-Hg mineralization at shallow submarine hydrothermal vents in Bahía Concepción, Baja California Sur, Mexico: Chemical Geology **224**: 96-112.

Carlo, D. E. and McMurtry, G. (1992). Rare earth element geochemistry of ferromanganese crusts from the Hawaiilan Archi-pelago, central Pasifc, Chem Geol. **95(3–4)**: 235–250.

Choi, J H. and Hariya Y. (1992). Geochemistry and depositional environment of Mn oxide deposits in the Tokora Belt, Northeastern Hokkaido, Japan. Economic Geology, **87**:1265-1274.

Craig, R. J. and Vaughan, J. D. (1994). Ore microscopy and ore petrography. A Wiley-Interscience Pub. New York.

Crook, K.A.W. (1974). Lithogenesis and geotectonics: The significance of compositional variation in flysch arenites (graywackes). The Society of Economic Paleontologists and Mineralogists (SEPM), Special publication **19**: 304-310.

Daniel Gemechu (1977). Aspects of Climate and Water Budget in Ethiopia. Addis Ababa University Press, Addis Ababa, Ethiopia.

Dereje Ayalew and Gezahegn Yirgu (2003). Crustal contribution to the genesis of Ethiopian plateau rhyolitic ignimbrites: Basalt and rhyolite geochemical provinciality. Journal of the Geological Society of London, **160**: 47–56.

Dereje Ayalew, Barbey, P., Marty, B., Reisberg, L., Gezahegn Yirgu and Pik, R. (2002). Source, genesis, and timing of giant ignimbrite deposits associated with Ethiopian continental flood basalts. Geochimica et Cosmochimica Acta, **66 (8):**1429-1448.

Fan, D. and Yang, P. (1999). Introduction to and classification of manganese deposits in china, Ore Geology Reviews, **15**: 1-13.

Fleet, A. J. (1983). Hydrothermal and hydrogenous ferromanganese deposits: The rare earth element evidence, in Rona, P.A., Boström, K., Laubier, L., (eds), Hydrothermal Process at Seafloor Spreading Centers: New York, Plenum Press, 535-555p.

Flohr, M. J. K. and Huebner, J. S. (1992). Mineralogy and geochemistry of two metamorphosed sedimentary manganese deposits, Sierra Nevada, California, USA, Lithos, **29**:57-85.

Folk, R. L. (1980). Petrology of sedimentary rocks. Hemphill Publishing, Austin, Texas.

Glasby, G.P., Stüben, D., Jeschke, G. and Garbe-Schönberg, C.D. (1997). A model for the formation of hydrothermal manganese crusts from the Pitcairn Island hotspot, Geochim. Cosmochim. Acta. **61**:4583–4597.

Gutzmer, J. & Beukes, N. J. (2009). Iron and manganese ore deposits: mineralogy, geochemistry and economic geology. Geology, **4**: 43-69.

Hayashi, K., Fujisawa, H., Holland, H. and Ohmoto, H. (1997). Geochemistry of 1.9 Ga sedimentary rocks from northeastern Labrador, Canada. Geochimica et Cosmochimica Acta, **61(19)**: 4115-4137.

Hein, J.R., Koschinsky, A., Halbach, P., Manheim, F.T., Bau, M., Kang, J. K. and Lubick, N. (1997). Iron and manganese oxide mineralization in the Pacific. Geol. Soc. Lond. Spec. Publ. **119**: 123–138.

Hein, J.R., Schulz, M.S., Dunham, R.E., Stern, R.J. and Bloomer, S.H. (2008). Diffuse flow hydrothermal manganese mineralization along the active Mariana and southern Izu-Bonin arc system, western Pacific. J. Geophys. Res. **113**: B08S14.

Hein, J.R., Spinardi, F., Okamoto, N., Mizell, K., Thorburn, D. and Tawake, A. (2015). Critical metals in manganese nodules from the Cook Islands EEZ, abundances and distributions. Ore Geol. Rev. **68**: 97–116.

Herron, M. M. (1988). Geochemical classification of terrigenous sands and shales from core or log data, Journal of Sedimentary Petrology, **58**: 820–829.

Hofmann, C., Courtillot, V., Feraud, G., Rochette, P., Gezahegn Yirgu, Ketefo, E. & Pik, R. (1997). Timing of the Ethiopian flood basalt event and implications for plume birth and global change. Nature, **389**: 838p.

https://en.climate-data.org/africa/ethiopia/amhara/debot-564611/ accessed on 28-03-2019.

https://investingnews.com/daily/resource-investing/battery-metals-investing/manganese-investing/op-manganese-producing-countries-south-africa-china-austraia/ accessed on 26-11-2018.

Josso, P., Pelleter, E., Pourret, O., Fouquet, Y., Etoubleau, J., Cheron, S. and Bollinger, C. (2016). A New Discrimination Scheme for Oceanic Ferromanganese Deposits using High Field Strength and Rare Earth Elements, Ore Geology Reviews.

Kahrazehi, M., Lotf, M., Ghaderi, M., Mohajjel, M. and Jafari, M. (2015). First report of Geochemical Characteristics of the Sangan Manganese Occurrence, Northeast Khash, Iran, Indian Journal of Science and Technology, **8(S3)**: 85–93.

Krauskopf, k. b. (1957). Separation of Manganese from Iron in Sedimentary processes, Geochimica et Cosmochimica Acta, Pergamon Press Ltd., London, **12**: 61-84.

Krinsley, D. H., K. Pye, Boggs, S. Jr. and Tovey, N. K. (1998). Backscattered scanning electron microscopy and image analysis of sediments and sedimentary rocks: Cambridge University Press, Cambridge, 193 p.

Kuleshov, V. and Maynard, J.B. (2017). Isotope Geochemistry: The origin and formation of manganese rocks and ores, Elsevier Inc., Amsterdam, 437pp.

Kurkura Kebeto., Aynalem Zenebe, Bheemalingeswara K., Kinfe Atshbeha, Solomon Gebresilassie and Kassa Amare (2012). Mineralogical and Geochemical Characterization of Clay and Lacustrine Deposits of Lake Ashenge Basin, Northern Ethiopia: Implication for Industrial Applications. Momona Ethiopian Journal of Science (MEJS). **4**:111-129.

Liakopoulos, A., Glasby, G.P., Papavassiliou C.T. and Boulegue, J. (2001). Nature and origin of the Vani manganese deposit, Milos, Greece: an overview. Ore Geology Reviews **18**: 181–209.

Marty, B., Pik, R. and Gezahegn Yirgu (1996). Helium isotopic variations in Ethiopian plume lavas: Nature of magmatic sources and limit on lower mantle contribution. Earth Planet. Sci. Lett. **144**: 223–237.

Maynard J. B. (1992). The Chemistry of Manganese Ores through Time: A Signal of Increasing Diversity of Earth-Surface Environments, Economic Geology, **105**:535–552.

Maynard, J. B. (2010). The Chemistry of Manganese Ores through Time: A Signal of Increasing Diversity of Earth-Surface Environments, Econ. Geol. **105**: 535–552.

McDonough, W. F. and Sun, S. S. (1995). The composition of the Earth. Chemical Geology, **120 (3)**: 223-253.

Melese Tadesse, Henok Bekele, Bezayit Mitiku, Meskerem Teshome, Asamenew Besufekade, Muhammed Edris, Getachew Burussa, Ezra Yehualaeshet, Shimeles Ashenafi and Tadesse Alemu (2011). Geology, Geochemistry and Gravity Survey of the Mychew Area. MOM,GSE.

Mengesha Tefera., Chernet T., and Haro W. (1996). Explanation of the Geological Map of Ethiopia. Ethiopian Institute of Geological Survey Addis Ababa, **3**: 79 pp.

Michard, A. (1989). Rare earth element systematics in hydrothermal fluids. Geochim. Cosmochim. Acta. **53**: 745–750.

Michard, A., Albarède, F., Michard, G., Minster, J.F. and Charlou, J.L. (1983). Rare-earth elements and uranium in high-temperature solutions from the East Pacific Rise hydrothermal vent field (13ºN): Nature, **303**: 795-797.

Miura, H. and Hariya, Y. (1997). Recent manganese oxide deposits in Hokkaido, Japan, in Nicholson, K., Hein, J.R., Bühn, B., Dasgupta, S. (eds), Manganese mineralization: geochemistry and mineralogy of terrestrial and marine deposits: The Geological Society of London, Special Publication **119**: 281-299.

Mohr, P. (1983) Ethiopian flood basalt province. Nature, **303**: 577–584.

Mohr, P. and Zanettin, B. (1988). The Ethiopian flood basalt province. In Continental flood basalts, edited by McDougall, J.D., Kluwer Acadamic Publication, Dordrecht, 63-110 p.

Nath, B. N., Pluger, W. L. and Roelandts, I. (1997). Geochemical constraints on the hydrothermal origin of ferromanganese encrustations from the Rodriguez Triple Junction, Indian Ocean, From Nicholson, K., Hein, J. R., Bfihn, B. & Dasgupta, S. (eds), 1997, Manganese Mineralization: Geochemistry and Mineralogy of Terrestrial and Marine Deposits, Geological Society Special Publication, **119**:199-211.

Nicholson, K. (1990). Stratiform manganese mineralisation near Inverness, Scotland: A Devonian sub-lacustrine hot-spring deposit? Mineralium Deposita, **25**:126-131.

Nicholson, K., Hein, J. R., Bühn, B. and Dasgupta, S. (1997). Manganese Mineralization: Geochemistry and Mineralogy of Terrestrial and Marine Deposits, Special Publication-Geological Society of London, **119**:5–27.

Nicoletti, M. and Petrucciani, C. (1973). Age of the alkaline rhyolites of the central eastern Ethiopian plateau and the edge of the rift. Atti Accademia Nazionale dei Lincei, Roma, Serie, **855**:471–476.

Oksuz, N. (2011). Geochemical characteristics of the Eymir (Sorgun-Yozgat) manganese deposit, Turkey, Journal of Rare Earths, **29**:282p.

Oksuz, N. and Okuyucu, N. (2014). Mineralogy, Geochemistry, and Origin of Buyukmahal Manganese Mineralization in the Artova Ophiolitic Complex, Yozgat, Turkey, Hindawi Publishing Corporation, Journal of Chemistry, Article ID 837972, 11p.

Papavassiliou, K., Voudouris, P., Kanellopoulos, C., Glasby, G., Alfieris, D. and Mitsis, I. (2017). New geochemical and mineralogical constraints on the genesis of the Vani hydrothermal manganese deposit at NW Milos island, Greece: Comparison with the Aspro Gialoudi deposit and implications for the formation of the Milos manganese mineralization, Ore geology Reviews, **80**:594-611.

Parr, J.M. (1992). Rare-earth element distribution in the exhalites associated with Broken Hill-type mineralisation at the Pinnacles deposit, New South Wales, Australia: Chemical Geology, **100**: 73-91.

Pettijohn, F. J., Potter, P. E. and Siever, R. (1972). Sand and Sandstones: Springer–Verlag, New York.

Pik, R., Daniel, C., Coulon, C., Gezahegn Yirgu, Hofman, C. and Dereje Ayalew (1998). The northwestern Ethiopian flood basalts: Classification and spatial distribution of magma types. J. Volcanol. Geotherm. Res, **81**: 91-111.

Pik, R., Deniel, C., Coulon, C., Gezahegn Yirgu, and Marty, B. (1999). Isotopic and trace element signatures of Ethiopian flood basalts: evidence for plume-lithosphere interactions. Geochim. Cosmochim. Acta, **63**:2263-2279.

Post, J. E. (1999). Manganese oxide minerals: Crystal structures and economic and environmental significance, Proc. Natl. Acad. Sci. **96**: 3447–3454.

Potter, P.E., (1978). Petrology and Chemistry of modern Big River Sand. Journal of Geology, **86(4)**: 423-449.

Rollinson H. R. (1993). Using geochemical data: evaluation, presentation, and interpretation. Pearson Education Asia (Pte) Ltd., Singapore (COS).

Rondeau B., Mazzero F., Bekele E., Gauthier J. P. and Fritsch E. (2009). Gem News International: New play-of-color opal from Wello, Ethiopia. G&G, **45(1)**: 59–60.

Roy, S. (1981). Genetic diversity of manganese deposition in the terrestrial geological record, **119**: 5-27.

Roy, S. (1992). Environments and processes of manganese deposition, Econ. Geol., **87**:1218-1236.

Roy, S. (1997). Genetic diversity of manganese deposition in the terrestrial geological record. In: Nicholson, K., Hein, J.R., Bu¨hn, B., Dasgupta, S. (Eds.), Manganese Mineralization: Geochemistry and Mineralogy of Terrestrial and Marine Deposits. Geol. Soc. Spec. Publ., **119**: 5–27.

Roy, S. (2006). Sedimentary manganese metallogenesis in response to the evolution of the Earth system, Earth-Science Reviews, **77**: 273–305.

Schilling J. G. (1973). Afar mantle plume: Rare earth evidence. Nature **242**: 2–5.

Shah, M. T. and Khan, A. (1999). Geochemistry and origin of Mn deposits in the Wazir is tanophiolite complex, north Waziristan, Pakistan, Miner Deposita, **34**:697–704.

Shah, M. T. and Moon, C. J. (2007). Manganese and ferromanganese ores from different tectonic settings in the NW Himalayas, Pakistan, Journal of Asian Earth Science, **29**: 455-465.

Solomon Tadesse (2009). Mineral Resources Potential of Ethiopia. Addis Ababa University Press. Addis Ababa. Ethiopia.

Solomon Tadesse, Milesi, J. P. and Deschamps, Y. (2003). Geology and mineral potential of Ethiopia: a note on geology and mineral map of Ethiopia, Journal of African Earth Sciences, **36**: 273–313.

Tesfaye Demissie, Genet Yohannes, Abraham Mammo, Yibeltal Tesfaye, Yonas Teshome, Getachew Burusa, Mohammed Edris and Meran Wenduante (2010). Geology, Geochemistry and Gravity Survey of the Dessie Area. MOM, GSE.

Toth, J R. (1980). Deposition of submarine crusts rich in manganese and iron. Geological Society of America Bulletin, **91**: 44-54.

ULLAH, K., ARIF, M. and SHAH, M. T. (2015). Petrography and geochemistry of the Kamlial Formation, southwestern Kohat plateau, Pakistan: implications for paleoclimate of the Western Himalayas, Turkish J Earth Sci. **24**:276-288.

Usui, A. and Someya, M. (1997). Distribution and composition of marine hydrogenetic and hydrothermal deposits in the northwest Pacific Nicholson, K., Hein, J. R., Biihn, B. & Dasgupta, S. (eds), 1997, Manganese Mineralization: Geochemistry and Mineralogy of Terrestrial and Marine Deposits, Geological Society Special Publication, **119**: 177- 198.

White R. S. and McKenzie D. P. (1989). Magmatism at rift zone: The generation of volcanic continental margins and flood basalts. J. Geophys. Res. **94**: 7685-7729.

Wolf, K. H. (1976). Handbook of strata-bound and stratiform ore deposits, II. Regional studies and specific deposits, Au, U, Fe, Mn, Hg, Sb, W and P deposits, Elsevier Scientific Publishing Company, Amsterdam, **7**: 649.

Worash Getaneh and Solomon Tadessse (2015). Textbook of Economic Geology, Addis Ababa University Press, 305P.

Yu, W., Algeo, T. J., Du Y., Maynard, B., Guo, H., Zhou, Q., Peng, T., Wang, P. and Yuan, L. (2016). Genesis of Cryogenian Datangpo manganese deposit: Hydrothermal influence and episodic postglacial ventilation of Nanhua Basin, South China, Palaeogeography, Palaeoclimatology, Palaeoecology, 54p.

Zanettin, B., Gregnanin, A., Justin Visentin, E., Morbidelli, M. and Piccirillo, E.M. (1974). Geological and petrological researches on the volcanics of central Ethiopia, Padova, Italy.

Zanettin, B., Justin Visentin, E. and Piccirillo, E.M. (1978). Volcanic Succession, Tectonics and Magmatology in the Central Ethiopia. Padova, Italy.

Zhang, W. and Cheng, C.Y. (2007). Manganese metallurgy review, Part I: Leaching of ores/ secondary materials and recovery of electrolytic /chemical manganese dioxide, Hydrometallurgy, **89**:137-159.

Appendix

1. Geochemical Analysis

Sample code	Name of sample	Wt. %	SiO_2	Al_2O_3	Fe_2O_3	CaO	MgO	Na_2O	K_2O	Cr_2O_3	TiO_2	MnO	P_2O_5	SrO	BaO	LOI	Total
KA 01	Ignimbrite	%	69.9	12.55	3.51	0.24	0.28	1.94	5.9	<0.002	0.56	0.2	0.03	0.01	0.01	5.69	100.82
KA 03	Mudstone	%	45	24.9	9.26	0.69	0.39	0.13	0.18	<0.002	1.35	0.04	0.02	0.01	0.02	18.2	100.19
KA 04	Fe-coated Mudstone	%	38	15.75	29.4	0.36	0.22	0.22	0.21	0.007	1.1	0.25	0.11	0.01	0.01	14.65	100.3
KA 06	Massive Mudstone	%	45.3	26.3	8.02	0.4	0.23	0.87	0.83	0.002	1.9	0.09	0.06	0.01	0.02	14.25	98.28
KA 08	Siltstone	%	48.8	25.7	7.28	0.31	0.16	0.86	0.82	<0.002	1.86	0.06	0.05	0.01	0.02	13.05	98.98
KA 20	White Claystone	%	48.5	27.4	8.8	0.22	0.08	0.09	0.13	<0.002	1.45	0.02	0.03	0.01	0.01	13.65	100.39
KA 05	Gray Indurated Sst	%	77.5	10.7	2.45	0.15	0.07	3.2	4.33	<0.002	0.45	0.06	0.03	<0.01	0.02	1.8	100.76
KA 13	White indurated Sst	%	73.9	12.4	3.01	0.1	0.06	3.87	4.91	<0.002	0.55	0.1	0.02	<0.01	0.02	1.19	100.13
KA 14	Brownish indurated Sst	%	77	11.4	2.68	0.12	0.09	3.31	4.53	<0.002	0.49	0.09	0.02	0.01	0.02	1.54	101.3
KA 21	Friable Sandstone	%	66.8	14.45	5.13	0.49	0.29	3.03	3.34	0.003	0.91	0.06	0.05	0.01	0.06	5.72	100.34
KA 22	Brown to reddish Sst	%	67	13.65	8.41	0.11	0.04	2.7	3.04	<0.002	0.62	0.09	0.05	<0.01	0.02	4.42	100.15
WG-4	Reddish Sandstone	%	67.2	15.3	4.82	0.58	0.44	2.79	3.29	<0.002	1	0.17	0.07	0.01	0.03	5.96	101.66
KA 19	Aphanetic Basalt	%	46.4	12.5	16.35	9.58	5.76	2.56	1.31	0.003	5.31	0.2	0.59	0.08	0.03	0.37	101.04
KA 07	Fe- ore	%	30.1	8.12	44.4	0.12	0.08	0.81	1.09	<0.002	0.63	2.33	0.08	0.01	0.32	11.55	99.64
KA 09	Massive Fe-ore	%	29.5	8.23	45.2	0.19	0.11	0.49	0.57	<0.002	0.8	1.22	0.06	0.01	0.16	12.65	99.19
KA 10	Fe-Mn ore	%	42.1	7.81	31.7	0.13	0.08	1.79	2.19	<0.002	0.32	4.74	0.01	0.01	0.73	8.32	99.93
KA 11	Mn- ore	%	34	7.36	2.66	0.14	0.07	1.74	3.47	0.004	0.35	33.1	<0.01	0.01	3.52	7.85	94.27
KA 12	Fine grain Mn- ore	%	3.76	2.36	1.28	0.26	0.07	0.22	3.19	0.007	0.12	59	0.2	0.19	4.82	12.35	87.83

Sample code	KA 01	KA 03	KA 04	KA 06	KA 08	KA 20	KA 05	KA 13	KA 14	KA 21	KA 22	WG 4	KA 19	KA 07	KA 09	KA 10	KA 11	KA 12
wt.(ppm)																		
Ba	99	159	107	205	188	124.5	177.5	176.5	174	480	163.5	252	239	2820	1390	6240	10000	10000
Ce	285	82.7	185	420	448	38.8	202	105.5	138	239	98.3	236	100	396	6150	258	755	1015
Cr	10	10	60	30	20	10	10	10	20	40	10	20	50	20	10	10	10	20
Cs	3.13	1.14	0.48	1.15	1.48	1.04	0.35	0.57	0.52	0.74	0.71	1.2	0.19	2.63	0.97	1.1	1.57	0.54
Dy	20.8	24.2	38.1	23.8	30.8	28.5	7.57	10.85	7.04	15.15	7.96	14.7	8.71	34.7	69.6	20.2	25	29.7
Er	11.15	15.2	26.3	17.1	19.95	22.5	3.64	6.42	3.71	7.55	4.3	8.17	3.99	16.55	34.7	8.64	9.57	17.7
Eu	5.51	5.72	5.62	5.71	9.21	3.69	3.05	2.68	2.23	5.22	3.05	4.77	3.82	12.95	11.7	8.93	13.25	5.79
Ga	38.1	67.9	48.9	75.7	76.4	81.8	27.1	33.4	28.4	36.1	33	37.6	26	27.4	39.8	23.1	29.8	24.9
Gd	23.7	22.7	25.1	20.1	32.6	14.25	10.55	10.05	7.67	19.55	9.76	17.5	11.9	46.5	52.5	30.5	46.7	28
Hf	33.8	53	30.9	55.7	54	48.8	7.7	15.4	9.5	14.5	13.7	15.6	10.5	14.3	15.6	7.6	8.5	5.3
Ho	4.07	5.03	8.52	5.39	6.51	6.77	1.41	2.23	1.3	2.78	1.51	2.94	1.58	6.1	13.1	3.49	4.12	6.43
La	142.5	111	64.4	194.5	344	47.8	99.2	46.2	46	150.5	84.2	118	40.6	392	78.9	240	603	145
Lu	1.39	2.35	3.67	2.68	3.05	4.04	0.46	0.85	0.49	0.86	0.8	1.1	0.39	1.95	3.12	0.79	0.85	2.03
Nb	248	302	275	284	293	273	47.3	79.6	53	77.8	76.2	82.4	53.8	85.5	91.9	36.6	36	24.7
Nd	143	115.5	77.4	165	292	53.2	97.8	54.9	54.7	134.5	81	124	58.9	432	115	278	531	126
Pr	37.4	28.7	19.5	48.2	85.5	13.9	25.1	14.2	14.3	34.8	22.6	31.7	13.3	118	27.4	72.4	143.5	32.7
Rb	223	8.1	4.2	11.8	14.6	9.2	51.3	81.7	51.1	42.3	21.4	34.6	28.4	25.2	10.3	19.8	33.4	29.1
Sm	29.1	25.2	21.3	28.4	47.5	12.9	15.95	11.65	10.3	24.1	14.2	22.2	13.3	72.4	41.4	48.7	79	27.1
Sn	9	15	9	17	16	14	3	5	3	5	4	5	3	5	5	2	3	2
Sr	19.1	42.8	20	29.6	25.8	12.8	12.9	7	8.2	61.5	7.5	44.1	667	19.5	15.8	20.8	140.5	1745
Ta	102.5	15.9	207	16.1	16	13.8	6.3	5.3	2.9	5.1	4.4	5.1	2.5	5	5.3	2.5	1.9	0.7

Tb	3.79	3.84	5.47	3.59	4.92	3.5	1.44	1.73	1.21	2.81	1.41	2.6	1.61	6.42	11.6	4.1	5.56	4.78
Th	24.7	35.4	20	36.5	36.1	30.5	5.57	10.9	6.63	12.1	9.96	10.6	3.71	10.4	11.2	5.43	6.19	4.31
Tm	1.59	2.28	4.01	2.74	3.09	3.72	0.5	0.92	0.51	0.96	0.68	1.17	0.51	2.27	4.5	1.07	1.13	2.37
U	8.85	6.59	18.15	6.55	9.87	3.88	1.64	2.89	1.62	2.54	1.6	2.62	1.13	9.76	23.2	15.35	4.51	15.75
V	47	67	192	91	77	31	12	16	15	38	27	48	511	90	121	14	12	115
W	3	4	5	6	7	4	2	2	2	2	3	2	3	9	13	1	<1	<1
Y	100.5	113	305	140.5	169	165.5	33	56.1	31.7	70.2	34.7	77	40.2	133	328	67.5	89.8	188.5
Yb	9.47	15.25	25.5	18	19.7	25.8	3.01	5.69	3.48	5.87	5.1	7.34	2.8	13.35	22.9	5.74	5.77	13.55
Zr	1340	2080	1270	2190	2200	2050	301	617	373	572	557	601	416	607	633	310	355	227
Ag	2.9	4.4	3	4.3	3.6	4.2	0.6	1	0.8	0.9	1.3	0.7	<0.5	2.9	2.5	3.2	17	33.5
As	<5	<5	14	8	11	8	<5	<5	5	<5	<5	<5	<5	76	79	5	5	5
Cd	0.5	<0.5	0.5	0.8	0.7	<0.5	<0.5	<0.5	<0.5	<0.5	<0.5	<0.5	1.6	<0.5	0.7	0.5	<0.5	18.3
Co	<1	1	28	4	1	<1	1	<1	1	4	2	6	52	45	343	6	4	48
Cu	1	<1	1	<1	<1	<1	1	<1	4	8	<1	2	308	4	1	1	1	35
Li	30	40	30	60	50	60	10	10	10	10	10	10	10	20	20	<10	10	10
Mo	6	3	18	4	3	<1	1	1	<1	1	2	2	<1	45	28	12	5	246
Ni	8	4	4	11	3	2	5	6	5	12	4	5	62	21	1	9	16	39
Pb	32	47	31	52	51	39	9	12	9	13	10	15	8	30	28	17	48	120
Sc	5	6	11	8	8	11	4	5	4	7	6	5	24	3	3	2	3	3
Tl	<10	<10	<10	<10	<10	<10	<10	<10	<10	<10	<10	<10	<10	20	10	<10	<10	<10
Zn	290	217	470	235	210	103	50	128	91	122	79	156	156	481	378	329	380	1570

2. Rare Earth Element Analysis

Sample	La	Ce	Pr	Nd	Sm	Eu	Gd	Tb	Dy	Ho	Er
KA - 07	392	396	118	432	72.4	13	47	6.4	35	6.1	17
KA - 09	79	6150	27.4	116	41.4	12	53	12	70	13	35
KA - 10	240	258	72.4	278	48.7	8.9	31	4.1	20	3.5	9
KA - 11	603	755	144	531	79	13	47	5.6	25	4.1	10
KA - 12	145	1015	32.7	126	27.1	5.8	28	4.8	30	6.4	18

Sample	Tm	Yb	Lu	Y	∑REE	LREE/HREE	Ce*	Eu*	Y/Ho
KA - 07	2.3	13	2	133	1551	11.13	0.42	0.57	21.8
KA - 09	4.5	23	3.1	328	6637	30.28	31.6	0.76	24.9
KA - 10	1.1	5.7	0.8	68	980.5	12.15	0.45	0.58	19.3
KA - 11	1.1	5.8	0.9	90	2224	21.52	0.56	0.54	21.8
KA - 12	2.4	14	2	189	1456	12.92	3.17	0.61	29.3

3. Petrographic analysis

Sample No	Q	F	R	M
KA01-A	28	30	12	30
KA01-B	30	25	10	35
KA-13	30	28	14	28
KA-14	34	20	22	26
KA-21	28	32	10	30
WG-4	30	20	28	22
Average	30	26	16	28